

A STUDY OF AB INITIO COMPUTATIONAL TECHNIQUES
AND THEIR APPLICATION TO CIS-TRANS
PHOTOISOMERIZATION OF RETINAL ANALOGS

CENTRE FOR NEWFOUNDLAND STUDIES

**TOTAL OF 10 PAGES ONLY
MAY BE XEROXED**

(Without Author's Permission)

ARPITA YADAV. B.Sc., M.Sc.





National Library
of Canada

Bibliothèque nationale
du Canada

Canadian Theses Service Service des thèses canadiennes

Ottawa, Canada
K1A 0N4

The author has granted an irrevocable non-exclusive licence allowing the National Library of Canada to reproduce, loan, distribute or sell copies of his/her thesis by any means and in any form or format, making this thesis available to interested persons.

The author retains ownership of the copyright in his/her thesis. Neither the thesis nor substantial extracts from it may be printed or otherwise reproduced without his/her permission.

L'auteur a accordé une licence irrévocable et non exclusive permettant à la Bibliothèque nationale du Canada de reproduire, prêter, distribuer ou vendre des copies de sa thèse de quelque manière et sous quelque forme que ce soit pour mettre des exemplaires de cette thèse à la disposition des personnes intéressées.

L'auteur conserve la propriété du droit d'auteur qui protège sa thèse. Ni la thèse ni des extraits substantiels de celle-ci ne doivent être imprimés ou autrement reproduits sans son autorisation.

ISBN 0-315-54985-8

A STUDY OF AB INITIO COMPUTATIONAL TECHNIQUES AND THEIR
APPLICATION TO CIS-TRANS PHOTOISOMERIZATION OF RETINAL ANALOGS

by

© Arpita Yadav, B.Sc., M.Sc.

A thesis submitted in partial fulfillment of the requirements
for the degree of Doctor of Philosophy.

Department of Chemistry
Memorial University of Newfoundland

April 1989

St. John's

Newfoundland
Canada

Dedicated

to

Amma & Pitaji

ABSTRACT

Ab initio Hartree Fock self consistent field calculations are performed on retinal analogs using the STO-3G basis set. Complete geometry optimizations are performed. The ground state properties (bond lengths, bond orders, net atomic charge distribution) of various cis and trans isomers of retinal analogs are studied in detail. Where necessary correlational effects are also taken into account by a simple model of strictly localized geminals. The effect of protonation on the properties of retinal Schiff base analogs is studied. Convergence in various properties is studied with increasing chain length justifying the use of smaller analogs mimicking retinal. Convergence, is however slower for retinal protonated Schiff base analogs. The retinal protonated Schiff base analogs show an increased conjugation in the vicinity of the NH_2^+ group. The cyclohexene ring is shown to have little effect on bonding and other properties of the molecule, but causes local torsional distortions. Methyl groups also cause torsional distortions as they introduce steric hindrance. The potential energy surfaces for conformational change around the 6-s-bond and 12-s-bond are studied in detail. The introduction of a methyl group at C13 leads to a skewed geometry around C12-C13 and C10-C11 single bonds. The results indicate that for retinal PSB the preferred conformation is planar 11-cis, 12-s-trans as compared to 11-cis, skewed 12-s-cis in retinal. The introduction of methyl groups on the cyclohexene ring leads to two stable skewed 6-s-cis conformations, one at 58.5° above the plane and the other at 65.0° below the plane, plane being defined by C1-C6-C5-C4. Planar 6-s-trans conformation is predicted to be a transition state for the isolated chromophore.

After a complete study of ground state properties, geometry relaxation studies are performed in the lowest lying triplet (^3B) excited state utilizing RHF and UHF methods. Since the UHF results suffer from significant spin contamination (even with the split valence 3-21G basis set), only the RHF results are considered. The RHF

results on the other hand, lead into the methodological difficulties concerning the intrinsic RHF instabilities. The 3B excited state results are also discussed from the solid state physics point of view. The results suggest highly delocalized spin density in the vicinity of the $NI_{2,2}^+$ group. $\pi \rightarrow \pi^*$ excitation energies are calculated using 'Singlet-triplet Approximation' and all singles doubles configuration interaction (SDCI) calculations. $\pi \rightarrow \pi^*$ excitation energies are studied as a function of chain length and rotation around the single bond. A red shift in the lowest $\pi \rightarrow \pi^*$ excitation energy is obtained on going from planar trans to planar cis conformation around a single bond or a double bond. Twisting around single bond leads to blue shift in accordance with the torsion model. SDCI calculations predict the lowest lying excited state to be 1A_g -like corresponding to the forbidden transition from the ground state.

Finally, based on ground and excited state results mechanisms for photocycles of rhodopsin, isorhodopsin and bacteriorhodopsin are discussed. Structural information on certain intermediates (bathorhodopsin, lumirhodopsin, metarhodopsin) is presented.

ACKNOWLEDGEMENTS

I wish to express my warmest gratitude to my research supervisor Professor Raymond A. Poirier for his excellent guidance and encouragement throughout this study. I would like to thank Dr. Peter R. Surján for many helpful discussions during his stay in St. John's.

I would also like to express my sincere thanks to Teresa Barker for typing the most difficult parts of this thesis. Special thanks to John Kane for drawing all the figures.

I thank Memorial University for financial support and Computing Services at Memorial University and Newfoundland and Labrador Computing Services for their generous allocation of computer time which made this work possible.

Last but not the least, I thank my husband, Veejendra, for his patience and constant encouragement.

Table of Contents

List of Tables	viii
List of Figures	x
Glossary	xiv
Definition of Terms	xvi
1. Introduction	1
1.1 Historical Background	1
1.1.1 Visual pigments (Rhodopsins)	1
1.1.2 Bacteriorhodopsin	3
1.1.3 Other rhodopsins	3
1.1.4 Some features of Rhodopsins	4
1.1.5 Primary events in the vision process (Rh) and the energy transfer process (bR)	4
1.1.6 Intermediates in the photocycles of bR and Rh	7
1.2 Recent Experimental Results	10
1.2.1 Structure elucidation based on Infrared, Resonance Raman, NMR and Absorption Spectroscopic data	10
1.2.2 Structure elucidation based on synthesis of artificial pigments	11
1.2.3 Conformation of 6-s-bond in bR	12
1.2.4 X-ray analysis data	13
1.3 λ_{\max} regulation in visual pigments: Models for Binding site	13
1.4 Mechanism proposed	15
1.5 Theoretical Results	18
1.5.1 Conformational Studies	19
1.5.2 Studies on charge distribution	19
1.5.3 Barriers to isomerization	20
1.5.4 Other theoretical investigations	20
1.5.5 Electronic Spectra Calculations	21
2. Computational details: The Methodology	24
2.1 The Hartree Fock Approximation	24
2.2 Choice of basis set	27

2.3	Closed Shell Hartree Fock: The Roothaan Equations	28
2.4	Open Shell spin Restricted Hartree Fock (RHF)	31
2.5	Open Shell spin Unrestricted Hartree Fock (UHF)	33
2.6	Mulliken population analysis and Bond orders	35
2.7	Geometry optimization using the optimally conditioned (OC) optimization algorithm	36
2.8	Singlet-triplet approximation (STA)	36
2.9	Strictly Localized Geminals (SLG) Approach	36
3.	Results and Discussion	38
3.1	Selection of analogs	38
3.2	Ground electronic state results	40
3.2.1	Optimized Geometries	40
3.2.2	Bond lengths and bond orders for chain analogs	40
3.2.3	Relative stabilities of various isomers of planar chain ana- logs	94
3.2.4	Ring analogs and full retinal PSB geometry	94
3.2.5	Effect of methyl substituents on the geometry and confor- mation of analogs	100
3.2.6	Effect of methyl substituents on the conformation of the cyclohexene ring	108
3.2.7	Net atomic charge distribution	119
4.	³ B Excited state results	128
4.1	Review of solid state aspects	128
4.1.1	Soliton-Antisoliton pairs	129
4.2	Ab initio RHF and UHF Results	131
4.2.1	UHF Results	141
4.3	Analogy with the allyl radical and methodological implications	143
4.3.1	The allyl radical structure and other related simple polyenes	143
4.3.2	RHF Instability	144
4.3.3	Retinal analogs as allyl-like moieties	144
4.3.4	Requirements for the search of true structure of triplet reti- nal analogs	146
4.4	Projected mechanistic implications	148
5.	Program developments for Configuration Interaction and Natural Orbi- tals	148

5.1	CI Wavefunction	148
5.1.1	Conventional CI procedure and Correlation energy	148
5.2	Setting up the CI Hamiltonian matrix	149
5.3	Practical Considerations	151
5.4	Direct CI	151
5.5	Program developments	152
5.6	One electron properties calculations from CI wavefunction	152
5.6.1	The reduced density matrix and natural orbitals	153
5.6.2	Setting up the reduced density matrix	153
5.6.3	Mulliken population analysis and one electron properties	157
6.	Applications of CI and STA to retinal analogs	159
6.1	Objectives of CI studies	159
6.2	Comparative study of excitation energies calculated using CI and STA	159
6.3	λ_{\max} regulation	161
6.4	Comparison of excited states level ordering obtained with STA and CI calculations	168
7.	Concluding Remarks	170
8.	References	179
	Appendix I	191
	Appendix II	192
	Appendix III	195
	Appendix IV	201

LIST OF TABLES

1. Planar all-trans chain analogs.	42
2. Planar 13-cis chain analogs.	43
3. Planar all-trans chain analogs.	44
4. Planar 11-cis chain analogs.	45
5. Planar 13-cis chain analogs.	47
6. Planar all-trans chain analogs.	49
7. Planar 11-cis chain analogs.	51
8. Planar 9-cis chain analogs.	53
9. Planar 13-cis chain analogs.	55
10. Planar all-trans retinal PSB analog.	57
11. All-trans, 5-methyl retinal PSB analog (C_8).	58
12. 11-cis, 12-s-trans, 13-methyl retinal analog (C_8).	60
13. 11-cis, 12-s-trans, 13-methyl retinal PSB analog (C_8).	62
14. Skewed 11-cis, 12-s-cis, 13-methyl retinal analog.	64
15. Skewed 11-cis, 12-s-cis, 13-methyl retinal PSB analog.	66
16. Cyclohexene ring (conformation 2) with an ethylenic branch at C6 (6-s-cis ring analog).	68
17. Cyclohexene ring (conformation 1) with an ethylenic branch at C6 (6-s-cis ring analog).	70
18. β -ionylidene ring (conformation 1) with an ethylenic branch at C6 (6-s-cis ring analog).	72

19. β -ionylidene ring (conformation 1) with an ethylenic branch at C6 (6-s-cis ring analog).	75
20. β -ionylidene ring (conformation 2) with an ethylenic branch at C6 (6-s-cis ring analog).	78
21. β -ionylidene ring (conformation 2) with an ethylenic branch at C6 (6-s-cis ring analog).	81
22. All-trans (6-s-cis) retinal PSB analog.	84
23. All-trans (6-s-trans) retinal PSB analog.	86
24. Total energies (a.u.) of various isomers of planar chain analogs. Relative energies (kJ mol^{-1}) with respect to the absolute minimum for that analog are given in brackets.	95
25. RIIF and UHF total energies (a.u.) at different optimized nuclear configurations in ^3B state. The relative energies (kJ mol^{-1}) with respect to the absolute minimum for that model are given in brackets. . . .	142
26. Excitation energies (eV) for lowest $\pi \rightarrow \pi^*$ transition.	160

LIST OF FIGURES

- Fig. 1. Variation in the SCF optimized C-C bond lengths for the (a) retinal, retinal SB and (b) retinal PSB analogs. The numbering of carbon atoms is as defined in the text. The different analogs are identified with different (dashed, dotted etc.) horizontal lines, for each bond; the vertical lines are just visual guidelines. Thick horizontal solid lines indicate coincidence. 88
- Fig. 2. Variation in the SCF optimized C-C bond orders for the (a) retinal, retinal SB and (b) retinal PSB analogs. For other notations, see fig. 1. 90
- Fig. 3. Variation in the SCF and MNDOC (from ref. 138) optimized C-C bond lengths for different analogs of (a) retinal, retinal SB and (b) retinal PSB. Experimental bond lengths (from ref. 69) for retinal are also shown. For other notations, see fig. 1. 92
- Fig. 4. Variation in the SCF optimized C-C bond lengths for the 6-s-cis retinal PSB analog along with the C-C bond lengths for the two building blocks. For other notations, see fig. 1. 97
- Fig. 5. Variation in the SCF optimized C-C bond orders for the 6-s-cis retinal PSB analog along with the C-C bond orders for the two building blocks. For other notations, see fig. 1. 99
- Fig. 6. The relative energy (kJ mol^{-1}) as a function of rigid rotation about the C12-C13 single bond. The torsion angle of 0° represents the 11-cis, 12-s-cis conformation. 104
- Fig. 7. The relative energy (kJ mol^{-1}) as a function of rotation about the C12-C13 single bond. Geometries for all the skewed 11-cis,

- 12-s-cis; 11-cis, 12-s-trans and planar 11-cis, 12-s-cis conformations have been fully optimized. Rigid rotations have been performed from the nearest optimized point. The torsion angle of 0° represents the planar 11-cis, 12-s-cis conformation. 106
- Fig. 8. The relative energy (kJ mol^{-1}) as a function of rotation about the C6-C7 single bond. The torsion angle of 0° represents the 6-s-cis retinal PSB. 111
- Fig. 9. The relative energy (kJ mol^{-1}) as a function of rigid rotation about the C6-C7 single bond. The torsion angle of 0° represents the planar 6-s-cis conformation. The energies are relative to β -ionylidene ring (conformation 2) with an ethylenic branch at C6 in the 6-s-cis conformation (6-s-cis above the plane). 114
- Fig. 10. The relative energy (kJ mol^{-1}) as a function of rotation about the C6-C7 single bond. The torsion angle of 0° represents the planar 6-s-cis conformation. The points where full geometry optimization has been carried out are shown in bold (except for the torsion angle under consideration for the points other than the two minima). Rigid rotations have been done from the nearest optimized point and are denoted by the same symbol. At the maximum there are two overlapping points at 160° and 165° 116
- Fig. 11. Variation in the SCF net atomic charges on the C, N, or O atoms for different chain analogs of (a) retinal, retinal SB and (b) retinal PSB. The numbering of carbon atoms is as defined in the text. 121

- Fig. 12. Variation in net atomic charges on the C,N, and O atoms for (a) retinal, retinal SB, and (b) retinal PSB analogs as obtained by ab initio SCF and SLG methods and semiempirical MNDOC (from ref. 138) and INDO-CISD (from ref. 108) calculations. The carbon atom numbering is as defined in the text. 124
- Fig. 13. Variation in the SCF net atomic charges on the C and N atoms for the 6-s-cis retinal PSB analog and the two building blocks. The numbering of carbon atoms is as defined in the text. 125
- Fig. 14. RHF optimized bond lengths for different resonance structures in 3B excited state of retinal SB and retinal PSB analogs with the STO-3G basis set. The resonance structures are shown schematically at the top of each diagram. The dots represent maximum spin densities. 133
- Fig. 15. RHF optimized bond lengths for different resonance structures in 3B excited state of retinal SB and retinal PSB analogs with the 3-21G basis set. For other notations, see fig. 14. 135
- Fig. 16. UHF optimized bond lengths for 3B excited state of retinal SB and retinal PSB analogs. The S^2 values as obtained in the calculation are shown. The expected value for S^2 is 2. For other notations, see fig. 14. 137
- Fig. 17. RHF optimized C-C bond orders for octatetraene in the 3B excited state. 140
- Fig. 18. Variation in the lowest $\pi \rightarrow \pi^*$ excitation energy (calculated using STA) with the chain length. 163
- Fig. 19. STA $\pi \rightarrow \pi^*$ excitation energies for a retinal chain analog as a function of torsion angle H13-C13-C12-H12. The torsion angle

of 180° represents the 12-s-trans conformation. The excited states are labelled considering analogy with simple polyenes having C_{2h} symmetry. 165

Fig. 20. HFSCF-SDCI $\pi \rightarrow \pi^*$ excitation energies for a retinal chain analog as a function of torsion angle H13-C13-C12-H12. The torsion angle of 180° represents the 12-s-trans conformation. The excited states are labelled considering analogy with simple polyenes having C_{2h} symmetry. 167

GLOSSARY

ATP	Adenosine tri-phosphate
B	Bathorhodopsin
BP mn	Bicycle pedal at centres m and n
bR	Bacteriorhodopsin
CI	Configuration interaction
CNDO/S	Complete neglect of differential overlap/ spectroscopic
CT-n	Concerted twist at centre n
HF	Hartree Fock
HT-n	Hula twist at centre n
I	Isorhodopsin
INDO-CISD	Intermediate neglect of differential overlap-configuration interaction singles and doubles
INDO-PSDCI	Intermediate neglect of differential overlap-partial singles and doubles configuration interaction
LCAO	Linear combination of atomic orbitals
MASS	Magic angle sample spinning
MNDOC	Modified neglect of diatomic overlap-correlated version
MO	Molecular Orbital
MRSD	Multi reference singles doubles
NMR	Nuclear Magnetic Resonance
PCILO	Perturbative configuration interaction with localized orbitals
PPP	Pariser-Parr-Pople
PSB	Protonated Schiff Base

QCFF/PI	Quantum mechanical modification of consistent force field for π-electrons
Rb	Rhodopsin
RHF	Restricted Hartree Fock
SB	Schiff Base
SCF	Self consistent field
UHF	Unrestricted Hartree Fock

Definition of Terms

(i) *Bleaching*

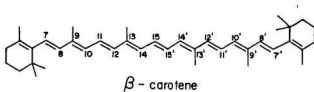
In presence of light the colour of the visual pigment slowly fades. This process is commonly referred to as 'bleaching'.

(ii) *Visual Purple*

In earlier works the visual pigment was referred to as the visual purple.

(iii) *Carotenoids*

Carotenoids are polyisoprenoid compounds linked 'head to tail' except in the middle of the molecule. The most common example of a carotenoid is β -carotene, $C_{40}H_{56}$.



(iv) *Rods and Cones*

The photoreceptor cells are of two types, which are called rods and cones because of their characteristic shapes. Rod cells make it possible to form black and white images in dim light; cones mediate colour or vision in bright light.

(v) *Opsin*

Opsin is a single polypeptide chain of 348 linked amino acids.

(vi) *Signal Transducer*

Visual pigments that photoisomerize and subsequently lead to the generation of an electrical signal are referred to as signal transducers. For example: Rhodopsin.

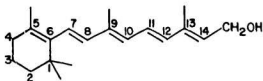
(vii) *Energy Transducer*

Visual pigments that convert light energy into a gradient of hydrogen ions across the membrane which subsequently leads to the synthesis of ATP are referred to as energy transducers. For example: **Bacteriorhodopsin**.

1. INTRODUCTION

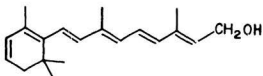
1.1 Historical Background

The first link between the 'chemistry of vision' and nutritional night blindness resulting from vitamin A deficiency came in the middle thirties when Wald made the observation that on bleaching or fading, visual purple produced a 'carotenoid', *retinene*, that could give rise to vitamin A¹. After many attempts Wald was the first to extract a photosensitive cone pigment working with chick retinas². The structure of vitamin A₁ resulted from the work of Karrer, Heilbron and others³⁻⁶.



Vitamin A₁ (retinol)

A similar compound vitamin A₂ was also discovered⁷⁻⁹ and its structure was studied:

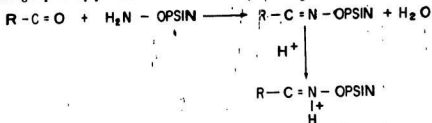


Vitamin A₂ (3-dehydroretinol)

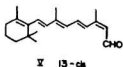
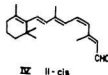
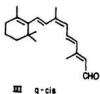
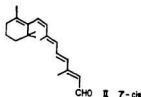
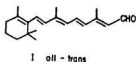
1.1.1 Visual pigments (Rhodopsins)

At this point it was known that visual pigments are made up of specific proteins, opsins, united with a prosthetic group based on vitamin A aldehydes, namely retinal or 3-dehydroretinal. The photoreceptor protein of rod cells is rhodopsin. In general, the visual pigments are referred to as rhodopsins (Rh). The nature of the prosthetic group- protein linkage was elucidated by Bownds¹⁰ and Akhtar et al¹¹.

They independently proved that the retinyl group is attached to the protein at an ϵ -amino group of a lysyl residue via a Schiff base (SB) linkage.



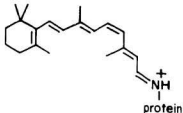
The general belief is that this Schiff base linkage is protonated¹². However, several investigators suggested that the ground state is not protonated¹³. The five isomeric forms of retinal were discovered^{14†}.



Wald and Hubbard studied the different isomers of retinal for the synthesis of Rh and thus differentiated between the 'active' and 'inactive' forms of retinal for the synthesis of Rh. The active form was first thought to be 11:13 di-cis, then either 7-cis or 11-cis^{15,16} based on the stereospecific synthetic work. Eventually the structure

† The conformation around the C6-C7 single bond is shown to be trans for historical reasons.

was unambiguously shown to be 11-cis¹⁷.



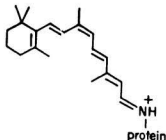
Rhodopsin

1.1.2 Bacteriorhodopsin

In 1971, Oesterhelt and Stoekenius discovered that the bacterium *Halobacterium halobium* when grown under anaerobic conditions develops a purple protein pigment bacteriorhodopsin (bR), which turned out to be an isomer of Rh^{18,19}. The role of bR is to convert light energy directly into a gradient of hydrogen ions across the membrane which subsequently leads to the synthesis of ATP. This discovery showed that very similar chromophoric systems are responsible for different roles in different organisms.

1.1.3 Other rhodopsins

Since then many other rhodopsins have been discovered: signal transducers such as: isorhodopsin, iodopsin, porphyropsin, slow rhodopsin and energy transducers such as: halorhodopsin, found in mammals, invertebrates and bacteria. In this context it may be useful to mention 'squid rhodopsin' which is a visual pigment that is photo sensitive but does not undergo 'bleaching'. Squid rhodopsin has some importance in the history of the subject because its peculiarity of not being bleached, permitted Hubbard and St. George to establish the primacy of the 11-cis to all-trans isomerization in rhodopsin. It is interesting to note that all these pigments contain different isomers of retinal as the chromophore.



Isorhodopsin

1.1.4 Some features of Rhodopsins

The most intriguing fact about Rh's is that they absorb over a wide range of wavelengths. The pigments of human colour vision absorb at 447, 540 and 577 nm²⁰ while other vertebrate rhodopsins absorb as low as 417 nm²¹ and as high as 620 nm²². Bacteriorhodopsin absorbs close to the upper limit at 568 nm. In contrast, simple retinal protonated Schiff bases (PSB) absorb at 440-450 nm and unprotonated SB absorb at 390 nm. Thus, the spectral properties of these rhodopsins reflect the sensitivity of the chromophore to the environment provided by the surrounding protein and the conformational differences between the chromophores.

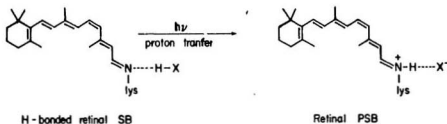
1.1.5 Primary events in the vision process (Rh) and the energy transfer process (bR)

Three basic steps were postulated for the reactions immediately following the photon absorption by the molecule:

- (i) a primary photochemical process;
- (ii) a dark reaction that replaced the decomposed photosensitive material, either from its products or from other precursors;
- (iii) a second dark process by which the primary photoproducts, alone or with other

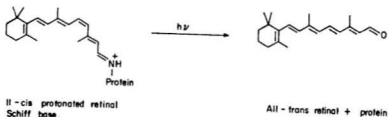
substances, initiated a nerve impulse²³.

Conjugated polyenes and carotenoids are well known for their tendency to undergo cis-trans isomerization on irradiation²⁴. Moreover, the process of vision is initiated by light not heat. Therefore, the involvement of an excited state that cannot be reached by possible increases in temperature seemed justified. Cis-trans isomerization was suggested as the primary step²⁵. However, it has been proposed that proton-transfer could be a fast competing process, as nitrogen can easily form hydrogen bonds or become protonated²⁶⁻²⁸. Rentzepis and co-workers found evidence for rapid proton-transfer in rhodopsin following light absorption²⁹⁻³¹. This led to the suggestion that in the ground state the retinal SB is not protonated but only H-bonded and the proton transfer takes place in the excited state as a result of photon absorption. The proton transfer is then followed by the cis-trans isomerization.



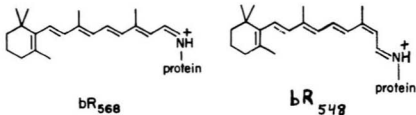
In the last ten years, a lot of experimental work has been done to understand the primary process in vision³²⁻⁴⁶. To summarize, we know that the initial conformation of the chromophore in Rh is 11-cis. During the process the geometry of the 11-cis retinal in Rh is changed to the all-trans form and in vertebrates the chromophore-opsin linkage is broken⁴⁷ whereas in invertebrates the photocycle does not lead to rupture of the chromophore-opsin bond³⁵. In vivo the photoreaction is

followed by enzymatic processes regenerating the original 11-cis pigment.

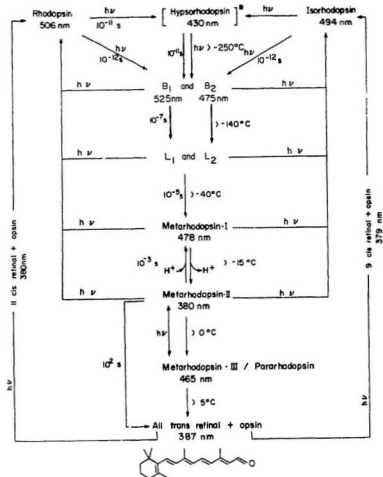
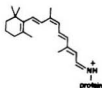
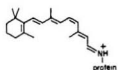


Primary event of the vision process in vertebrate rhodopsin .

In bR the chromophore is the all-trans (light adapted) or about 1:1 all-trans and 13-cis (dark adapted)⁴⁸. This is due to the fact that the light adapted bR₅₆₈, in the dark slowly converts to dark- adapted bR which contains an approximately equal mixture of all-trans and 13-cis retinal PSB chromophores (denoted bR₅₆₈ and bR₅₄₈, respectively).



Light absorption causes isomerization about the C13=C14 bond and the deprotonation of the Schiff base nitrogen. This results in the transport of protons across the cell membrane. The pigment returns to the light adapted bR₅₆₈ in the dark in ~ 10 msec. This makes bR very convenient for biophysical studies. Like invertebrates, in bR the chromophore does not detach from the opsin during the photocycle⁴⁸.



Intermediates in the photocycle of Rh

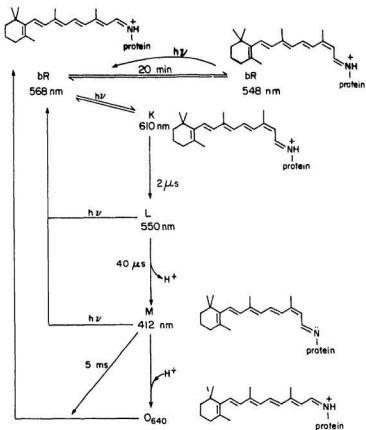
*Hypsorhodopsin has been observed only in the case of cattle rhodopsin.

Absorption maxima (in nm) and decay times (in seconds) of the intermediates are shown. Transition temperatures between intermediates are also listed.

Adapted from:

T. Yoshizawa and S. Horiuchi in *Biochemistry and Physiology of visual pigments*, 73, Ed: H. Langer, Springer-Verlag, New York (1973)

V. Balogh-Nair and K. Nakanishi, *New Comprehensive Biochemistry*, Vol. 3 Stereochemistry, Ed: Ch. Tamm, Elsevier Biomedical Press, 289 (1982)



Intermediates in the photocycle of bR

Absorption maxima and decay times of intermediates are shown.

Adapted from:

R.A. Mathies in Spectroscopy of biological molecules, Ed. C. Sandorfy and T. Theophanides, D. Reidel Publishing Company, Holland, page 303 (1984)

T. Alsuth, P. Hildebrandt, M. Stockburger in Spectroscopy of biological molecules, Ed. C. Sandorfy and T. Theophanides, D. Reidel Publishing Company, Holland, page 329 (1984)

R.R. Birge, Ann. Rev. Biophys. Bioeng., 10, 341 (1981)

1.2 Recent Experimental Results

1.2.1 Structure elucidation based on Infrared, Resonance Raman, NMR and Absorption Spectroscopic data

Most of the spectroscopic work has been done to elucidate the structures of the intermediates in the photocycles of Rh and bR and to determine where the deprotonation/reprotonation takes place in the photocycle. Oseroff and Callender^{49,50} studied the structures of Rh, isorhodopsin (I) and bathorhodopsin (B) using resonance Raman spectroscopy and showed that they were all protonated. Based on their results they also suggested that B had a highly distorted geometry. The structure of retinal chromophore in bR has also been studied using resonance Raman spectroscopy⁵¹. Elegant vibrational analysis of the retinal isomers⁵² and the all-trans retinal PSB⁵³ has been reported. Raman spectra of a series of all-trans retinal PSB isotopic derivatives were obtained. The 'fingerprint' assignments of all-trans retinal PSB and all-trans retinal were compared and it was shown that the major effect of the SB formation was a shift of the C14-C15 stretch from 1111 cm^{-1} in the aldehyde to 1163 cm^{-1} in the SB. This shift was attributed to the increased C14-C15 bond order that results from the reduced electronegativity of the SB nitrogen compared with the aldehyde oxygen.

More recently, the vibrational analysis of the 13-cis retinal chromophore in the dark-adapted bR⁵⁴ and the all-trans retinal chromophore in the light-adapted bR⁵⁵ have been reported. A detailed analysis of the 'fingerprint region' led to the identification of the spectral features and vibrational coupling patterns which are diagnostic of the C13=C14 and C=N conformations in retinal pigments. The vibrational analysis of the 13-cis retinal chromophore in the dark-adapted bR indicated that the C13=C14 bond is in the cis conformation and the C15=N Schiff base bond is in the syn conformation.

Recent results, based on photolysis experiments⁵⁶, indicate that two B intermediates are formed from Rh as well as I. Both the B intermediates comprise strained all-trans structures with slightly different arrangements within their protein pockets. B₁ decays to L₁ (lumirhodopsin 1) and B₂ decays to L₂ (lumirhodopsin 2).

The picosecond fluorescence kinetic data and quantum yield measurements from bovine rhodopsin by A.G. Doukas et al⁵⁷ have further confirmed the cis-trans isomerization about the C11=C12 bond of retinal in the vision process.

The syn-anti isomerization of the imine function could play an important role in the mechanism of vision. Using ¹³C solid state NMR and MASS technique Harbison et al⁵⁸ showed that the lyophilized dark-adapted bR is composed of a mixture of all-trans, 15-anti (E) and 13-cis, 15-syn (Z) isomers.

Apart from the above spectroscopic studies more information on the structures of intermediates came from the synthesis of artificial pigments.

1.2.2 Structure elucidation based on synthesis of artificial pigments

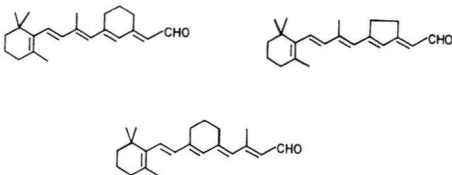
Some evidence for the involvement of particular bonds in isomerization came from the synthesis of artificial pigments with locked single or double bonds. J.M. Fang et al⁵⁹ synthesized fixed 13-ene structures that inhibited proton pumping.



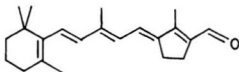
Based on their results they suggested that 13-ene plays a more important role than the ring site in initiating proton pumping in bR.

Later, in 1986 Albeck et al⁶⁰ based on their synthesis of artificial bR pigments

concluded that rotations around single bonds C12-C13, C10-C11 and isomerizations



of C11=C12 and C9=C10 are not required either for initiating the photocycle of all trans bR or for forming its M intermediate. C.H. Chang et al also arrived at



the same conclusion from their study of the C13=C14 locked chromophore⁶¹.

1.2.3 Conformation of the 6-s-bond in bR

As evident from the above results much of the present research has been on bR due to a number of experimental advantages. In the context of bR it is important to mention the recent work regarding the 6-s-bond conformation. Since bR absorbs at 568 nm which is in the upper range, spectroscopists have tried to explain this unusual 'opsin shift' in bR that shifts its λ_{max} to the red. It was noticed that the spectra of bR were sensitive to modifications in the ring region of the molecule⁶². Sheves et al⁶³ studied the effects caused by introducing steric hindrance in the vicinity of the bR ring. Harbison et al⁶⁴ and Childs et al⁶⁵ used solid state ¹³C NMR

spectroscopy to study the ring portion of the bR chromophore. Their results indicated that in the solid state the chromophore has a 6-s-trans conformation in the protein in contrast to an energetically favoured 6-s-cis conformation for retinoids in solution. They also showed that the chromophore conformation may be 25-30% 6-s-trans in solution⁶⁶. Locked 6-s-trans and cis chromophores synthesized by van der Steen et al⁶⁷ indicated that part of the opsin shift in bR arises when the chromophore changes from a 40° twisted 6-s-cis to a planar 6-s-trans conformation upon binding to the protein. However, the recent NMR and absorption spectroscopic data indicated that a s-cis ring chain conformation in bR cannot be ruled out⁶⁸.

1.2.4 X-ray analysis data

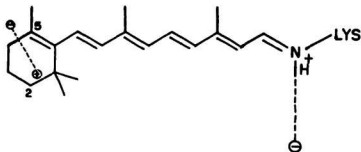
The above indirect methods have been used to determine the conformation of retinal salts and related compounds as no reliable X-ray structure of a retinylidene iminium salt has yet been reported in the literature. X-ray crystal structures of vitamin A isomers are limited to the following compounds: all-trans⁶⁹, 11-cis^{70,71} and 13-cis retinal⁷²; all-trans retinoic acid^{73,74}; β -ionylidene crotonic acid⁷⁵; all-trans vitamin A acetate⁷⁶ and methyl 7-cis, 9-cis retinoate⁷⁷. It has to be noted that for a given compound the ring-chain⁷⁴ conformation may change from s-cis to s-trans depending on the method of crystallization. A very unusual case is in 13-cis retinal where simultaneous presence of both conformers in one unit cell was reported⁷⁷.

1.3 λ_{\max} regulation in visual pigments: Models for Binding site

As we know, rhodopsins absorb over a wide range of wavelength, that is the λ_{\max} varies a great deal from one species to the other. Despite a lot of effort, no definite explanation has yet been obtained about the frequency regulation. The factors affecting λ_{\max} can be divided into two: electrostatic and conformational.

Nakanishi, Honig and coworkers⁷⁸⁻⁸² studied the chromophore- protein interactions by synthesizing dihydrorretinals and suggested the external point charge theory. They suggested the presence of a negative charge 3.0 Å⁺ above C5 and a positive

charge 3.0 \AA^* from the negative charge, that is, an ion-pair protein/chromophore interaction near the β -ionone moiety⁸³.



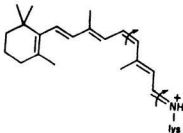
Point charge model for bR

However, the results of Sheves et al⁶³ and Lugtenburg et al⁸⁴ indicate that the major role in λ_{\max} regulation is played by the charge separation between the protonated Schiff base and its opsin counterion. Blatz and coworkers correlated the λ_{\max} of protonated all-trans retinylidene n-butyl amine with some physico-chemical properties of the counterions⁸⁵. Their results also indicated that λ_{\max} could be regulated by the distance between the counterion (anion) and the protonated Schiff base (cation) itself. Kakitani⁸⁶ suggested that a major factor in λ_{\max} regulation could be conformational: the twisting around double bond leads to the *bathochromic shift* (red shift) and that around single bond leads to the *hypochromic shift* (blue shift) so that, the wavelength regulation of the visual pigments can be achieved by different combinations of the double and single bond twistings.

1.4 Mechanisms proposed

During the past years, a number of mechanisms have been proposed for the vertebrate and invertebrate visual cycles, some of which are summarized below:

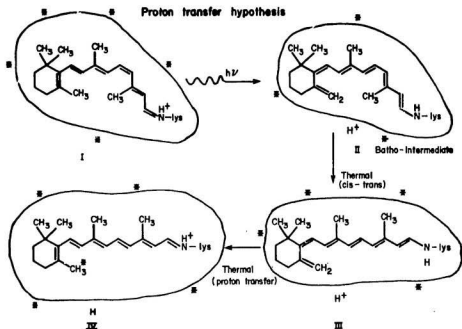
The first mechanism for the vision process was proposed by Warshel⁸⁷ in 1976. He proposed a '*bicycle pedal mechanism*' that involves concerted rotation around parallel pairs of double bonds in the lowest excited singlet state.



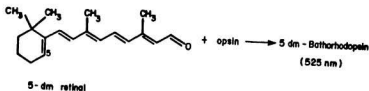
'Bicycle pedal': One step concerted rotation
around the C11=C12 and C15=N bonds

The mechanism was proposed in order to take into account the fact that retinal is bound to a restrictive active site in which the cyclohexene ring, at one end of the molecule, is trapped in a hydrophobic cleft and the other end of the molecule is bonded by a Schiff base bond to a lysine residue of the protein, that is the rotation takes place inside the protein cavity.

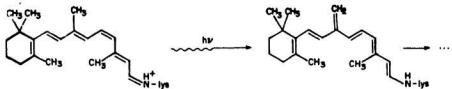
Fransen et al⁸⁸ suggested the proton transfer hypothesis that involved the transfer of a proton from the methyl group at C5 to some site on opsin.



Kropf²⁶ synthesized 5-demethyl retinal which on combination with opsin still gave rise to a batho intermediate.



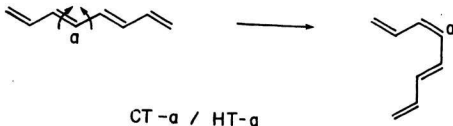
This experiment does contradict the hypothesis proposed by Fransen et al but, does not exclude the possibility of proton transfer taking place from some site other than the 5-methyl. For example, proton transfer from 9-methyl could take place as shown below



Furthermore, it is not surprising that the 5-demethyl retinal PSB synthesized by Kropf underwent photoisomerization as in general any conjugated polyene would photoisomerize. Therefore, a few more experiments are suggested before any conclusion can be drawn about the proton transfer hypothesis, for example, an experiment involving a comparative study of rate of photoisomerization and quantum yields for the methylated and demethylated retinal PSB.

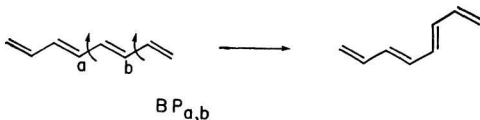
A mechanism for the proton pump in bR was suggested in 1978 by Schulten and Tavan⁸⁹. The mechanism is based on the fact that the PSB exhibits a high barrier for thermal isomerization in the ground state but a low barrier in the excited state and that the SB follows the reverse trend.

Liu and Asato⁹⁰ proposed a mechanism for the vision process that involves simultaneous twisting of two adjacent bonds called the *concerted twisting process* (CT-n; concerted twist at centre n). It is also known as the *Hula-twist process* (HT-n) and is a volume-conserving process.



The mechanism has been proposed based on molecular model construction and photochemical and bioorganic reasoning. Specific structures for the intermediates in the vision process have also been proposed.

Later, a combination of HT-n and a modified version of Warshel's 'bicycle-pedal' mechanism BP_{mn} (bicycle pedal at centres m and n) was proposed to explain the photocycle of bR and invertebrate and vertebrate rhodopsin photocycles⁹¹⁻⁹⁴.



Modified version of Warshel's "bicycle-pedal"

HT-n is proposed to take place in the excited state as it involves rotation around a formal single bond accompanied by isomerization of a neighbouring double bond, whereas, the BP_{mn} is proposed for all ground state conformational changes as it involves simultaneous rotation around two formal single bonds.

1.6 Theoretical Results[†]

Attempts to utilize computational chemistry for understanding the process of vision in the past have been limited mainly to methods such as Huckel and Pariser-Parr-Pople (PPP) π -electron methods. Crude theoretical models have been applied largely due to the size of the molecule. More recently, INDO-CISD (intermediate neglect of differential overlap configuration interaction singles and doubles) and

[†] Please see appendix III for details of different theoretical methods.

MNDOC (modified neglect of diatomic overlap correlated version) molecular orbital methods have been applied. In most of the cases geometry optimizations were not performed.

1.5.1 Conformational Studies

In 1970 Langlet et al⁹⁵ applied the PCILO (perturbative configuration interaction with localized orbitals) method to study the 6-*s*-cis/trans conformation of the cyclohexene ring with respect to the side chain in retinal. The calculations showed that the skewed-*s*-cis conformation is 2.5-2.8 kcal mol⁻¹ more stable than the planar-*s*-trans conformation. Honig et al⁹⁶ calculated the torsional potential of the cyclohexene ring in retinal for rotation around the C6-C7 and C12-C13 bonds utilizing a LCAO-MO-CI semiempirical method of PPP type corrected for the nearest neighbour overlap⁹⁷. Further conformational investigation on retinal was carried out by Dhingra and Saran⁹⁸ who utilized the PCILO method to study the preferred conformation around various single bonds and the relative stability of various isomers. Based on their results they proposed structures of the intermediate species in the photoreaction cycles of Rh⁹⁹ and bR¹⁰⁰.

1.5.2 Studies on charge distribution

Minimal basis set ab initio MO calculations with a 3x3 CI treatment were performed by Salem and Bruckmann on a nonatetraenylidene methyliminium molecule^{101,102}. Based on the calculated charge distributions in the ground and lowest singly excited $\pi \pi^*$ singlet states a specific hypothesis was suggested. According to their hypothesis the lowest $\pi \pi^*$ singlet excited state creates a sudden polarization within the molecule that triggers a sudden short lived electrical signal, causing charge transfer from one end of the molecule to the other. Warshel and Deakyne¹⁰³ studied the effect of torsion, bond alternation and charge stabilization on the ground and excited state energies of retinal PSB using the QCFF/PI method. Their results indicated that the light energy may be used not only for cis-trans isomerization

about double bonds but also for trapping charge stabilized intermediates. Hays et al¹⁰⁴ studied the effects of dipoles and aromatic amino acid side chain models on the absorption of Rh by using perturbation theory.

1.5.3 Barriers to isomerization

Being a photoisomerization problem there has been a continued interest in calculating barriers to isomerization around various single and double bonds in the ground and excited states and to study the effect of counterion and other external point charges on these barriers^{105,106}. Tavan et al¹⁰⁷ used the MNDOC method to study the effect of substituents at C13 on the barrier to isomerization around C13=C14 double bond. Seltzer¹⁰⁵ studied the energy barriers to cis-trans isomerization in a model for retinal PSB utilizing the MNDO method. The study indicated that in the ground state a negative charge near C13 lowers the barrier to bicycle-pedal isomerization but does not lower the barrier for Hula-twist. MNDO/CI calculations¹⁰⁶ in the ground and excited states on a model of retinal PSB indicated that a mechanism involving complete rotation around one double bond assisted by a partial rotation of the second double bond is more favourable as compared to a strictly bicycle-pedal motion.

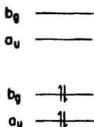
1.5.4 Other theoretical investigations

The INDO-CISD-MO theory coupled with the semiempirical molecular dynamics procedures has been utilized to investigate the quantum yields for photoisomerization¹⁰⁸⁻¹¹⁰. Force constant calculations have also been carried out for some analogs of retinal PSB^{111,112}. Kakitani et al^{113,114} proposed the torsion model to interpret the properties of Rh and its intermediates. Based on the model they^{115,116} analyzed the optical absorption wavelengths, oscillator strengths and rotational strengths of visual pigments and intermediates at low temperatures.

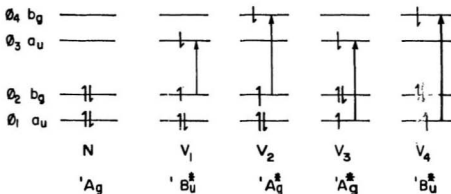
1.5.5 Electronic Spectra Calculations

The electronic spectra of conjugated polyenes in general have been investigated thoroughly, for example, ethylene, cis/trans butadiene, hexatriene etc.

Taking the example of trans butadiene in the ground state the MO energy level scheme for its π system under the simple Hückel approximation is:



Let us consider other configurations generated from the ground state configuration, in which only one electron is excited at a time.



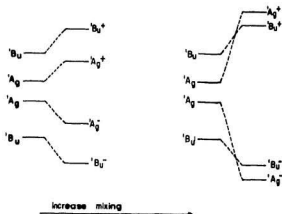
M.O. energy level schemes for the π -system of trans butadiene.

Each configuration is labelled with a symmetry symbol. Symbols N and V_i are according to Mulliken's notation which has not been universally adopted. The symmetry of each configuration (or state)[†] is determined from the product representations of the MO wave functions (refer to appendix I).

The spin and symmetry of the states determine which transitions are allowed. According to spin selection rule: $\Delta S=0$, and according to symmetry selection rule (Laporte's rule) transitions between states of the same parity, (u or g) are forbidden. $u \rightarrow g$ and $g \rightarrow u$ but $g \nrightarrow g$ and $u \nrightarrow u$.

Based on the above rules in trans butadiene there are $4 \pi \pi^*$ bands: two ${}^1A_g \rightarrow {}^1B_u^*$ bands (allowed) and the other two ${}^1A_g \rightarrow {}^1A_g^*$ transitions (forbidden). In cis butadiene however, all the four bands are symmetry allowed.

For a MO wavefunction (with configuration interaction) the two 1A_g configurations will mix, leading to a ${}^1A_g + {}^1A_g \rightarrow {}^1A_g^+$ and a ${}^1A_g - {}^1A_g \rightarrow {}^1A_g^-$ (The + and - signs refer to the sign in the linear combination resulting from configuration mixing). If the mixing is large the ${}^1A_g^-$ state can become lower than the ${}^1B_u^+$ state and be the lowest excited singlet state.



[†] The configurations may be referred to as states to a first approximation.

The advancement of two-photon spectroscopy has made it possible to study the lowest lying 1A_g state which corresponds to the forbidden transition from the ground state. In two-photon spectroscopy transitions of $g \rightarrow g$ type are allowed. Visual pigments do not have the C_{2h} symmetry but behave analogously to the simple conjugated polyenes and approximately follow the same nomenclature.

(CNDO/S) SCF-MO-CI calculations¹¹⁷ have been performed to study the excited states of all-trans and 11-cis retinal. MRSD π CI and single excitation σ π CI treatment on 2,4-pentadienal and 2,4,6,8-nonatetraenal (all-trans and 11-cis forms of aldehyde, SB, PSB of the model system) using a split valence basis set indicated large energy lowering (~ 1 eV) of the first allowed $\pi \pi^*$ excited state on protonation of the SB¹¹⁸. Birge and co workers¹¹⁹ have utilized the INDO-PSDCI MO theory to study models of the binding site, oscillator strengths of Rh and B, and barriers to isomerization in ground and excited states. They have also calculated molecular two photon absorptivities based on the combined use of PPP π -electron method including full SDCI (singles and doubles configuration interaction) and Monson and McClain's two-photon orientational averaging procedures¹²⁰⁻¹²⁴. Their results indicated that the $^1A_g^-$ covalent state is strongly two-photon allowed in long chain polyenes. All-trans retinal and the retinal SB also have the $^1A_g^-$ -like lowest lying state. However, in retinal PSB a reversal in the level ordering was noticed that makes the $^1B_u^+$ -like state the lowest. This reversal in level ordering (also obtained by two-photon laser spectroscopy) was considered as an indication for the presence of a protonated SB in Rh.

2. COMPUTATIONAL DETAILS: THE METHODOLOGY

Ab initio Hartree Fock self consistent field (HF SCF) MO calculations have been performed throughout using the program MUNGAUSS¹²⁵.

2.1 The Hartree Fock Approximation

The essence of the Hartree Fock approximation is to replace the complicated many electron problem by a one electron problem in which electron-electron repulsion is treated in an average way.

The ground state of an N-electron system can be written as a single Slater determinant

$$| \Psi_0 \rangle = | \psi_1 \bar{\psi}_1 \cdots \psi_1 \bar{\psi}_1 \cdots \psi_{N/2} \bar{\psi}_{N/2} \rangle$$

where each spatial molecular orbital (ψ_i | $i=1,2,\dots,N/2$) is doubly occupied. According to the variation principle the best wavefunction is the one that gives the lowest possible energy

$$E_0 = \langle \Psi_0 | H | \Psi_0 \rangle$$

H is the full electronic Hamiltonian. The variational flexibility in the wave function is in the choice of orbitals. By minimizing E_0 with respect to the choice of orbitals one can derive the HF equations which determine the optimal orbitals. HF equations are eigenvalue equations of the form

$$f(1) \psi_i(1) = \epsilon_i \psi_i(1)$$

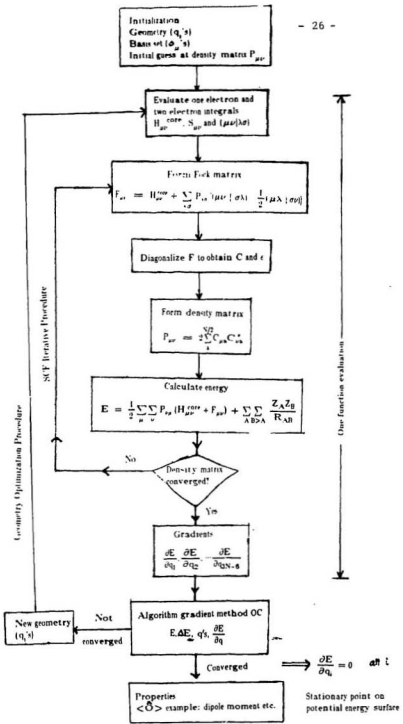
where $f(1)$ is an effective one electron operator, called the Fock operator.

$$f(1) = -\frac{1}{2} \nabla_1^2 - \sum_{A=1}^M \frac{Z_A}{r_{1A}} + v^{\text{HF}}(1) = h(1) + v^{\text{HF}}(1)$$

The Fock operator $f(1)$ is the sum of a core hamiltonian operator $h(1)$ and an effective one electron potential operator called the Hartree Fock potential $v^{\text{HF}}(1)$. $v^{\text{HF}}(1)$ is the average potential experienced by the electron 1 due to the presence of

the other electrons. Therefore, $\psi^{\text{HF}}(1)$ depends on the orbitals of the other electrons. Thus, the HF equations are non-linear and must be solved iteratively. The procedure for solving the HF equations is called the self consistent field (SCF) method.

The following flow chart gives a brief outline of the closed shell HF SCF procedure along with the geometry optimization procedure:



2.2 Choice of basis set

Molecular orbitals are expressed as a linear combination of a set of functions

$$\psi_i = \sum_{\mu=1}^K C_{\mu i} \phi_{\mu}$$

Due to the large size of retinal the calculations have been limited to the minimal STO-3G basis set¹²⁶. Only in some cases has a larger split valence 3-21G basis set been used¹²⁷. In STO-3G basis set a linear combination of Gaussian type orbitals (GTO) (contraction) is tailored to fit the shape of Slater type orbitals (STO). In general, a contraction has the form

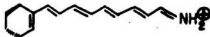
$$\phi_{\mu}(r - R_A) = \sum_{p=1}^L d_{p\mu} g_p(\alpha_{p\mu}, r - R_A)$$

$\alpha_{p\mu}$ and $d_{p\mu}$ are exponents and contraction coefficients respectively. L is the length of the contraction. For STO-3G L=3 and in 3-21G L=3 for core and 2 and 1 for valence orbitals which are split into two.

Minimal basis	Split-valence
H/He	H/He
1s	1s' 1s''
Li → Ne	Li → Ne
1s	1s
2s 2p _x 2p _y 2p _z	2s' 2p _x ' 2p _y ' 2p _z ' 2s'' 2p _x '' 2p _y '' 2p _z ''

Certain basis set exponents are optimized with the constraint that the 2s exponent is equal to the 2p exponent (2s=2p) and similarly 3s=3p=3d and so on. In these cases the functions are referred to as 2sp and 3spd respectively.

The basis size for the largest retinal PSB analog is shown below as an example:



	STO-3G basis set	3-21G basis set
number of basis functions	100	184
number of two electron integrals	12,753,775	579,377,820
number of one electron integrals	5050	34040

2.3 Closed Shell Hartree Fock: The Roothaan Equations

The Hartree Fock Hamiltonian is defined as

$$H_0 = \sum_{i=1}^N f(i)$$

where $f(i)$ is a Fock operator for the i^{th} electron.

The closed shell restricted (α and β spin orbitals are constrained to have the same spatial function) ground state for an N -electron system can be described as:

$$| \Psi_0 \rangle = | \psi_1 \bar{\psi}_1 \dots \psi_{N/2} \bar{\psi}_{N/2} \dots \psi_{N/2} \bar{\psi}_{N/2} \rangle$$

Each of the occupied spatial molecular orbitals (ψ_a , $a=1,2, \dots, N/2$) is doubly occupied. As described before the Fock operator is a sum of a core hamiltonian operator and an effective one electron potential operator called the Hartree Fock potential $U^{\text{HF}}(1)$.

$$f(1) = h(1) + U^{\text{HF}}(1) = h(1) + \sum_a^{N/2} 2J_a(1) - K_a(1)$$

J_a and K_a are the coulomb and exchange operators respectively which are defined as follows:

$$J_a(1) = \int d\tau_2 \psi_a^*(2) \frac{1}{r_{12}} \psi_a(2)$$

$$K_a(1) \psi_i(1) = \left[\int d\mathbf{r}_2 \psi_a^*(2) \frac{1}{r_{12}} \psi_i(2) \right] \psi_a(1)$$

The coulomb term represents the average local potential at \mathbf{r}_1 arising from an electron in ψ_a . The exchange term arises from the antisymmetric nature of the single determinant and does not have a simple classical interpretation.

The closed shell HF energy is given by

$$E_0 = \langle \Psi_0 | H | \Psi_0 \rangle$$

The calculation of molecular orbitals now becomes equivalent to the problem of solving the spatial integro-differential equations.

$$f(1) \psi_i(1) = c_i \psi_i(1) \quad (1)$$

Roothaan¹²⁸ showed that by introducing a set of known spatial basis functions the differential equation could be converted to a set of algebraic equations and solved by standard matrix techniques. Introducing a set of K known basis functions $\{\phi_\mu(\mathbf{r})\}_{\mu=1,2,\dots,K}$ and expanding the unknown molecular orbitals in the linear expansion

$$\psi_i = \sum_{\mu=1}^K C_{\mu i} \phi_\mu \quad i = 1, 2, \dots, K \quad (2)$$

Substituting the linear expansion (2) into the Hartree Fock equation (1) we get

$$f(1) \sum_{\nu} C_{\nu i} \phi_{\nu}(1) = c_i \sum_{\nu} C_{\nu i} \phi_{\nu}(1)$$

Multiplying by $\phi_{\mu}^*(1)$ on the left and integrating

$$\sum_{\nu} C_{\nu i} \int d\mathbf{r}_1 \phi_{\mu}^*(1) f(1) \phi_{\nu}(1) = c_i \sum_{\nu} C_{\nu i} \int d\mathbf{r}_1 \phi_{\mu}^*(1) \phi_{\nu}(1) \quad (3)$$

One can define an overlap matrix S, a $K \times K$ hermitian matrix, which has elements

$$S_{\mu\nu} = \int d\mathbf{r}_1 \phi_{\mu}^*(1) \phi_{\nu}(1)$$

Also defining a Fock matrix F that has the elements

$$F_{\mu\nu} = \int d\mathbf{r}_1 \phi_{\mu}^*(1) f(1) \phi_{\nu}(1)$$

It is also a $K \times K$ hermitian matrix. The basis functions $\{\phi_{\mu}\}$ are not in general orthogonal to each other and hence overlap with a magnitude $0 \leq |S_{\mu\nu}| \leq 1$. The diagonal elements of S are unity and the off-diagonal elements are less than unity. The sign of the off-diagonal terms depends on the relative sign of the two basis functions, and their relative orientation and separation in space. With these definitions the integrated HF equation (3) can be written as

$$\sum_{\nu} F_{\mu\nu} C_{\nu i} = \epsilon_i \sum_{\nu} S_{\mu\nu} C_{\nu i} \quad i = 1, 2, \dots, K$$

These are Roothaan's equations which can be written as the single matrix equation.

$$FC = SC\epsilon \quad (4)$$

C is a $K \times K$ square matrix of the expansion coefficients $C_{\mu i}$.

$$C = \begin{pmatrix} C_{11} & C_{12} & \dots & C_{1K} \\ C_{21} & C_{22} & \dots & C_{2K} \\ \vdots & \vdots & \ddots & \vdots \\ C_{K1} & C_{K2} & \dots & C_{KK} \end{pmatrix}$$

and ϵ is a diagonal matrix of the orbital energies ϵ_i .

$$\epsilon = \begin{pmatrix} \epsilon_1 & & & 0 \\ & \epsilon_2 & & \\ 0 & & \ddots & \\ & & & \epsilon_K \end{pmatrix}$$

As the Fock matrix depends on the expansion coefficients the resulting Roothaan equations are nonlinear

$$F(C)C = SC\epsilon$$

and are solved iteratively. (See Appendix IIa for details.) For an orthogonal basis set i.e. $S=I$ Roothaan's equations have the form of the usual matrix eigenvalue problem

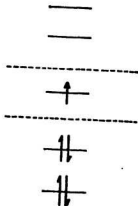
and the eigenvectors C and eigenvalues ϵ are calculated by diagonalizing F . Therefore the procedures for orthogonalizing the basis functions are considered. (Refer to Appendix IIb)

2.4 Open shell spin Restricted Hartree-Fock (RHF)

In the open shell RHF formalism all electrons except those that are explicitly required to occupy open shell orbitals, occupy closed shell orbitals. The wavefunctions thus obtained are eigenfunctions of the spin operator S^2 .

If the number of α - electrons $N_\alpha >$ number of β - electrons N_β there are N_β doubly occupied M.O.'s and $(N_\alpha - N_\beta)$ singly occupied M.O.'s. If K is the total number of basis functions then there will also be $(K - N_\alpha)$ unoccupied M.O.'s. For example: The case of a five electron doublet is shown below

$$(\psi_1\alpha) (\psi_1\beta) (\psi_2\alpha) (\psi_2\beta) (\psi_3\alpha)$$



Given a basis set $\{\phi_\mu | \mu = 1, 2, \dots, K\}$ the doubly occupied orbitals can be expanded as

$$\psi_i = \sum_{\mu} C_{\mu i} \phi_{\mu} \quad i = 1, 2, \dots, N_\beta$$

and $(N_\alpha - N_\beta)$ singly occupied orbitals can be expanded as

$$\psi_k = \sum_{\mu} C_{\mu k} \phi_{\mu} \quad k = N_t + 1, \dots, N_a$$

The energy expression for the five electron doublet wavefunction can be written as

$$\begin{aligned} E &= (2h_{11} + 2h_{22}) + h_{33} + (2J_{11} - K_{11} + 2J_{22} - K_{22} + 4J_{12} - 2K_{12}) \\ &\quad + (2J_{13} - K_{13} + 2J_{23} - K_{23}) \\ &= 2(h_{11} + h_{22}) + 2(J_{11} + J_{22} + J_{13} + J_{23}) - (K_{11} + K_{22} + K_{13} + K_{23}) \\ &\quad + h_{33} + 4J_{12} - 2K_{12} \\ &= E_{closed} + E_{open} \end{aligned}$$

In general, the energy expression for any wavefunction involving both closed shell and open shell orbitals can be written as

$$E = E_c + \sum_i^{open} 2f_i h_{ii} + \sum_{i,j}^{open} (a_{ij} J_{ij} + b_{ij} K_{ij})$$

a_{ij} and b_{ij} are referred to as the coupling coefficients. $a_{ij} = 2$ and $b_{ij} = 1$ for closed shell. The energy expression for the closed shell part (E_c) is written as

$$E_c = 2 \sum_p^{closed} h_{pp} + \sum_{p,q}^{closed} (2 J_{pq} - K_{pq})$$

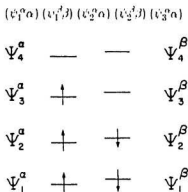
The generalized Fock operator is defined as

$$F_i = f_i h_{ii} + \sum_j (a_{ij} J_j + b_{ij} K_j)$$

As compared to the closed shell RHF in the open shell RHF the problem now cannot be expressed as a single matrix equation. Therefore other iterative optimization procedures are employed. An example of such optimization procedures is given in ref. 129. Some multiconfiguration SCF (MCSCF) procedures are also based on such optimization techniques. For open shell RHF different types of procedures have been employed. For example, a procedure involving setting up three Fock matrices which leads to three diagonalizations per iteration¹³⁰. This approach is computationally expensive to use.

2.5 Open shell spin Unrestricted Hartree-Fock (UHF)

In this approach, different spatial orbitals are assigned to α and β electrons. There are two distinct sets of molecular orbitals $\{\psi_j^\alpha \mid j=1,2,\dots,K\}$ and $\{\psi_j^\beta \mid j=1,2,\dots,K\}$. For example: The electron configuration for a five electron doublet can be written as



Since the RHF is a special case of the UHF function, according to the variation principle the optimized UHF energy is below the optimized RHF value. But, the UHF wavefunctions are not eigenfunctions of the total spin operator. Therefore, the UHF wavefunctions are contaminated by functions corresponding to states of higher spin multiplicity.

In UHF theory, the two sets of M.O.'s are defined by two sets of coefficients,

$$\psi_i^\alpha = \sum_{\mu=1}^K C_{\mu i}^\alpha \phi_\mu; \quad \psi_i^\beta = \sum_{\mu=1}^K C_{\mu i}^\beta \phi_\mu$$

These coefficients are varied independently, leading to UHF generalizations of Roothaan equations¹³¹.

$$\sum_{\nu} F_{\mu\nu}^\alpha C_{\nu j}^\alpha = \epsilon_j^\alpha \sum_{\nu} S_{\mu\nu} C_{\nu j}^\alpha \quad j = 1,2,\dots,K \quad (5)$$

$$\sum_{\nu} F_{\mu\nu}^{\beta} C_{ij}^{\beta} = \epsilon_j^{\beta} \sum_{\nu} S_{\mu\nu} C_{ij}^{\beta} \quad j = 1, 2, \dots, K \quad (6)$$

The two Fock matrices are defined by,

$$F_{\mu\nu}^{\alpha} = H_{\mu\nu}^{\text{core}} + \sum_{\lambda} \sum_{\sigma} P_{\lambda\sigma}^T(\mu\nu | \sigma\lambda) - P_{\lambda\sigma}^{\alpha}(\mu\lambda | \sigma\nu) \quad (7)$$

and

$$F_{\mu\nu}^{\beta} = H_{\mu\nu}^{\text{core}} + \sum_{\lambda} \sum_{\sigma} P_{\lambda\sigma}^T(\mu\nu | \sigma\lambda) - P_{\lambda\sigma}^{\beta}(\mu\lambda | \sigma\nu) \quad (8)$$

The two density matrices are defined as,

$$P_{\mu\nu}^{\alpha} = \sum_a^{N_a} C_{\mu a}^{\alpha} (C_{\nu a}^{\alpha})^* \quad (9)$$

$$P_{\mu\nu}^{\beta} = \sum_a^{N_b} C_{\mu a}^{\beta} (C_{\nu a}^{\beta})^* \quad (10)$$

The total density matrix is defined as $P^T = P^{\alpha} + P^{\beta}$ and a total spin density matrix is defined as $P^s = P^{\alpha} - P^{\beta}$. The integrals $S_{\mu\nu}$, $H_{\mu\nu}^{\text{core}}$ and $(\mu\nu|\sigma\lambda)$ appearing in the UHF equations are the same as those defined in the Roothaan procedure for closed shell calculations. Equations (5) and (6) lead to the following two matrix equations

$$F^{\alpha} C^{\alpha} = S C^{\alpha} \epsilon^{\alpha} \quad (11)$$

$$F^{\beta} C^{\beta} = S C^{\beta} \epsilon^{\beta} \quad (12)$$

ϵ^{α} and ϵ^{β} are diagonal matrices of orbital energies. C^{α} and C^{β} are KxK matrices of expansion coefficients. The above equations (11 and 12) are referred to as the Pople-Nesbet equations. Since F^{α} and F^{β} depend on both C^{α} and C^{β} the two eigenvalue equations have to be solved simultaneously.

Solution to the Pople-Nesbet Equations

The procedure is essentially identical with the case of the Roothaan's equations. An initial guess of both the density matrices P^{α} and P^{β} is taken and F^{α} and F^{β} are

formed. At each step of the iterative procedure the two matrix eigenvalue problems (11) and (12) are solved for C^α and C^β and new P^α and P^β are formed. The procedure is repeated until self consistent solutions to both are obtained simultaneously.

2.6 Mulliken population analysis and Bond orders

The total number of electrons $N = 2 \sum_{\alpha} \int d\mathbf{r} |\psi_{\alpha}(\mathbf{r})|^2$. This divides the total number of electrons into two electrons per MO. After substituting the basis expansion we get,

$$N = \sum_{\mu} \sum_{\nu} P_{\mu\nu} S_{\nu\mu} = \sum_{\mu} (PS)_{\mu\mu} = \text{tr} PS$$

It is possible to interpret $(PS)_{\mu\mu}$ as the number of electrons associated with ϕ_{μ} . This is called Mulliken population analysis. The above definition for the number of electrons associated with ϕ_{μ} is not unique as $\text{tr} PS = \text{tr} SP$ and

$$N = \sum_{\mu} \{S^n P S^{1-n}\}_{\mu\mu} \text{ for any } n$$

For the Mulliken population analysis $n=1$. The number of electrons associated with an atom in a molecule can be obtained by summing over all basis functions centred on that atom, and the net atomic charge can be calculated as

$$q_A = z_A - \sum_{\mu \in A} (PS)_{\mu\mu} \quad (13)$$

where z_A = atomic number of atom A.

Bond orders (B_{AB}) and atomic valency (V_A) indices have been calculated at the optimized geometries according to the definition given by Mayer¹³². Bond order index between atoms A and B is defined as

$$B_{AB} = \sum_{\mu \in A} \sum_{\nu \in B} (PS)_{\mu\nu} (PS)_{\nu\mu} \quad (14)$$

The valence of an atom in a molecule is given by the sum of bond orders formed by the atom.

$$V_A = \sum_{B(\neq A)} B_{AB} \quad (15)$$

2.7 Geometry optimization using the optimally conditioned (OC) optimization algorithm

Geometry optimizations have been performed using a variable metric algorithm proposed by Davidson¹³³. For convergence the gradient length was required to be $< 5.0 \times 10^{-4}$ where the gradient length is defined as $\left(\frac{\sum \epsilon_i^2}{N} \right)^{1/2}$ where N = number of optimizable parameters.

2.8 Singlet-triplet approximation (STA)

Singlet and triplet excitation energies have been calculated within the singlet-triplet approximation as follows:

For $k \rightarrow l^*$ transition

$$^3\Delta E = \epsilon_{l^*} - \epsilon_k - J_{kl^*}$$

$$^1\Delta E = \epsilon_{l^*} - \epsilon_k - J_{kl^*} + 2K_{kl^*}$$

where ϵ are orbital energies and J and K refer to the usual coulomb and exchange integrals. The above formulae are derived by considering the gains and losses in energies when going from one state of the molecule to another assuming a frozen orbital approximation. An example for the CO molecule is given in ref. 134.

2.9 Strictly Localized Geminals (SLG) Approach

Correlational effects are taken into account in some cases by a model of strictly localized geminals. This approach corresponds to a first order many body perturbation theory with a correlated, but fully localized reference state. The basis set is partitioned by assigning each basis function to a chemical bond possessing two electrons (geminals). A zeroth-order wavefunction is constructed as an antisymmetrized

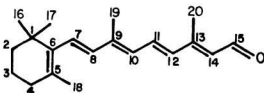
product of two electron group wave functions (geminals) expanded in disjunct but overlapping subspaces of basis orbitals. The geminals are obtained by solving the two electron Schrodinger equations exactly for each chemical bond within the corresponding local basis set. Therefore it gives a fully correlated description of two-electron chemical bonds. A second quantized formalism of the above approach is given in ref. 135.

Obviously, the SLG method cannot describe any conjugational effect, thus its error can be considered as a measure of the conjugation.

3. RESULTS AND DISCUSSION

In the introductory part we have seen that any attempts to utilize computational chemistry for understanding the vision process in the past have been limited mainly to methods such as Huckel and PPP π -electron methods. In this work we have utilized ab initio Hartree Fock M.O. calculations to study the properties of retinal. Since retinal is a large molecule for ab initio calculations let us first consider the approach to the problem, that is, the selection of the analogs.

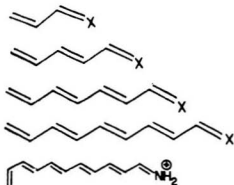
The numbering of carbon atoms in retinal is shown below. The same numbering shall be referred to throughout the text.



3.1 Selection of Analogs

A series of retinal analogs is investigated¹³⁶, starting with the smallest analog from the heteroatom end and then gradually increasing the chain length up to and including the double bond of the cyclohexene ring. At first the methyl substituents are not incorporated. Full geometry optimizations (no constraints) are performed in each case[†]. Similarly, the analogs of retinal SB and retinal PSB are also studied. After studying the chain part of the molecule in detail the ring end of the molecule is studied separately. The cyclohexene ring is studied with an ethylenic branch at C6. Finally, the optimized geometry for the largest chain analog is combined with the optimized cyclohexene ring analog. The geometrical parameters common to both

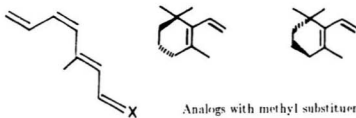
[†] When studying only the chain part it is assumed to be planar except in certain cases.



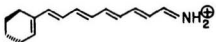
$\text{X} = \text{O}, \text{NH}, \text{NH}_2^+$
Chain Analogs



Cyclohexene ring analogs



Analogues with methyl substituents



Full retinal PSB analog
(without methyl substituents)

Analogues Studied

units are averaged. Full retinal PSB is thus studied¹³⁷ (without any methyl substituents).

3.2 Ground electronic state results

As a first step the properties of retinal, its SB and PSB are studied in its ground electronic state. Convergence in bond lengths, bond orders and charge distribution is studied as a function of chain length. This determines the smallest possible analogs that can be used to study the properties of retinal, its SB and PSB respectively.

3.2.1 Optimized Geometries

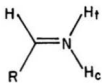
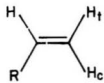
The STO-3G optimized geometries of the various cis and trans analogs for the chain part of the molecule are given in tables 1 to 15. The optimized geometries of the analogs for the cyclohexene ring end of the molecule are given in tables 16 to 21. The optimized geometries for the full retinal PSB analog (without any methyl substituents) are given in tables 22 and 23.

In general, the tables reflect the large difference in the behaviour of retinal analogs and retinal PSB analogs. The retinal SB analogs however, behave very similarly to the retinal analogs. The geometries of the various cis isomers are very close to the geometries of their respective trans isomers, except for the bond angle involving the cis bond which is $3-4^\circ$ larger than the respective bond angle for the trans isomer. For example, the bond angle C10-C11-C12 for the 11-cis retinal chain analog is predicted to be 127.2° (c.f. table 7) as compared to 124.1° (c.f. table 6) for the respective trans isomer.

3.2.2 Bond lengths and bond orders for chain analogs

The C-C bond lengths for different analogs of retinal, retinal SB and retinal PSB are shown in fig. 1 and the C-C bond orders for the same analogs are given in fig. 2. In the case of retinal analogs, bond length (r_{ab}) and bond orders (B_{ab}) are fairly independent of chain length, that is, they show a convergence with increasing

In the following tables the hydrogens labelled trans and cis are defined as follows



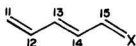


Table 1 Planar all-trans chain analogs

Bond	Bond lengths (Å)		
	X=O	X=NH	X=NH ₂ ⁺
C15-X	1.2214	1.2797	1.3220
C14-C15	1.5052	1.4926	1.4272
C13-C14	1.3203	1.3213	1.3560
C12-C13	1.4859	1.4854	1.4648
C11-C12	1.3144	1.3144	1.3261
C15-H	1.1037	1.0908	1.0986
C14-H	1.0833	1.0844	1.0805
C13-H	1.0857	1.0851	1.0927
C12-H	1.0841	1.0841	1.0823
C11-H _e	1.0821	1.0821	1.0870
C11-H _t	1.0816	1.0816	1.0868
N-H _e	—	1.0487	1.0273
N-H _t	—	—	1.0268
Angle	Bond Angles (degrees)		
	X=O	X=NH	X=NH ₂ ⁺
H-C15-X	121.6	117.5	115.8
H-C14-C15	116.3	116.2	118.3
H-C13-C14	119.7	119.8	119.1
H-C12-C13	115.8	115.9	117.0
H _e -C11-C12	122.0	122.0	122.3
H _t -C11-C12	122.0	122.0	121.5
H _e -N-C15		108.6	121.4
H _t -N-C15			121.6
C11-C15-X	124.1	127.0	124.2
C13-C14-C15	122.4	123.3	120.0
C12-C13-C14	124.4	124.2	124.3
C11-C12-C13	123.7	123.8	121.5

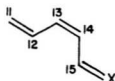


Table 2 Planar 13-cis chain analogs

Bond	Bond lengths (Å)		
	X=O	X=NH	X=NH ₂ ⁺
C15-X	1.2225	1.2803	1.3215
C14-C15	1.5060	1.4934	1.4202
C13-C14	1.3224	1.3231	1.3570
C12-C13	1.4875	1.4865	1.4671
C11-C12	1.3146	1.3147	1.3261
C15-H	1.1011	1.0887	1.0070
C14-H	1.0837	1.0846	1.0806
C13-H	1.0854	1.0852	1.0028
C12-H	1.0820	1.0822	1.0804
C11-H _c	1.0822	1.0821	1.0873
C11-H _t	1.0817	1.0816	1.0871
N-H _c	—	1.0489	1.0270
N-H _t	—	—	1.0276
Angle	Bond Angles (degrees)		
	X=O	X=NH	X=NH ₂ ⁺
H-C15-X	121.1	117.0	115.5
H-C14-C15	114.2	114.5	116.9
H-C13-C14	118.3	118.2	116.2
H-C12-C13	117.4	117.3	118.8
H _c -C11-C12	122.0	122.1	122.2
H _t -C11-C12	122.0	121.9	121.6
H _c -N-C15	—	108.7	121.7
H _t -N-C15	—	—	121.4
C14-C15-X	122.9	126.0	123.4
C13-C14-C15	126.4	126.7	123.1
C12-C13-C14	127.4	127.2	128.8
C11-C12-C13	122.8	122.9	120.7

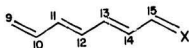


Table 3 Planar all-trans chain analogs

Bond	Bond lengths (Å)	
	X=O	X=NH ₂ ⁺
C15-X	1.2215	1.3291
C14-C15	1.5043	1.4117
C13-C14	1.3215	1.3685
C12-C13	1.4808	1.4412
C11-C12	1.3234	1.3457
C10-C11	1.4844	1.4723
C9-C10	1.3146	1.3215
C15-H	1.1038	1.0973
C14-H	1.0833	1.0798
C13-H	1.0857	1.0926
C12-H	1.0838	1.0811
C11-H	1.0846	1.0902
C10-H	1.0843	1.0827
C9-H _c	1.0819	1.0853
C9-H _t	1.0814	1.0849
N-H _c	—	1.0253
N-H _t	—	1.0248
Angle	Bond Angles (degrees)	
	X=O	X=NH ₂ ⁺
H-C15-X	121.6	115.4
H-C14-C15	116.3	118.7
H-C13-C14	119.5	118.5
H-C12-C13	116.2	117.8
H-C11-C12	119.9	119.3
H-C10-C11	115.8	116.6
H _c -C9-C10	122.0	122.2
H _t -C9-C10	122.0	121.7
H _c -N-C15	—	121.3
H _t -N-C15	—	121.5
C14-C15-X	124.2	124.6
C13-C14-C15	122.3	120.2
C12-C13-C14	124.5	124.6
C11-C12-C13	123.7	121.4
C10-C11-C12	124.0	124.3
C9-C10-C11	123.9	122.2

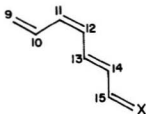


Table 4 Planar 11-cis chain analogs

Bond	Bond lengths (Å °)	
	X=O	X=NH ₂ ⁺
C15-X	1.2216	1.3285
C14-C15	1.5044	1.4128
C13-C14	1.3218	1.3677
C12-C13	1.4817	1.4433
C11-C12	1.3251	1.3468
C10-C11	1.4852	1.4742
C9-C10	1.3149	1.3216
C15-H	1.1038	1.0973
C14-H	1.0833	1.0799
C13-H	1.0839	1.0907
C12-H	1.0838	1.0811
C11-H	1.0846	1.0902
C10-H	1.0824	1.0808
C9-H _c	1.0820	1.0855
C9-H _t	1.0815	1.0851
N-H _c	—	1.0248
N-H _t	—	1.0254
Angle	Bond Angles (degrees)	
	X=O	X=NH ₂ ⁺
H-C15-X	121.6	115.5
H-C14-C15	116.2	118.6
H-C13-C14	119.0	118.2
H-C12-C13	114.8	116.3
H-C11-C12	118.2	116.9
H-C10-C11	117.2	118.3
H _c -C9-C10	122.0	122.1
H _t -C9-C10	122.0	121.7
H _c -N-C15	—	121.6
H _t -N-C15	—	121.3

C14-C15-X	124.1	124.4
C13-C14-C15	122.4	120.2
C12-C13-C14	123.6	123.8
C11-C12-C13	126.7	124.5
C10-C11-C12	127.2	128.4
C9-C10-C11	123.1	121.4

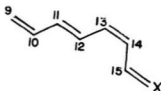


Table 5 Planar 13-cis chain analogs

Bond	Bond lengths (Å °)	
	N=O	X=NH ₂ ⁺
C15-X	1.2227	1.3286
C14-C15	1.5049	1.4137
C13-C14	1.3236	1.3603
C12-C13	1.4822	1.4438
C11-C12	1.3236	1.3455
C10-C11	1.4844	1.4724
C9-C10	1.3146	1.3216
C15-H	1.1011	1.0958
C14-H	1.0835	1.0798
C13-H	1.0855	1.0927
C12-H	1.0817	1.0794
C11-H	1.0847	1.0903
C10-H	1.0842	1.0825
C9-H _e	1.0819	1.0854
C9-H _t	1.0814	1.0850
N-H _e	—	1.0256
N-H _t	—	1.0249
Angle	Bond Angles (degrees)	
	N=O	X=NH ₂ ⁺
H-C15-X	121.1	115.2
H-C14-C15	114.3	117.3
H-C13-C14	118.2	115.7
H-C12-C13	117.8	119.5
H-C11-C12	120.0	119.3
H-C10-C11	115.9	116.7
H _e -C9-C10	122.0	122.2
H _t -C9-C10	122.0	121.7
H _e -N-C15	—	121.3
H _t -N-C15	—	121.6
C14-C15-X	123.0	123.8
C13-C14-C15	126.3	123.2

C12-C13-C14	127.4	128.9
C11-C12-C13	122.8	120.7
C10-C11-C12	124.0	124.4
C9-C10-C11	123.9	122.2

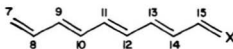


Table 6 Planar all-trans chain analogs

Bond	Bond lengths (Å)	
	X=O	X=NH ₂ ⁺
C15-X	1.2216	1.3342
C14-C15	1.5038	1.4018
C13-C14	1.3210	1.3769
C12-C13	1.4797	1.4281
C11-C12	1.3248	1.3554
C10-C11	1.4791	1.4547
C9-C10	1.3237	1.3372
C8-C9	1.4839	1.4772
C7-C8	1.3147	1.3187
C15-H	1.1038	1.0963
C14-H	1.0832	1.0794
C13-H	1.0857	1.0924
C12-H	1.0837	1.0806
C11-H	1.0847	1.0906
C10-H	1.0839	1.0817
C9-H	1.0844	1.0884
C8-H _c	1.0843	1.0830
C7-H _c	1.0818	1.0842
C7-H _t	1.0813	1.0837
N-H _c	—	1.0240
N-H _t	—	1.0234
Angle	Bond Angles (degrees)	
	X=O	X=NH ₂ ⁺
H-C15-X	121.6	115.2
H-C14-C15	116.3	119.0
H-C13-C14	119.5	118.2
H-C12-C13	116.2	118.1
H-C11-C12	119.8	118.9
H-C10-C11	116.1	117.2
H-C9-C10	120.0	119.5
H-C8-C9	115.8	116.3
H _c -C7-C8	122.0	122.1
H _t -C7-C8	122.0	121.8
H _c -N-C15	—	121.2
H _t -N-C15	—	121.5

C14-C15-X	124.2	124.7
C13-C14-C15	122.4	120.3
C12-C13-C14	124.5	124.8
C11-C12-C13	123.7	121.4
C10-C11-C12	124.1	124.6
C9-C10-C11	123.9	122.0
C8-C9-C10	124.0	124.2
C7-C8-C9	124.0	122.7

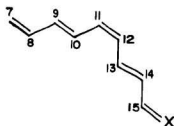


Table 7 Planar 11-cis chain analogs

Bond	Bond lengths (Å ⁺)	
	X=O	X=NH ₂ ⁺
C15-X	1.2217	1.3337
C14-C15	1.5040	1.4028
C13-C14	1.3221	1.3762
C12-C13	1.4806	1.4300
C11-C12	1.3265	1.3566
C10-C11	1.4799	1.4568
C9-C10	1.3239	1.3371
C8-C9	1.4841	1.4773
C7-C8	1.3116	1.3187
C15-H	1.1038	1.0964
C14-H	1.0833	1.0795
C13-H	1.0839	1.0907
C12-H	1.0837	1.0806
C11-H	1.0847	1.0905
C10-H	1.0822	1.0799
C9-H	1.0845	1.0885
C8-H	1.0843	1.0829
C7-H _c	1.0818	1.0813
C7-H _t	1.0813	1.0839
N-H _c	—	1.0235
N-H _t	—	1.0211
Angle	Bond Angles (degrees)	
	X=O	X=NH ₂ ⁺
H-C15-X	121.6	115.3
H-C14-C15	116.3	118.9
H-C13-C14	119.0	117.9
H-C12-C13	114.8	116.7
H-C11-C12	118.1	116.4
H-C10-C11	117.5	118.9
H-C9-C10	120.0	119.5

H-C8-C9	115.8	116.4
H _c -C7-C8	122.0	122.1
H _c -C7-C8	122.0	121.8
H _c -N-C15	—	121.5
H _c -N-C15	—	121.2
C14-C15-X	124.2	124.6
C13-C14-C15	122.4	120.3
C12-C13-C14	123.7	124.0
C11-C12-C13	126.7	124.4
C10-C11-C12	127.2	128.6
C9-C10-C11	123.1	121.2
C8-C9-C10	124.0	124.3
C7-C8-C9	124.0	122.6

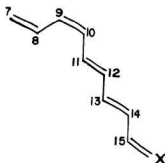


Table 8 Planar 9-cis chain analogs

Bond	Bond lengths (Å)	
	X=O	X=NH ₂ ⁺
C15-X	1.2216	1.3337
C14-C15	1.5038	1.4025
C13-C11	1.3210	1.3762
C12-C13	1.4798	1.4293
C11-C12	1.3250	1.3548
C10-C11	1.4700	1.4565
C9-C10	1.3254	1.3383
C8-C9	1.4847	1.4787
C7-C8	1.3140	1.3188
C15-H	1.1038	1.0961
C14-H	1.0832	1.0795
C13-H	1.0857	1.0921
C12-H	1.0838	1.0807
C11-H	1.0828	1.0886
C10-H	1.0840	1.0817
C9-H	1.0844	1.0884
C8-H	1.0825	1.0812
C7-H _c	1.0810	1.0843
C7-H _t	1.0814	1.0830
N-H _c	—	1.0235
N-H _t	—	1.0241
Angle	Bond Angles (degrees)	
	X=O	X=NH ₂ ⁺
H-C15-X	121.6	115.3
H-C14-C15	116.3	119.0
H-C13-C14	119.5	118.2
H-C12-C13	116.2	118.0
H-C11-C12	119.3	118.5

H-C10-C11	114.7	115.8
H-C9-C10	118.3	117.3
H-C8-C9	117.2	118.0
H _c -C7-C8	122.0	122.1
H _f -C7-C8	122.0	121.8
H _c -N-C15	—	121.5
H _f -N-C15	—	121.2
C14-C15-X	124.2	124.7
C13-C14-C15	122.4	120.3
C12-C13-C14	124.5	124.8
C11-C12-C13	123.6	121.4
C10-C11-C12	123.3	123.7
C9-C10-C11	126.9	125.1
C8-C9-C10	127.1	128.0
C7-C8-C9	123.2	121.9

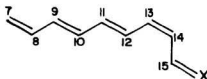


Table 9 Planar 13-cis chain analogs

Bond	Bond lengths (Å)	
	X=O	X=NH ₂ ⁺
C15-X	1.2228	1.3335
C14-C15	1.5045	1.1039
C13-C14	1.3239	1.3778
C12-C13	1.3811	1.4308
C11-C12	1.3251	1.3551
C10-C11	1.4790	1.4549
C9-C10	1.3237	1.3372
C8-C9	1.4839	1.4771
C7-C8	1.3147	1.3188
C15-H	1.1011	1.0949
C14-H	1.0835	1.0704
C13-H	1.0855	1.0925
C12-H	1.0816	1.0790
C11-H	1.0847	1.0906
C10-H	1.0839	1.0815
C9-H	1.0844	1.0885
C8-H	1.0843	1.0830
C7-H _c	1.0818	1.0843
C7-H _t	1.0813	1.0838
N-H _c	—	1.0243
N-H _t	—	1.0236
Angle	Bond Angles (degrees)	
	X=O	X=NH ₂ ⁺
H-C15-X	121.0	115.0
H-C14-C15	114.3	117.6
H-C13-C14	118.1	115.5
H-C12-C13	117.8	119.8
H-C11-C12	119.8	118.7
H-C10-C11	116.2	117.3
H-C9-C10	120.0	119.5
H-C8-C9	115.8	116.3
H _c -C7-C8	122.0	122.1
H _t -C7-C8	122.0	121.8

H _c -N-C15	-	121.2
H _t -N-C15	-	121.5
C14-C15-N	123.0	124.0
C13-C14-C15	126.3	123.2
C12-C13-C14	127.5	129.0
C11-C12-C13	122.8	120.6
C10-C11-C12	124.1	124.7
C9-C10-C11	123.8	122.0
C8-C9-C10	124.0	124.3
C7-C8-C9	124.0	122.6

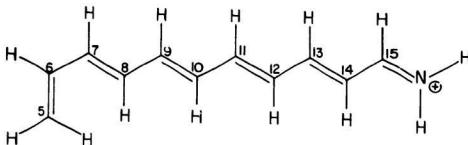
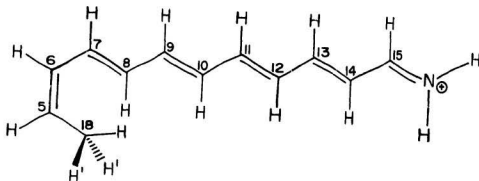


Table 10 Planar all-trans retinal PSB analog

Bond lengths (Å ^o)			
C15-N	1.3379	N-H _e	1.0231
C14-C15	1.3954	N-H _t	1.0225
C13-C14	1.3826	C15-H	1.0957
C12-C13	1.4199	C14-H	1.0792
C11-C12	1.3617	C13-H	1.0923
C10-C11	1.4455	C12-H	1.0804
C9-C10	1.3437	C11-H	1.0907
C8-C9	1.4618	C10-H	1.0812
C7-C8	1.3318	C9-H	1.0888
C6-C7	1.4855	C8-H	1.0812
C5-C6	1.3170	C7-H	1.0872
		C6-H	1.0833
		C5-H _t	1.0829
		C5-H _e	1.0824
Bond Angles (degrees)			
H-C15-N	115.1	C14-C15-N	121.8
H-C14-C15	119.1	C13-C14-C15	120.3
H-C13-C14	118.0	C12-C13-C14	121.9
H-C12-C13	118.4	C11-C12-C13	121.3
H-C11-C12	118.6	C10-C11-C12	124.7
H-C10-C11	117.5	C9-C10-C11	121.9
H-C9-C10	119.1	C8-C9-C10	124.5
H-C8-C9	116.5	C7-C8-C9	122.0
H-C7-C8	118.5	C6-C7-C8	125.5
H-C6-C7	114.8	C5-C6-C7	125.6
H _t -C5-C6	123.0		
H _e -C5-C6	121.2		
H _e -N-C15	121.2		
H _t -N-C15	121.1		

Table 11 All-trans, 5-methyl retinal PSB analog (C₉)

Bond lengths (Å °)			
C15-N	1.3392	N-H _c	1.0228
C14-C15	1.3929	N-H _t	1.0221
C13-C14	1.3840	C15-H	1.0955
C12-C13	1.4167	C14-H	1.0791
C11-C12	1.3641	C13-H	1.0922
C10-C11	1.4422	C12-H	1.0803
C9-C10	1.3457	C11-H	1.0908
C8-C9	1.4630	C10-H	1.0810
C7-C8	1.3344	C9-H	1.0890
C6-C7	1.4822	C8-H	1.0776
C5-C6	1.3245	C7-H	1.0880
C5-C18	1.5179	C6-H	1.0833
		C5-H	1.0874
		C18-H	1.0801
		C18-H'	1.0882
Bond Angles (degrees)			
H _c -N-H _c	117.4	H-C9-C10	119.0
H _c -N-C15	121.2	H-C9-C8	116.5
H-C15-N	115.0	H-C8-C9	115.9
H-C15-C14	120.1	H-C8-C7	123.0
H-C14-C15	119.2	H-C7-C8	116.4
H-C14-C13	120.4	H-C7-C6	112.6
H-C13-C14	117.9	H-C6-C7	111.9
H-C13-C12	117.2	H-C6-C5	116.2
H-C12-C13	118.4	H-C5-C6	115.8
H-C12-C11	120.2	C18-C5-C6	131.7
H-C11-C12	118.5	H-C18-C5	113.7
H-C11-C10	116.7	H'-C18-C5	109.3
H-C10-C11	117.6	H-C10-C9	120.6
Torsion Angles (degrees)			
H-C18-C5-C6	0.0	H'-C18-C5-C6	121.3

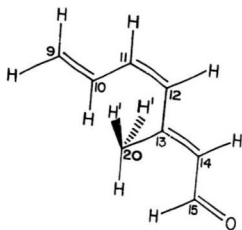


Table 12 11-cis, 12-s-trans, 13-methyl retinal analog (C_s)

Bond lengths (Å °)			
C15-O	1.2234	C15-H	1.1006
C14-C15	1.5034	C14-H	1.0829
C13-C14	1.3297	C20-H	1.0820
C13-C20	1.5265	C20-H'	1.0863
C12-C13	1.4079	C12-H	1.0837
C11-C12	1.3256	C11-H	1.0849
C10-C11	1.4859	C10-H	1.0790
C9-C10	1.3153	C9-H _t	1.0819
		C9-H _c	1.0815
Bond Angles (degrees)			
H-C15-O	120.7	H-C11-C12	115.8
H-C15-C14	116.8	H-C11-C10	112.6
H-C14-C15	113.1	H-C10-C11	118.6
H-C14-C13	119.0	H-C10-C9	119.2
C20-C13-C14	123.2	H _t -C9-C10	122.1
C20-C13-C12	120.0	H _c -C9-C10	121.9
H-C20-C13	111.6	H'-C20-C13	110.5
H-C12-C13	111.7	H-C12-C11	115.5
Torsion Angles (degrees)			
H-C20-C13-C14	0.0	H'-C20-C13-H	120.1

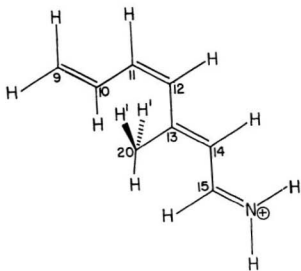


Table 13 11-*cis*, 12-*s-trans*, 13-methyl retinal PSB analog (C₄)

Bond lengths (Å °)			
C15-N	1.3321	N-H _l	1.0210
C14-C15	1.4063	N-H _e	1.0216
C13-C14	1.3819	C15-H	1.0912
C13-C20	1.5259	C14-H	1.0791
C12-C13	1.4635	C20-H	1.0817
C11-C12	1.3442	C20-H'	1.0872
C10-C11	1.4758	C12-H	1.0807
C9-C10	1.3248	C11-H	1.0900
		C10-H	1.0872
		C9-H _l	1.0850
		C9-H _e	1.0853
Bond Angles (degrees)			
H _l -N-H _e	117.2	H-C12-C13	113.1
C15-N-H _e	121.5	H-C12-C11	116.0
H-C15-N	114.6	H-C11-C12	114.5
H-C15-C14	122.1	H-C11-C10	112.7
H-C14-C15	116.3	H-C10-C11	119.7
H-C14-C13	118.6	H-C10-C9	119.8
C20-C13-C14	122.7	H _l -C9-C10	122.3
C20-C13-C12	121.2	H _e -C9-C10	121.7
H-C20-C13	112.5	H'-C20-C13	109.5
Torsion Angles (degrees)			
H-C20-C13-C14	0.0	H'-C20-C13-H	120.6

Table 14 Skewed 11-cis, 12-s-cis, 13-methyl retinal analog

Bond lengths (Å °)			
C15-O	1.2228	C15-H	1.1009
C14-C15	1.5049	C14-H	1.0823
C13-C14	1.3247	C20-H	1.0824
C13-C20		C20-H'	1.0873
C12-C13	1.5028	C20-H''	1.0878
C11-C12	1.3212	C12-H	1.0850
C10-C11	1.4872	C11-H	1.0846
C9-C10	1.3141	C10-H	1.0827
		C9-H _t	1.0814
		C9-H _c	1.0819
Bond Angles (degrees)			
H-C15-O	120.8	H-C12-C13	111.2
H-C15-C14	116.4	H-C12-C11	118.2
H-C14-C15	113.6	H-C11-C12	118.2
H-C14-C13	119.3	H-C11-C10	114.7
C20-C13-C14	125.1	H-C10-C11	116.7
C20-C13-C12	113.5	H-C10-C9	120.0
H-C20-C13	112.7	H _c -C9-C10	122.1
H'-C20-C13	109.7	H _t -C9-C10	122.0
H''-C20-C13	109.9		
Torsion Angles (degrees)			
C14-C15-H15-O	180.0	H10-C10-C11-H11	189.6
H14-C14-C15-H15	180.2	C9-C10-H10-C11	180.9
C13-C14-H14-C15	179.2	H9 _c -C9-C10-H10	180.0
C20-C13-C14-H14	182.5	H9 _t -C9-C10-H10	-0.2
H20-C20-C13-C14	1.8	H20'-C20-C13-H20	120.9
C12-C13-C20-C14	182.2	H12-C12-C13-C20	44.3
C11-C12-H12-C13	178.6	H11-C11-C12-H12	2.1
C10-C11-H11-C12	178.4		

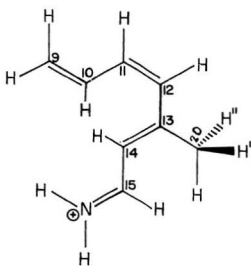


Table 15 Skewed 11-cis, 12-s-cis, 13-methyl retinal PSB analog

Bond lengths (Å)			
C15-N	1.3293	N-H _t	1.0247
C14-C15	1.4124	N-H _c	1.0252
C13-C14	1.3743	C15-H	1.0949
C13-C20	1.5287	C14-H	1.0773
C12-C13	1.4725	C20-H	1.0820
C11-C12	1.3372	C20-H'	1.0883
C10-C11	1.4801	C20-H''	1.0887
C9-C10	1.3190	C12-H	1.0820
		C11-H	1.0892
		C10-H	1.0802
		C9-H _t	1.0843
		C9-H _c	1.0847
Bond Angles (degrees)			
H _t -N-C15	121.5	H-C12-C13	113.7
H _c -N-H _t	117.1	H-C12-C11	117.7
H-C15-N	114.8	H-C11-C12	115.9
H-C15-C14	121.8	H-C11-C10	114.0
H-C14-C15	116.3	H-C10-C11	118.1
H-C14-C13	119.7	H-C10-C9	120.2
C20-C13-C14	124.1	H _c -C9-C10	122.2
C20-C13-C12	113.7	H _t -C9-C10	121.8
H-C20-C13	113.7	H'-C20-C13	108.6
H''-C20-C13	108.7		
Torsion Angles (degrees)			
C15-N-H _t -H _c	180.5	C10-C11-H11-C12	176.3
H15-C15-N-H _t	-0.3	H10-C10-C11-H11	193.5
C14-C15-H15-N	179.7	C9-C10-H10-C11	182.4
H14-C14-C15-H15	180.2	H9 _c -C9-C10-H10	179.1
C13-C14-H14-C15	177.6	H9 _t -C9-C10-H10	-1.3
C20-C13-C14-H14	185.9	H20-C20-C13-C14	-1.4
H20'-C20-C13-H20	121.6	C12-C13-C20-C14	183.1
H12-C12-C13-C20	24.9	C11-C12-H12-C13	177.3
H11-C11-C12-H12	3.6		

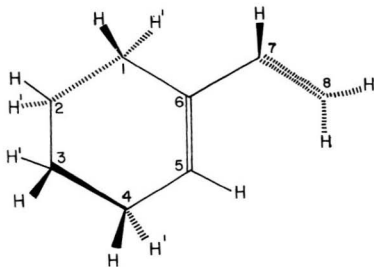


Table 16 Cyclohexene ring (conformation 2) with an ethylenic branch at C6
(*trans*-*cis* ring analog)

Bond lengths (Å)			
C1-C2	1.5424	C1-H	1.0906
C2-C3	1.5400	C1-H'	1.0888
C3-C4	1.5422	C2-H	1.0879
C4-C5	1.5235	C2-H'	1.0880
C5-C6	1.3175	C3-H	1.0880
C6-C7	1.5006	C3-H'	1.0878
C7-C8	1.3127	C4-H	1.0891
		C4-H'	1.0912
		C5-H	1.0827
		C7-H	1.0849
		C8-H _t	1.0810
		C8-H _c	1.0806
Bond Angles (degrees)			
C6-C1-C2	112.6	C5-C6-C1	122.0
H-C1-C6	109.3	C5-C6-C7	123.0
H-C1-C6	108.8	C6-C7-C8	126.5
H-C2-C1	109.7	H-C7-C6	114.6
H-C2-C1	109.5	H _c -C8-C7	122.8
H-C3-C4	109.9	H _c -C8-C7	121.5
H-C3-C4	109.5	C3-C4-C5	112.0
H-C4-C5	109.5	H-C4-C5	109.1
H-C5-C4	115.3	H-C5-C6	120.1
Torsion Angles (degrees)			
C1-C5-H5-C6	179.8	H2'-C2-C1-H1	163.8
H4-C4-C5-H5	-41.7	C7-C6-C5-C4	179.6
H4-C4-C5-H5	-74.6	H7-C7-C6-C5	199.4
C3-C4-C5-H5	164.0	C8-C7-C6-C5	20.3
H3'-C3-C4-H4	-71.0	H8 _c -C8-C7-H7	181.2
H3-C3-C4-H4	-47.0	H8 _c -C8-C7-H7	0.9
C1-C6-C5-H5	181.0	H1-C1-C6-C5	105.6
H1'-C1-C6-C5	-138.3	C2-C1-C6-C5	-16.1
H2-C2-C1-H1	-46.0		

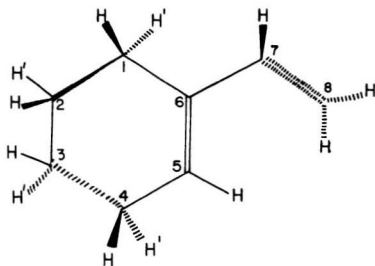


Table 17 Cyclohexene ring (conformation I) with an ethylenic branch at C6
(6-s-cis ring analog)

Bond lengths (Å)			
C1-C2	1.5425	C1-H	1.0887
C2-C3	1.5399	C1-H'	1.0906
C3-C4	1.5423	C2-H	1.0880
C4-C5	1.5234	C2-H'	1.0878
C5-C6	1.3176	C3-H	1.0877
C6-C7	1.5007	C3-H'	1.0880
C7-C8	1.3127	C4-H	1.0911
		C4-H'	1.0894
		C5-H	1.0828
		C7-H	1.0848
		C8-H _i	1.0811
		C8-H _e	1.0807
Bond Angles (degrees)			
C6-C1-C2	112.6	H-C5-C4	115.2
H-C1-C6	109.2	H-C5-C6	120.0
H'-C1-C6	109.0	C5-C6-C1	122.0
H-C2-C1	109.5	C5-C6-C7	122.8
H'-C2-C1	109.7	C6-C7-C8	126.2
H-C3-C4	109.9	H-C7-C6	114.8
H'-C3-C4	109.6	H _i -C8-C7	121.6
C3-C4-C5	112.1	H _e -C8-C7	122.7
H-C4-C5	109.1	H'-C4-C5	109.3
Torsion Angles (degrees)			
C4-C5-H5-C6	180.8	C7-C6-C5-C4	180.8
H4-C4-C5-H5	72.0	H7-C7-C6-C5	201.8
H1'-C4-C5-H5	-44.2	C8-C7-C6-C5	22.7
C3-C4-C5-H5	193.6	H8 _e -C8-C7-H7	181.3
H3'-C3-C4-H4	-162.9	H8 _i -C8-C7-H7	1.0
H3-C3-C4-H4	-41.9	C1-C6-C5-H5	181.4
H1-C1-C6-C5	137.5	H1'-C1-C6-C5	-106.4
C2-C1-C6-C5	15.4	H2-C2-C1-H1	-47.1
H2'-C2-C1-H1	70.7		

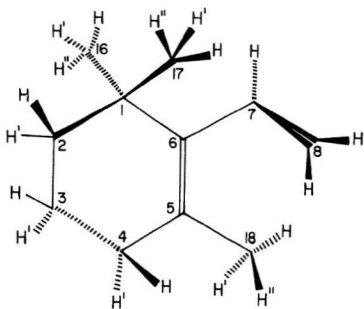


Table 18 β -ionylidene ring (conformation 1) with an ethylenic branch at C6
(6-s-cis ring analog)

Bond lengths (Å)			
C1-C2	1.5520	C17-H	1.0845
C1-C17	1.5520	C17-H'	1.0857
C1-C16	1.5547	C17-H''	1.0854
C2-C3	1.5355	C16-H	1.0856
C3-C4	1.5379	C16-H'	1.0846
C4-C5	1.5322	C16-H''	1.0846
C5-C6	1.3223	C2-H	1.0877
C6-C7	1.5084	C2-H'	1.0875
C7-C8	1.3109	C3-H	1.0877
C5-C18	1.5275	C3-H'	1.0866
		C4-H	1.0907
		C4-H'	1.0884
		C7-H	1.0854
		C8-H _t	1.0812
		C8-H _c	1.0809
		C18-H	1.0826
		C18-H'	1.0868
		C18-H''	1.0881
Bond Angles (degrees)			
C6-C1-C2	110.7	C3-C4-C5	113.4
C16-C1-C6	109.6	H-C4-C5	108.4
H-C16-C1	110.2	H'-C4-C5	109.1
H'-C16-C1	110.9	C4-C5-C18	112.6
H''-C16-C1	111.3	C6-C5-C18	124.1
C17-C1-C6	110.3	H-C18-C5	112.1
H-C17-C1	111.3	H'-C18-C5	109.9
H'-C17-C1	110.0	H''-C18-C5	110.5
H''-C17-C1	110.7	C5-C6-C7	122.6
H-C2-C1	109.0	C5-C6-C1	123.2
H'-C2-C1	109.2	C6-C7-C8	125.7
H-C3-C4	109.8	H-C7-C6	115.5
H'-C3-C4	109.8	H _t -C8-C7	121.8
		H _c -C8-C7	122.4
Torsion Angles (degrees)			
H18''-C18-C5-C6	227.7	H16-C16-C1-C6	183.8
H18'-C18-C5-C6	109.3	H16''-C16-C1-H16	119.6
H18-C18-C5-C6	-11.6	H16''-C16-C1-H16	-119.9
C4-C5-C18-C6	180.9	C17-C1-C6-C5	-104.2
H4-C4-C5-C18	73.7	H17'-C17-C1-C16	-60.9
H4'-C4-C5-C18	-41.9	H17-C17-C1-H17'	119.5
C3-C4-C5-C18	195.4	H17''-C17-C1-H17'	-120.2
H3-C3-C4-H4	-44.1	C2-C1-C6-C5	17.2
H3'-C3-C4-H4	-161.8	H2'-C2-C1-C16	70.7
C1-C6-C5-C18	178.5	H2-C2-C1-C16	-46.3
C16-C1-C6-C5	136.4	C7-C6-C5-C4	179.2

H8 _c -C8-C7-H7	178.6	H7-C7-C6-C5	123.9
H8 _f -C8-C7-H7	-1.1	C8-C7-C6-C5	-58.5

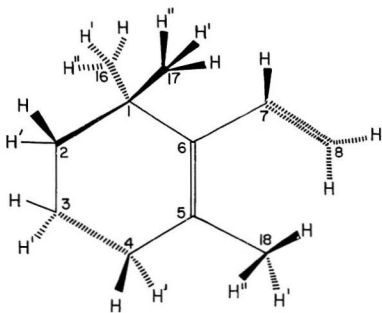


Table 19 β -ionylidene ring (conformation 1) with an ethylenic branch at C6
(*6-s-cis* ring analog)

Bond lengths (Å)			
C1-C2	1.5538	C17-H	1.0843
C1-C17	1.5535	C17-H'	1.0856
C1-C16	1.5540	C17-H''	1.0855
C2-C3	1.5359	C16-H	1.0856
C3-C4	1.5373	C16-H'	1.0850
C4-C5	1.5310	C16-H''	1.0847
C5-C6	1.3212	C2-H	1.0877
C6-C7	1.5107	C2-H'	1.0875
C7-C8	1.3105	C3-H	1.0878
C5-C18	1.5273	C3-H'	1.0868
		C4-H	1.0906
		C4-H'	1.0887
		C7-H	1.0851
		C8-H _c	1.0814
		C8-H _c	1.0812
		C18-H	1.0831
		C18-H'	1.0880
		C18-H''	1.0871
Bond Angles (degrees)			
C6-C1-C2	111.0	C3-C4-C5	112.8
C16-C1-C6	109.0	H-C4-C5	108.8
H-C16-C1	110.3	H'-C4-C5	109.0
H'-C16-C1	110.4	C4-C5-C18	112.7
H''-C16-C1	111.2	C6-C5-C18	123.9
C17-C1-C6	110.7	H-C18-C5	112.1
H-C17-C1	111.5	H'-C18-C5	110.6
H'-C17-C1	109.7	H''-C18-C5	109.9
H''-C17-C1	110.9	C5-C6-C7	123.5
H-C2-C1	109.0	C5-C6-C7	121.9
H'-C2-C1	109.1	C6-C7-C8	124.9
H-C3-C4	109.9	H-C7-C8	116.1
H'-C3-C4	109.8	H _c -C8-C7	121.9
		H _c -C8-C7	122.3
Torsion Angles (degrees)			
H18''-C18-C5-C6	132.5	C17-C1-C6-C5	-108.6
H18-C18-C5-C6	11.8	H17-C17-C1-C16	-57.8
H18'-C18-C5-C6	-109.2	H17'-C17-C1-H17	119.7
C4-C5-C18-C6	181.0	H17''-C17-C1-H17	-120.3
H4-C4-C5-C18	74.3	C2-C1-C6-C5	12.8
H4'-C4-C5-C18	-41.5	H2'-C2-C1-C16	72.7
C3-C4-C5-C18	196.0	H2-C2-C1-C16	-41.3
H3-C3-C4-H4	-46.0	C7-C6-C5-C4	181.6
H3'-C3-C4-H4	-164.0	H7-C7-C6-C5	243.5
C1-C6-C5-C18	181.4	C8-C7-C6-C5	65.0
C16-C1-C6-C5	132.3	H8-C8-C7-H7	180.7

H16 ^L -C16-C1-C6	186.4	H8 _t -C8-C7-H7	0.7
H16 ^H -C16-C1-H16 ^L	119.5	H16-C16-C1-H16 ^L	-119.5

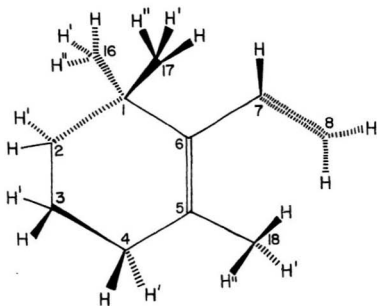


Table 20 β -ionylidene ring (conformation 2) with an ethylenic branch at C6
(6-s-cis ring analog)

Bond lengths (Å)			
C1-C2	1.5530	C17-H	1.0856
C1-C17	1.5547	C17-H'	1.0846
C1-C16	1.5529	C17-H''	1.0846
C2-C3	1.5358	C16-H	1.0857
C3-C4	1.5380	C16-H'	1.0854
C4-C5	1.5320	C16-H''	1.0846
C5-C6	1.3220	C2-H	1.0875
C6-C7	1.5090	C2-H'	1.0877
C7-C8	1.3108	C3-H	1.0866
C5-C18	1.5274	C3-H'	1.0877
		C4-H	1.0884
		C4-H'	1.0907
		C7-H	1.0855
		C8-H _t	1.0813
		C8-H _c	1.0810
		C18-H	1.0826
		C18-H'	1.0881
		C18-H''	1.0869
Bond Angles (degrees)			
C6-C1-C2	110.7	C3-C4-C5	113.4
C16-C1-C6	110.2	H-C4-C5	109.1
H-C16-C1	110.0	H'-C4-C5	108.4
H'-C16-C1	110.7	C4-C5-C18	112.6
H''-C16-C1	111.3	C6-C5-C18	124.1
C17-C1-C6	109.6	H-C18-C5	112.1
H-C17-C1	110.2	H'-C18-C5	110.5
H'-C17-C1	110.8	H''-C18-C5	109.9
H''-C17-C1	111.3	C5-C6-C1	123.2
H-C2-C1	109.2	C5-C6-C7	122.5
H'-C2-C1	109.0	C6-C7-C8	125.6
H-C3-C4	109.8	H-C7-C6	115.5
H'-C3-C4	109.8	H _t -C8-C7	121.8
		H _c -C8-C7	122.4
Torsion Angles (degrees)			
H18''-C18-C5-C6	130.6	C17-C1-C6-C5	-136.8
H18-C18-C5-C6	9.8	H17-C17-C1-C16	-63.9
H18'-C18-C5-C6	-111.1	H17''-C17-C1-H17	119.8
C4-C5-C18-C6	179.2	H17'-C17-C1-H17	-119.6
H4-C4-C5-C18	42.1	C2-C1-C6-C5	-17.5
H4'-C4-C5-C18	-73.5	H2-C2-C1-C16	47.7
C3-C4-C5-C18	164.7	H2'-C2-C1-C16	164.7
H3'-C3-C4-H4	-72.8	C7-C6-C5-C4	180.7
H3-C3-C4-H4	45.0	H7-C7-C6-C5	238.2
C1-C6-C5-C18	181.6	C8-C7-C6-C5	60.6
C16-C1-C6-C5	103.9	H8 _c -C8-C7-H7	181.4

H16-C16-C1-C6	181.6	H8 _c -C8-C7-H7	1.3
H16 ^u -C16-C1-H16	120.2	H16 ^l -C16-C1-H16	-119.5

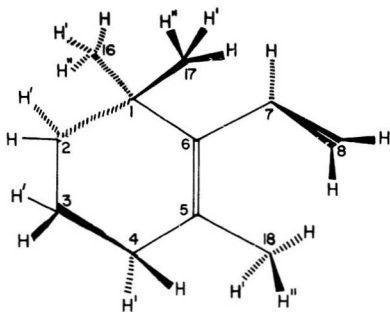


Table 21 β -ionylidene ring (conformation 2) with an ethylenic branch at C6
(6-s-cis ring analog)

Bond lengths (Å)			
C1-C2	1.5535	C17-H	1.0856
C1-C17	1.5540	C17-H'	1.0851
C1-C16	1.5535	C17-H''	1.0847
C2-C3	1.5360	C16-H	1.0853
C3-C4	1.5375	C16-H'	1.0855
C4-C5	1.5310	C16-H''	1.0843
C5-C6	1.3213	C2-H	1.0875
C6-C7	1.5105	C2-H'	1.0877
C7-C8	1.3106	C3-H	1.0867
C5-C18	1.5274	C3-H'	1.0878
		C4-H	1.0888
		C4-H'	1.0905
		C7-H	1.0850
		C8-H _l	1.0814
		C8-H _c	1.0812
		C18-H	1.0831
		C18-H'	1.0871
		C18-H''	1.0880
Bond Angles (degrees)			
C6-C1-C2	111.0	C3-C4-C5	112.9
C16-C1-C6	110.8	H-C4-C5	108.9
H-C16-C1	109.7	H'-C4-C5	108.8
H'-C16-C1	110.9	C4-C5-C18	112.7
H''-C16-C1	111.5	H-C18-C5	112.1
C17-C1-C6	109.0	H'-C18-C5	109.8
H-C17-C1	110.3	H''-C18-C5	110.6
H'-C17-C1	110.4	C18-C5-C6	123.9
H''-C17-C1	111.2	C5-C6-C1	123.4
H-C2-C1	109.1	C5-C6-C7	121.9
H'-C2-C1	109.0	C6-C7-C8	124.9
H-C3-C4	109.8	H-C7-C6	116.1
H'-C3-C4	109.9	H _l -C8-C7	121.9
		H _c -C8-C7	122.3
Torsion Angles (degrees)			
H18'-C18-C5-C6	226.8	C17-C1-C6-C5	-132.9
H18''-C18-C5-C6	108.5	H17-C17-C1-C16	-67.0
H18-C18-C5-C6	-12.5	H17'-C17-C1-H17	119.5
C4-C5-C18-C6	178.9	H17-C17-C1-H17	-119.5
H4-C4-C5-C18	42.2	C2-C1-C6-C5	-13.4
H4'-C4-C5-C18	-73.6	H2-C2-C1-C16	45.8
C3-C4-C5-C18	164.6	H2'-C2-C1-C16	162.7
H3'-C3-C4-H4	-71.4	C7-C6-C5-C4	178.3
H3-C3-C4-H4	46.5	H7-C7-C6-C5	117.4
C1-C6-C5-C18	178.5	C8-C7-C6-C5	-64.0
C16-C1-C6-C5	108.0	H8 _c -C8-C7-H7	179.3

H16-C16-C1-C6	178.6	H8-C8-C7-H7	-0.7
H16 ^u -C16-C1-H16	120.3	H16 ^l -C16-C1-H16	-119.7

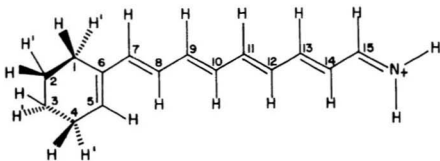


Table 22 All-trans (6-s-cis) retinal PSB analog

Bond lengths (Å °)			
C15-N	1.3491	N-H ₁	1.0218
C14-C15	1.3908	N-H _c	1.0225
C13-C14	1.3867	C15-H	1.0952
C12-C13	1.4138	C14-H	1.0791
C11-C12	1.3662	C13-H	1.0921
C10-C11	1.4390	C12-H	1.0802
C9-C10	1.3475	C11-H	1.0909
C8-C9	1.4597	C10-H	1.0800
C7-C8	1.3345	C9-H	1.0802
C6-C7	1.4879	C8-H	1.0804
C5-C6	1.3234	C7-H	1.0878
C4-C5	1.5221	C5-H	1.0842
C3-C4	1.5116	C4-H	1.0912
C2-C3	1.5395	C4-H'	1.0893
C1-C2	1.5117	C3-H	1.0874
C6-C1	1.5325	C3-H'	1.0879
		C2-H	1.0880
		C2-H'	1.0875
		C1-H	1.0887
		C1-H'	1.0907
Bond Angles (degrees)			
C6-C1-C2	112.3	C6-C7-C8	127.6
H-C1-C6	109.3	H-C8-C7	121.8
H'-C1-C6	109.0	H-C8-C9	116.4
H-C2-C1	109.5	H-C9-C8	116.4
H'-C2-C1	109.5	H-C9-C10	118.9
H-C3-C4	109.6	H-C10-C9	120.5
H'-C3-C4	109.6	H-C10-C11	117.7
C3-C4-C5	112.3	H-C11-C10	116.7
H-C4-C5	108.5	H-C11-C12	118.4
H'-C4-C5	109.0	H-C12-C11	120.2
H-C5-C4	115.2	H-C12-C13	118.5
H-C5-C6	120.3	H-C13-C12	117.2
C5-C6-C1	122.1	H-C13-C14	117.8
C5-C6-C7	122.6	H-C14-C13	120.4
H-C7-C6	114.7	H-C14-C15	119.3
H-C15-C14	120.1	H-C15-N	115.0
H _c -N-C15	121.2	H ₁ -N-C15	121.4
Torsion Angles (degrees)			
C4-C5-H5-C6	181.0	C2-C1-C6-C5	16.7
H4-C4-C5-H5	71.7	H2-C2-C1-H1	-47.7
H4'-C4-C5-H5	-44.2	H2'-C2-C1-H1	70.0
C3-C4-C5-C6	14.4	C7-C6-C5-C4	180.3
H3-C3-C4-H4	-41.7	H7-C7-C6-C5	183.9
H3'-C3-C4-H4	-162.5	C8-C7-C6-C5	4.1
C1-C6-C5-H5	180.8	H8-C8-C7-H7	180.4
H1-C1-C6-C5	138.7	H1'-C1-C6-C5	-105.0

The C9 to N part of the chain is kept planar.

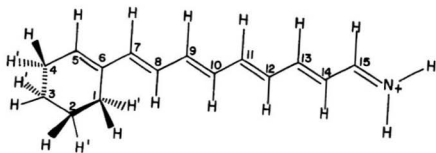


Table 23 All-trans (6-s-trans) retinal PSB analog

Bond lengths (Å °)			
C15-N	1.3107	N-H _t	1.0217
C14-C15	1.3898	N-H _e	1.0223
C13-C14	1.3878	C15-H	1.0951
C12-C13	1.4126	C14-H	1.0791
C11-C12	1.3673	C13-H	1.0921
C10-C11	1.4379	C12-H	1.0802
C9-C10	1.3484	C11-H	1.0900
C8-C9	1.4587	C10-H	1.0809
C7-C8	1.3347	C9-H	1.0893
C6-C7	1.4834	C8-H	1.0801
C5-C6	1.3247	C7-H	1.0877
C4-C5	1.5214	C5-H	1.0856
C3-C4	1.5417	C4-H	1.0912
C2-C3	1.5396	C4-H'	1.0892
C1-C2	1.5430	C3-H	1.0874
C6-C1	1.5300	C3-H'	1.0880
		C2-H	1.0880
		C2-H'	1.0876
		C1-H	1.0881
		C1-H'	1.0904
Bond Angles (degrees)			
C6-C1-C2	112.1	C6-C7-C8	126.5
H-C1-C6	109.6	H-C8-C7	121.5
H'-C1-C6	109.2	H-C8-C9	116.6
H-C2-C1	109.4	H-C9-C8	116.5
H'-C2-C1	109.4	H-C9-C10	118.8
H-C3-C4	109.7	H-C10-C9	120.5
H'-C3-C4	109.6	H-C10-C11	117.7
C3-C4-C5	111.9	H-C11-C10	116.8
H-C4-C5	108.6	H-C11-C12	118.4
H'-C4-C5	109.1	H-C12-C11	120.1
H-C5-C4	115.7	H-C12-C13	118.6
H-C5-C6	119.6	H-C13-C12	117.2
C5-C6-C1	122.3	H-C13-C14	117.8
C5-C6-C7	118.9	H-C14-C13	120.3
H-C7-C6	115.1	H-C14-C15	119.3
H-C15-C14	120.2	H-C15-N	115.0
H _e -N-C15	121.2	H _t -N-C15	121.4
Torsion Angles (degrees)			
C4-C5-H5-C6	180.3	C2-C1-C6-C5	15.6
H4-C4-C5-H5	72.9	H2-C2-C1-H1	-16.7
H4'-C4-C5-H5	-43.0	H2'-C2-C1-H1	70.9
C3-C4-C5-C6	14.9	C7-C6-C5-C4	181.4
H3-C3-C4-H4	-45.2	H7-C7-C6-C5	-3.8
H3'-C3-C4-H4	-163.1	C8-C7-C6-C5	175.6
C1-C6-C5-H5	180.4	H8-C8-C7-H7	179.8
H1-C1-C6-C5	137.1	H1'-C1-C6-C5	-106.1

The C9 to N part of the chain is kept planar.

Figure 1

Variation in the SCF optimized C-C bond lengths for retinal, retinal SB (a) and retinal PSB (b) analogs. The numbering of carbon atoms is as defined in the text. The different analogs are identified with different (dashed, dotted etc.) horizontal lines, for each bond; the vertical lines are just visual guidelines. Thick horizontal solid lines indicate coincidence.

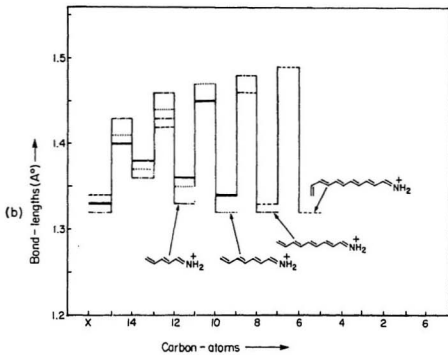
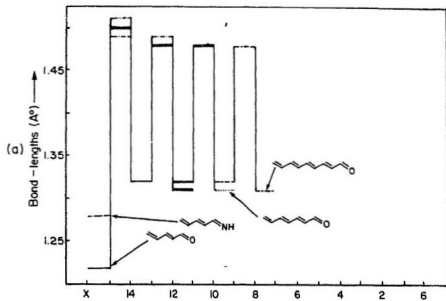


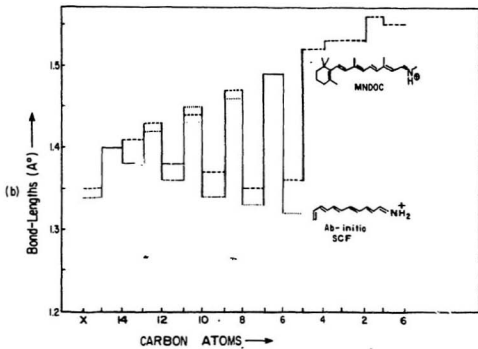
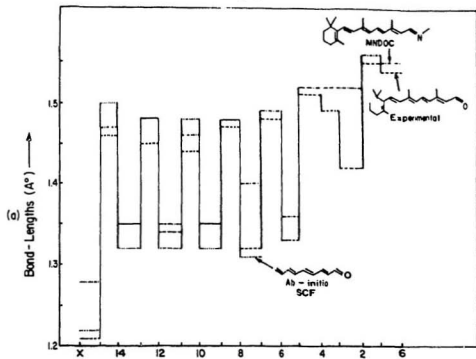
Figure 2

Variation in the SCF optimized C-C bond orders for retinal, retinal SB (a) and retinal PSB (b) analogs. For other notations, see fig. 1.



Figure 3

Variation in the SCF and MNDOC (from ref. 138) optimized C-C bond lengths for different analogs of retinal, retinal SB (a) and retinal PSB (b). Experimental bond lengths (from ref. 69) for retinal are also shown. For other notations, see fig. 1.



chain length. In turn, the same quantities in case of retinal PSB show a slower convergence, that is, slightly more variation in r_{ab} and B_{ab} . As a consequence, the smallest analogs (up to three double bonds) do not give a good estimation of the corresponding properties of the larger retinal PSB analogs.

It is also evident from figs. 1 and 2 that r_{ab} and B_{ab} values for the retinal SB analogs are very similar to those for the retinal analogs, while the corresponding quantities for retinal PSB are rather different. In the case of the former two, the single and double bonds are easily identified indicating a limited conjugation along the whole chain. In other terms, the C-C bond lengths of the retinal and retinal SB show a strong regular alternation. On the other hand, the retinal PSB analogs show an increased conjugation around the NH_2^+ group manifested in a decreased alternation of bond lengths and bond orders. The conjugation subsequently dies off on moving towards the cyclohexene ring end of the molecule. Experimental results⁵³ show an increase in the frequency of the C14-C15 stretch on protonation of the Schiff base, which is in agreement with the above results. The bond order of the C11-C12 double bond is reduced considerably on protonation of the Schiff base thereby facilitating the rotation of the C11-C12 double bond or in other words facilitates the cis-trans isomerization. (c.f. fig. 2)

In fig. 3 the optimized geometries for the retinal and the retinal PSB analogs are compared with the experimental and the theoretical data available from semiempirical calculations. The bond lengths for the retinal analog are very close to the experimental geometry for retinal obtained by X-ray crystallography⁶⁹. The MNDOC results¹³⁸ for the retinal SB predict a very long bond length for the C7-C8 double bond and therefore predict the dihedral angle between the plane of the ring and the chain to be 83° which is larger than the experimentally observed angle of 62° ⁶⁹. Also, MNDOC does not assign enough torsional stability to the C6-C7 π single bond to compete with the steric interaction between the methyl groups at C1 and C5 and

the hydrogens at C7 and C8. The present ab initio results for the retinal PSB analog are in general agreement with the MNDOC results (c.f. fig. 3), though the latter seems to overestimate most of the bond lengths.

3.2.3 Relative stabilities of various isomers of planar chain analogs

The relative stabilities of various isomers of planar chain analogs are given in table 24. In each case the planar trans isomer is predicted to be the most stable. For retinal analogs the 11-cis isomer is more stable than the 13-cis isomer. Due to the absence of methyl groups on these analogs the trend observed does not agree with the trend reported by Dhingra and Saran⁹⁸ for retinal. It is to be noted that the retinal PSB analogs show a different trend as compared to the retinal analogs. For the retinal PSB analogs the 11-cis isomer is predicted to be less stable as compared to the 13-cis isomer. This is due to the increased conjugation in the vicinity of the NH_2^+ group in retinal PSB analogs.

3.2.4 Ring analogs and full retinal PSB geometry

The cyclohexene ring end of the molecule is studied with an ethylenic branch (C7-C8) at C6. Two practically degenerate conformations of the cyclohexene ring are optimized (tables 16 and 17) excluding the methyl groups at C1 and C5. The lowest energy conformation is used to construct the full retinal PSB (tables 22 and 23) by combining it with the optimized geometry for the largest chain analog. To start with the geometrical parameters common to both units are averaged. Then, all the geometrical parameters are relaxed, except the C9 to NH_2^+ part of the molecule which is kept planar. Since the C9 to NH_2^+ part of the molecule is conjugated, no significant torsional distortions are expected. (The gradients for the fixed angles are all well within the convergence criteria.)

Fig. 4 illustrates the C-C bond length alternation for the 6-7-s-cis retinal PSB structure along with those of the two building blocks. The differences in the corresponding bond lengths are essentially negligible. The cyclohexene ring simply

Table 24 Total energies (a.u.) of various isomers of planar chain analogs. Relative energies (kJ mol^{-1}) with respect to the absolute minimum for that analog are given in brackets.


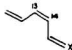

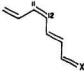
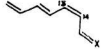
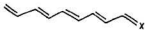
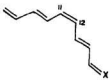
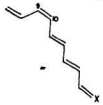
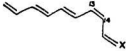
Planar analog	X=O	X=NH	X=NH ₂ ⁺
	-264.251123 (0.00)	-244.719182 (0.00)	-245.173513 (0.00)
	-264.247430 (9.70)	-244.716072 (8.17)	-245.169841 (9.64)
	-340.199000 (0.00)		-321.129012 (0.00)
	-340.198066 (7.70)		-321.125333 (9.66)
	-340.195341 (9.61)		-321.125464 (9.32)
	-416.146919 (0.00)		-397.081293 (0.00)
	-416.144007 (7.65)		-397.077640 (9.59)
	-416.144024 (7.60)		-397.077812 (9.14)
	-416.143277 (9.56)		-397.077852 (9.03)

Figure 4

Variation in the SCF optimized C-C bond lengths for the 6-*s-cis* retinal PSB analog along with the C-C bond lengths for the two building blocks. For other notations, see fig. 1.

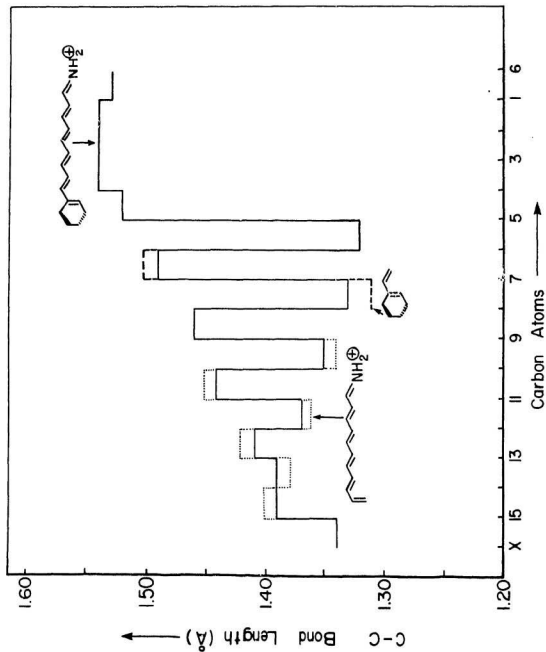
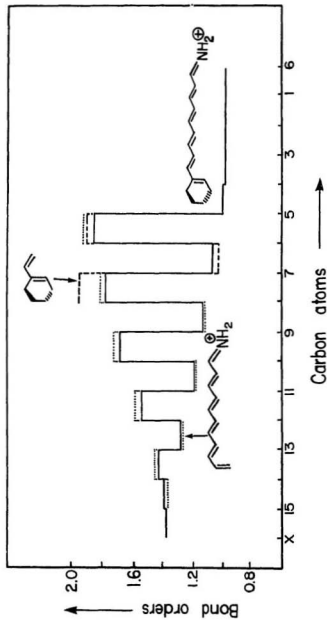


Figure 5

Variation in the SCF optimized C-C bond orders for the 6-s-cis retinal PSB analog along with the C-C bond orders for the two building blocks. For other notations, see fig. 1.



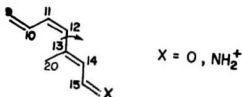
causes local torsional distortions in the full retinal PSB. (c.f. table 22) The torsional angle (C8-C7-C6-C5) between the plane of the ring and the chain is predicted to be only 4° . For retinal in the solid state a value of 60° is observed⁶⁹ whereas MNDOC calculations¹³⁸ predict a torsional angle of 83° . The larger values obtained from experiment and MNDOC calculations are partly due to the steric interaction of the methyl groups at C1 and C5 with the hydrogens at C7 and C8. The conformation of the cyclohexene ring is characterized by the C2-C1-C6-C5 (and C3-C4-C5-C6) torsion angle. The C2-C1-C6-C5 torsion angle measures 19° for the retinal in the solid state⁶⁹ and is predicted to be 21° by the MNDOC calculations¹³⁸. The ab initio results (c.f. tables 22 and 23) predict the torsion angle to be 17° in the 6-7-s-cis retinal PSB and 16° in the 6-7-s-trans retinal PSB in good agreement with the experiment. Fig. 4 again shows the strong conjugational effect in the vicinity of the NH_2^+ group which dies off near C9, as observed in the case of smaller analogs. (c.f. fig. 1) The same trend is reproduced in the bond orders. (fig. 5) The MNDOC results¹³⁸ are in good overall agreement with the ab initio results except for the C5-C6 double bond which is predicted to be longer (1.36 \AA as compared to 1.32 \AA). The 6-7-s-cis retinal PSB and the 6-7-s-trans retinal PSB show the same conjugation effect and bond length alternation. (tables 22 and 23)

3.2.5 Effect of methyl substituents on the geometry and conformation of the analogs

The geometry of the largest chain analog with the methyl substituent at C5 is shown in table 11. The introduction of the methyl group at C5 slightly reduces the effect of conjugation throughout the chain. All the C-C single bonds become slightly longer and the C=C double bonds slightly shorter. (c.f. tables 10 and 11) This effect is probably a result of electron donating properties of the methyl group to the π system.

To study the effect of a methyl group at C13 the chain analog corresponding to

four C-C double bonds is selected. The optimized geometries are given in tables 12-15. In all the cases the 11-cis isomer is studied to mimic the 11-cis retinal chromophore in rhodopsin. The cyclohexene ring end of the molecule is eliminated as it is not expected to have any significant effect on this part of the molecule.



Tables 12 and 13 illustrate the optimized geometries for 11-cis, 12-s-trans (trans orientation around the C12-C13 single bond) retinal and retinal PSB analogs with the C_s symmetry constraint. On comparing the geometries with their corresponding demethyl analogs (c.f. table 4) we find that the introduction of the methyl group increases the C12-C13 bond length by $\sim 0.02 \text{ \AA}$ and the C13-C14 bond length by $\sim 0.04 \text{ \AA}$. Also, the corresponding bond angles are increased. This is due to the steric interaction introduced between the hydrogens on the methyl group attached to C13 and the hydrogen at C10. To alleviate this strain it has been suggested that the 11-cis retinal chromophore in rhodopsin is distorted around C10-C11 or C11-C12 or C12-C13 bonds¹³⁹. The rotation around C11-C12 is hard to accomplish because of the large potential barrier associated with a double bond. Therefore, it is more likely to be distorted around C10-C11 or C12-C13 single bonds. Dhingra and Saran⁹⁸ however suggest that the rotation around C10-C11 will not relieve the strain.

The optimized geometries for the distorted 11-cis, 12-s-cis retinal analog and retinal PSB analog are shown in tables 14 and 15 respectively. In retinal analog the torsion around C12-C13 single bond is predicted to be 44.3° and the torsion around C10-C11 single bond is predicted to be 9.6° (table 14). The X-ray diffraction data

for 11-cis retinal⁷⁰ predicts the torsion around C12-C13 single bond to be 38.7° . The present ab initio results on the retinal analog are in good agreement with the X-ray diffraction data for 11-cis retinal. On the other hand the X-ray data does not predict any significant distortion around the C10-C11 single bond but predicts a slight distortion around the C14-C15 single bond. The present ab initio results are also in good agreement with the proton NMR results on 11-cis retinal¹⁴⁰ that indicate a skewed geometry around the C12-C13 single bond. The results for the retinal PSB analog (table 15) indicate a distortion of 24.9° around the C12-C13 single bond and an increased distortion around the C10-C11 single bond of 13.5° . The calculations also predict small distortions around the C13-C14 (5.9°) and C11-C12 (3.6°) double bonds due to the reduced bond orders in retinal PSB. Therefore, the retinal PSB analog is significantly more distorted than the retinal analog.

The potential energy surfaces for 11-cis retinal and retinal PSB analogs resulting from rigid rotations around 12-s-bond are given in fig. 6. Fig. 7 shows the potential energy surfaces after full geometry optimizations have been performed. The results are compared with previous theoretical investigations^{98,96,141}. In all the previous theoretical investigations only 11-cis retinal was studied and rigid rotations were performed. Geometry relaxation was not taken into account. The aim of this study is to see whether 11-cis retinal PSB follows the same trend as 11-cis retinal although their conjugational properties are significantly different.

Rigid rotations around the 12-s-bond predict the 11-cis, 12-s-trans structure to be more stable than the 11-cis, skewed 12-s-cis structure in both the cases: retinal and retinal PSB. (c.f. fig. 6) However, the barrier to 12-s-trans/cis interconversion is predicted to be much higher (47.2 kJ mol^{-1} as compared to 15.9 kJ mol^{-1}) for the retinal PSB analog as compared to the retinal analog. This is due to the increased conjugational effect in retinal PSB analog that increases the bond order of 12-s-bond. The 11-cis, 12-s-cis structure as expected is predicted to be an energy maximum due

Figure 6

The relative energy (kJ mol^{-1}) as a function of rigid rotation about the C12-C13 single bond. The torsion angle of 0° represents the 11-cis, 12-s-cis conformation.

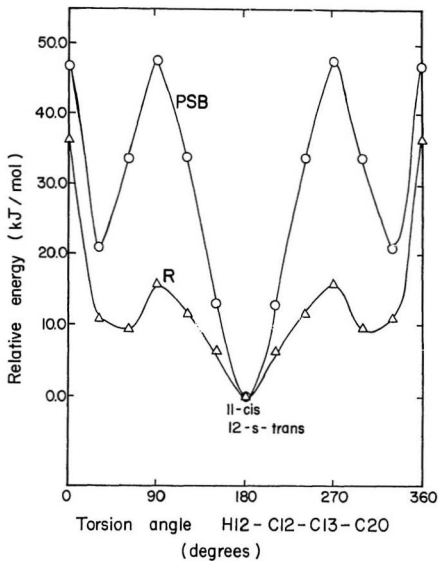
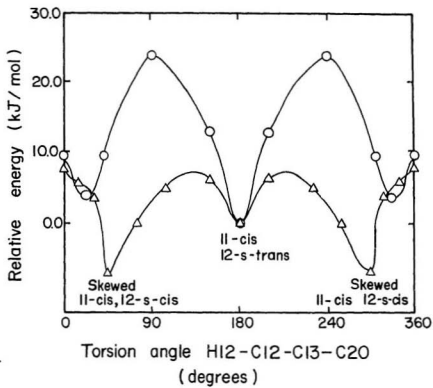


Figure 7

The relative energy (kJ mol^{-1}) as a function of rotation about the C12-C13 single bond. Geometries for all the skewed 11-cis, 12-s-cis; 11-cis, 12-s-trans and planar 11-cis, 12-s-cis conformations have been fully optimized. Rigid rotations have been performed from the nearest optimized point. The torsion angle of 0° represents the planar 11-cis, 12-s-cis conformation.



to steric interaction between the methyl hydrogens at C20 and the hydrogen at C10.

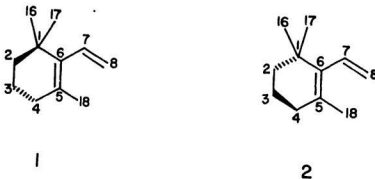
The potential energy surfaces obtained after geometry relaxation (fig. 7) show overall the same features as the results of rigid rotation (fig. 6) but the relative stabilities of the two conformers are changed. For the retinal analog the 11-cis, skewed 12-s-cis structure is now predicted to be 7.0 kJ mol^{-1} lower in energy than the planar 11-cis, 12-s-trans structure and the barrier to 12-s-cis/trans interconversion is predicted to be $-15.3 \text{ kJ mol}^{-1}$. The barrier for the conversion of one skewed 12-s-cis retinal analog to the other through the planar 11-cis, 12-s-cis transition state is also predicted to be of the same magnitude. The present ab initio results for this retinal analog are in overall agreement with the previous theoretical investigations^{96-98,141}. In all the cases skewed 12-s-cis structure was predicted to be lower in energy than the 12-s-trans structure. However, the earlier studies had reported the presence of skewed 12-s-trans structure^{96,97,141} whereas the present results indicate the presence of a planar 12-s-trans structure. The results obtained by Dhingra and Saran⁹⁸ using the PCIO method also support the existence of a planar 12-s-trans structure. The energy difference between the skewed 12-s-cis and 12-s-trans structures being very small (in the range of $4.2\text{-}17.5 \text{ kJ mol}^{-1}$) it has been suggested that 11-cis retinal exists as an equilibrium mixture of the two 12-s-cis/trans structures in solution. The crystal structure being the skewed 12-s-cis. ^1H NMR studies on 11-cis retinal in acetone at low temperature suggest that a distorted 12-s-trans conformation is preferred⁹⁷. The solvent effect could shift the equilibrium towards one conformation or the other as the energy difference between the two is very small.

For the retinal PSB analog the planar 11-cis, 12-s-trans structure is predicted to be 4.2 kJ mol^{-1} more stable than the skewed 11-cis, 12-s-cis structure and the barrier for 12-s-cis/trans interconversion is predicted to be $-23.8 \text{ kJ mol}^{-1}$. The barrier for interconversion from one skewed 12-s-cis to the other through the planar 11-cis, 12-s-cis transition state is predicted to be 5.4 kJ mol^{-1} . These results indicate that for

retinal PSB the preferred conformation is planar 11-cis, 12-s-trans as compared to 11-cis, skewed 12-s-cis in retinal. This is due to the strong conjugational effects in retinal PSB. However, since the energy difference between the two conformations in retinal PSB is small, the possibility of existence as an equilibrium mixture of the two in solution cannot be ruled out. The solvent effect could shift the equilibrium towards one or the other.

3.2.6 Effect of methyl substituents on the conformation of the cyclohexene ring

After studying the effect of methyl groups on the conformation of the chain part of the molecule, let us now consider the effect of the methyl groups on the cyclohexene ring end of the molecule, mainly their effect on the ring puckering and the torsional angle (C8-C7-C6-C5) between the plane of the ring and the chain. The chain part of the molecule is not expected to have any significant effect on the conformation of this part of the molecule as the effect of conjugation dies off near C10. Therefore only the β -ionylidene ring with an ethylenic branch at C6 is studied and both the possibilities for ring puckering (conformation 1 and 2) have been considered.



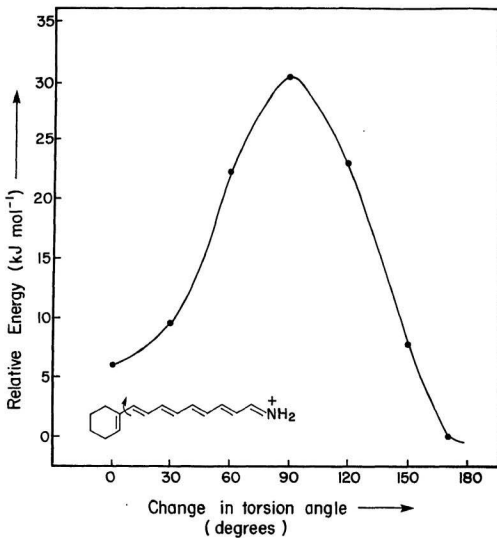
The optimized geometries for β -ionylidene ring with an ethylenic branch

($C7=C8$) at C6 are shown in tables 18-21. Two skewed 6-s-cis conformations have been obtained for each of the ring conformations. For both ring conformations the planar 6-s-trans structure has been predicted to be the transition state. The two skewed-6-s-cis structures correspond to 6-s-cis above the plane and 6-s-cis below the plane, the plane being defined by C1-C6-C5-C4. It has to be noted that a planar 6-s-trans structure is obtained when the methyl groups on C1 and C18 are replaced by hydrogen atoms (c.f. table 23 and fig. 8). In table 17 the optimized geometry for the cyclohexene ring (conformation 1) with an ethylenic branch at C6 is given. The torsion angle C8-C7-C6-C5 is observed to be 22.7° . Table 18 gives the optimized geometry for β -ionylidene ring (conformation 1) with an ethylenic branch at C6 (6-s-cis above the plane). On comparing the geometry for the β -ionylidene ring with the corresponding cyclohexene ring conformation (c.f. table 17) the major change observed is in the torsion angle C8-C7-C6-C5 which changes from 22.7° to -58.5° due to the steric hindrance introduced by the methyl groups. Table 19 gives the optimized geometry for β -ionylidene ring (conformation 1), 6-s-cis below the plane. Similar to the 6-s-cis above the plane (c.f. table 18) the C8-C7-C6-C5 torsion angle is now observed to be 65.0° .

Now we consider the effect of the methyl groups on conformation 2 for the cyclohexene ring. Table 16 gives the geometry for the cyclohexene ring in conformation 2 without any methyl groups. The torsion angle C8-C7-C6-C5 is noted to be 20.3° . Table 20 gives the optimized geometry for the β -ionylidene ring (conformation 2) with an ethylenic branch at C6 in the conformation 6-s-cis below the plane. It is noted that in general the geometries are the same (bond lengths and bond angles are similar; c.f. table 16 and 20). The most significant effect of the addition of methyl groups is on the torsion angle C8-C7-C6-C5 which changes from 20.3° to 60.6° for the 6-s-cis below the plane. Table 21 gives the optimized geometry for the β -ionylidene ring (conformation 2) with an ethylenic branch at C6 in the conforma-

Figure 8

The relative energy (kJ mol^{-1}) as a function of rotation about the C6-C7 single bond. The torsion angle of 0° represents the 6-s-cis retinal PSB.



tion 6-s-cis above the plane. Similar to the 6-s-cis below the plane the C8-C7-C6-C5 torsion angle is now observed to be -64.0° .

Comparing these results to the X-ray crystallographic data reported so far in the literature for retinal and related compounds

6-s-cis conformers	C8-C7-C6-C5	Reference
Vitamin-A acid (triclinic)*	35° or 42°	74
11-cis retinal	41.4°	70
Vitamin-A acetate	58°	76
All-trans retinal	62°	69
13-cis retinal	65.4°	72
Present results (ring analog)	58.5°	
6-s-trans conformers		
Vitamin-A acid (monoclinic)	6°	74
13-cis retinal	174.9°	72

Therefore, the only case where planar 6-s-trans structure has been reported is in monoclinic vitamin-A acid or in 13-cis retinal where simultaneous occurrence of both 6-s-cis/trans structures has been observed in a single unit cell. Once again not to forget that there is no X-ray data reported for the iminium salts of retinal.

The potential energy surface as a result of rigid rotations around the 6-s-bond is given in fig. 9 and after full geometry optimizations is shown in fig. 10. The results are compared with the previous quantum mechanical calculations. Langlet et al⁹⁵ applied the PCIO method to study the rotation around 6-s-bond in the aldehyde of crotonic acid which was chosen as an analog for retinal and reported 6-s-trans to be $10.5\text{--}11.7 \text{ kJ mol}^{-1}$ less stable than the 6-s-cis structure. A barrier of 33.4 kJ mol^{-1}

* The most common modification of vitamin A acid is a monoclinic one. This is a metastable form which transforms irreversibly into the triclinic one at about 80° C .

Figure 9

The relative energy (kJ mol^{-1}) as a function of rigid rotation about the C6-C7 single bond. The torsion angle of 0° represents the planar 6-s-cis conformation. The energies are relative to β -ionylidene ring (conformation 2) with an ethylenic branch at C'6 in the 6-s-cis conformation (6-s-cis above the plane).

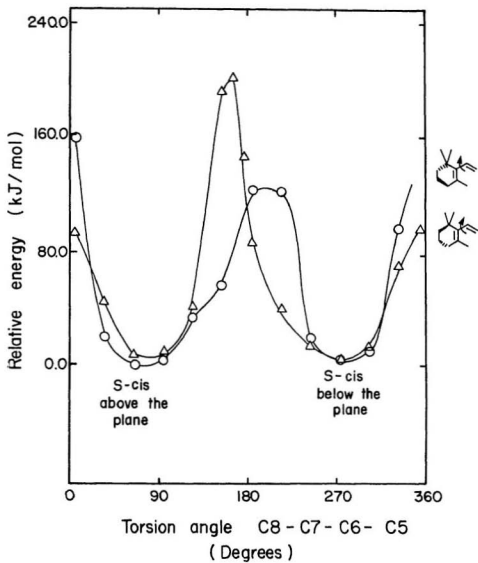
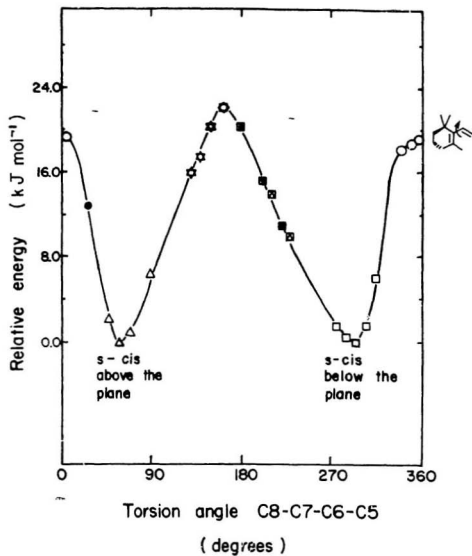


Figure 10

The relative energy (kJ mol^{-1}) as a function of rotation about the C6-C7 single bond. The torsion angle of 0° represents the planar 6-s-cis conformation. The points where full geometry optimization has been carried out are shown in bold (except for the torsion angle under consideration for the points other than the two minima). Rigid rotations have been done from the nearest optimized point and are denoted by the same symbol. At the maximum there are two overlapping points at 160° and 165° .



was calculated for 6-s-cis/trans interconversion. Other theoretical investigations^{96,98,142} also suggest that a skewed-s-cis conformation is the most stable in retinal. In all the previous theoretical investigations the geometry was adopted from the X-ray data on retinal and rigid rotations were performed around 6-s-bond. In the studies by Langlet et al⁹⁵ and Pullman et al¹⁴² the methyl groups were relaxed when necessary keeping the rest of the geometry fixed. Honig et al⁹⁶ included the relaxation of bond lengths and bond angles in their study.

In the present study the results of rigid rotations as well as full geometry optimizations are presented¹⁴³. In both the cases the potential energy surface reflect the same features (c.f. figs. 9 and 10). Only the barriers to rotation are drastically reduced after the geometry optimization. In both the cases two minima corresponding to skewed-s-cis structures are obtained and the planar-s-trans corresponds to an energy maximum. In fig. 10 the two skewed-s-cis conformations are observed at 58.5° above the plane and 65.0° below the plane. This is in agreement with the reported crystal structures of all-trans and 11-cis retinal in which 6-s-bond is cis and twisted by 40° to 62°. The results of rigid rotation from the two minima have also been plotted. Rigid rotations have been done from the nearest optimized points to avoid any artifacts due to fixed geometry during the rigid rotation. In the region of the s-cis above the plane Langlet et al⁹⁵ observed two minima at 45° and 75° separated by a small barrier whereas we observe only one minimum corresponding to skewed-s-cis above the plane (58.5°). The planar-s-trans conformation is 21.7 kJ mol⁻¹ higher in energy than the skewed-s-cis conformations. Several other points have been fully optimized in the region of planar-s-trans to eliminate any artificial features that may be introduced due to fixed geometry. In the region of the s-cis below the plane, again only one minimum corresponding to skewed-s-cis (65.0° below the plane) is observed whereas Langlet et al observed two minima at 90° and 45° below the plane separated by a small barrier. The observation of two minima

separated by a small barrier in both the skewed-s-cis regions could be due to partial methyl relaxation that disappears on full geometry optimization.

The planar-s-cis conformation as expected, due to steric interactions with the methyl group at C5, is a saddle point connecting the two skewed-s-cis conformations with a calculated barrier of 18.9 kJ mol⁻¹.

One would expect two barriers in the region of the 6-s-trans conformation, corresponding to the two methyl groups on C1. However, the ring puckering disposes one methyl group at C1 far from the rotating group and as a result only one barrier (21.7 kJ mol⁻¹) is observed corresponding to the planar-s-trans transition state. The differences in the geometry used and the partial relaxation of geometry as compared to full optimization could be responsible for the differences between our results and those of Langlet et al⁹⁵ and Honig et al⁹⁶. The present ab initio results are in good overall agreement with the results obtained by Dhinra and Saran using the PCILO method⁹⁸. However, the barrier to rotation around the 6-s-bond obtained in the present study is drastically reduced (21.7 kJ mol⁻¹ as compared to 197 kJ mol⁻¹) due to geometry relaxation. The observation of two minima corresponding to 6-s-trans structures near the planar-s-trans maximum by Pullman et al¹⁴² seems to be an artifact of the extended Huckel theory. In the treatment by PCILO method such minima corresponding to 6-s-trans structures are not observed. The planar-s-trans structure was however noted to be an energy maximum in both the case^{12,98} in agreement with the present ab initio results.

The present results also clarify that merely changing the ring puckering will not lead to an observation of the planar-s-trans minimum. The results of rigid rotation with the different puckering (c.f. fig. 9) are the same except that the planar-s-trans maximum is slightly shifted.

In section 1.2.3 some experimental results on the conformation of 6-s-bond in bR were discussed. Recent solid state ¹³C NMR and absorption spectroscopic data⁶⁸

indicate the possibility of a 6-s-cis ring chain conformation in bR. However, the solid state ^{13}C NMR spectroscopy results obtained by Harbison et al⁶⁴ and Childs et al⁶⁵ indicate the presence of a 6-s-trans conformation in the solid state. The present ab initio results show that the isolated chromophore has a 6-s-cis ring chain conformation. The observation of 6-s-trans conformation in the experiments could perhaps be due to certain protein-chromophore interactions that lead to a 6-s-trans ring chain conformation.

3.2.7 Net atomic charge distribution

The net atomic charges of retinal, retinal SB and retinal PSB are often studied because of their importance in understanding the energetics of the interaction between the chromophore and protein residual charges in simple electrostatic terms. The atomic charge distribution is also useful in monitoring the changes in the electronic structure of different analogs. The atomic charges have been determined by means of Mulliken's population analysis, which is expected to give reasonable relative values in the minimal basis set used.

In fig. 11 net atomic charges are plotted for various analogs of different chain lengths. An alternation pattern of the atomic charges can be observed in each case. The heteroatom is always strongly negative, C15 is positive, and the charge alternation on remaining carbon atoms decreases subsequently. However, similar to the cases of bond lengths and bond orders, the retinal and retinal SB analogs show a rather different behaviour compared to retinal PSB. In the former case (fig. 11a), the charges after C15 are all negative with a minor alternation while in fig. 11b for retinal PSB analogs we see a much larger alternation which keeps the odd-numbered carbon atoms slightly positive. The charge alternation is almost the same for cis and trans isomers.

The alternation of atomic charges along a chain introduced by a heteroatom as an 'impurity' is well known. It can be understood by simple topological Hückel-type

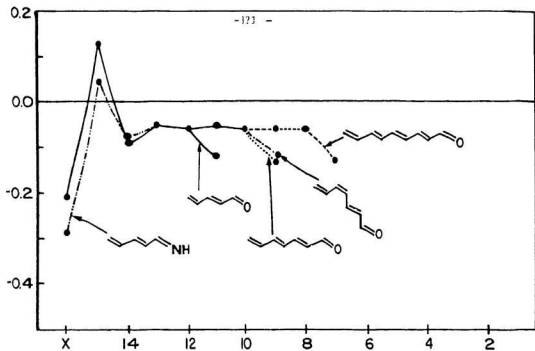
Figure 11

Variation in the SCF net atomic charges on the C,N, or O atoms for different chain analogs of (a) retinal and retinal SB and (b) retinal PSB. The numbering of carbon atoms is as defined in the text.

(a)



NET ATOMIC CHARGES



(b)

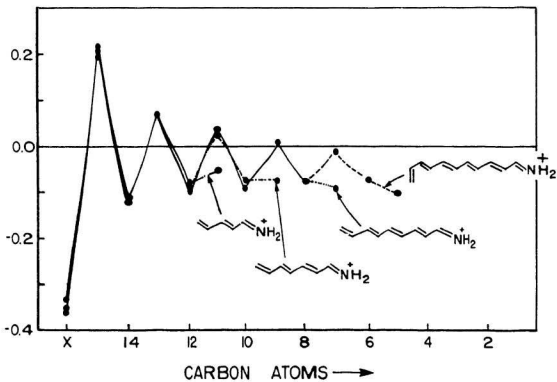
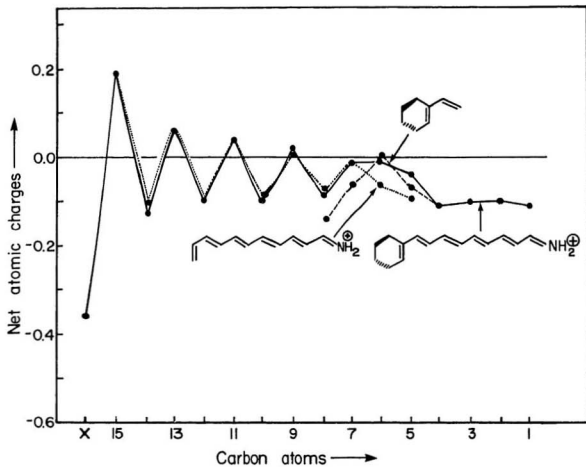


Figure 12

Variation in net atomic charges on the C, N, and O atoms for (a) retinal, retinal SB, and (b) retinal PSB analogs as obtained by ab initio SCF and SLG methods and semiempirical MNDOC (from ref. 138) and INDO-CISD (from ref. 108) calculations. The carbon atom numbering is as defined in the text.

Figure 13

Variation in the SCF net atomic charges on the C and N atoms for the 6-*s-cis* retinal PSB analog and the two building blocks. The numbering of carbon atoms is as defined in the text.



models¹⁴⁴ or, alternatively, on the basis of the induction of local dipoles. The reason of the remarkable difference between 11a and b is less obvious, though it has been studied formerly in several cases. In fig. 12 some previous INDO-CISD and MNDOC results have been collected from the literature^{108,138}. The charges obtained by the SLG wavefunction are also plotted. All the methods agree in the overall pattern of the charges though the MNDOC results seem to overestimate the actual values. The significance of the SLG method is important in this respect, because it does not take into account any delocalization or conjugation effects, and still shows a similar charge distribution. This implies that the essential difference between the charge distribution of retinal PSB and the retinal and retinal SB analogs reflected by fig. 11 and 12 is not to be attributed to the increased conjugation of the former. The increased charge alternation in retinal PSB should be a consequence of the extra positive charge on N which induces larger local dipoles in the bonds over the whole molecule, an effect which is properly accounted for by the simple SLG wavefunction where the bonds are electrostatically coupled.

Fig. 13 illustrates the net atomic charge distribution for the 6-7-3-cis retinal PSB along with those of the two building blocks. An alternation pattern is observed as for the smaller chain analogs (c.f. fig. 11), which is due to the local dipoles induced by the heteroatom. Net atomic charges for the retinal PSB are superimposable with those for the two building blocks. The differences are only at the terminal atoms which are generally more negative. The induced dipole effect is more prominent in the vicinity of the NH_2^+ group. C5 and C6 are predicted to be slightly more positive as compared to C1-C4 keeping the overall net atomic charge on these carbons negative. MNDOC results predict more positive net atomic charges for the ring carbon atoms¹³⁸.

An interesting difference in the charge alternation pattern has been observed upon rotation around the C11-C12 'double bond' in the excited state¹⁰⁸. The INDO-

CISD calculations for the excited state predict an extra polarization at 90° of rotation around the C11-C12 bond. However, the charges obtained by the properly correlated SLG wavefunction do not show the spurious extra polarization at 90° reported in refs. 108 and 101. The extra polarization is therefore most likely an artifact of the calculations. It should be emphasized that the HF- based methods are incapable of describing rotations around double bonds and do lead to charge polarization. Therefore, based on these results the sudden polarization charge transfer hypothesis can be eliminated as a possible mechanism in the vision process.

4. ³B EXCITED STATE RESULTS

To understand the photoisomerization process leading to vision or the energy transfer process it is important to have a good understanding of both the ground state and the lowest lying singlet and triplet excited state potential energy surfaces. In the past, the excited state studies on retinal have been mainly concerned with the prediction of absorption spectra i.e. excitation energies^{118,123,124,145} (section 1.5.5) mainly due to its analogy with the simple polyenes. The photoisomerization process in polyenes has been the subject of a number of theoretical studies¹⁴⁶⁻¹⁵⁶. Geometrical relaxation studies in several low lying excited states are important for proposing mechanisms of photochemical reactions involving these relaxed species as intermediates. Therefore, the present study focusses on the geometry relaxation studies for retinal SB and retinal PSB analogs in the lowest lying triplet excited state¹⁵⁷. Methodological implications are discussed. The results are also discussed based on the qualitative knowledge accumulated in solid state theory.

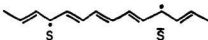
4.1 Review of Solid State Aspects

Recently polyenes have been studied by solid state physicists^{158,159}. The theoretical analysis of various phenomena of polyenes is usually done by rather primitive models like the simple Hückel model. The basic picture of the excited state of polyenes is concerned with the assumption of a local bond rupture process.



'Localized' excited state indicating the rupture of a π bond.

However, the solid state physicists mostly deal with much more delocalized states



'Delocalized' excited state resembling a soliton-antisoliton pair.

These excited states resemble bound soliton-antisoliton pairs, known in solid state physics as elementary excitations, in long conjugated chains.

4.1.1 Soliton-Antisoliton Pairs

Finite polyenes are known to have alternating geometries, that is, they consist of consecutive double and single bonds. For longer and longer chains, the difference between 'single' and 'double' bonds tends to decrease, but many experimental¹⁶⁰ and theoretical^{153,161-163} arguments show that some alternation persists in the infinite chain. For very long chains the bond length alternation value $|r_{>} - r_{<}| \simeq 0.06 \text{ \AA}$ is generally accepted¹⁶². That is, a regular bond length alternation is characteristic for long chains in their ground electronic state. An interesting defect in the bond length alternation occurs in chains consisting of an odd number of carbons, because the chain ends always prefer double bonds.



Doublet Ground state bond length alternation in odd polyenes.

The odd chain is said to contain a neutral (spin carrying) *phase kink* or *soliton*. In the above fig. the dot indicates the place of the soliton which corresponds to maximum spin density location. Recent ab initio calculations¹⁶⁴ confirm that maximum spin densities appear at the place of a phase kink. The origin of the term 'soliton' is connected to 'solitary wave' which appear as solutions of certain non-linear differential equations. Such equations are useful to describe polyacetylene in a continuum model¹⁶⁵. The soliton as described above appears as the ground state solution of an *odd chain*, or as a special bond length alternation defect, *phase kink*, in long chains. In finite polyenes containing an *even* number of carbons, a special excitation is observed if the geometry of the chain is allowed to relax in an electronically excited state. The typical alternation pattern is shown below:



Soliton-antisoliton pair as an excitation in long even polyenes.

Bond lengths shown in A° were optimized by the model Hamiltonian of Surján and Kuzmany¹⁵⁵.

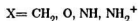
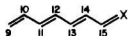
The soliton-antisoliton pair ($S\bar{S}$ pair) is considered as an elementary excitation in the $(CH)_x$ chain.

Theoretical treatment of such phenomena has been dealt with using simple π -electron models augmented with an empirical account of the core. Several models of this type have been proposed in the literature^{153,155,166-168}. In longer chains, it was noticed that the solitons are rather delocalized in the sense that they affect the bond lengths within a wide interval of approximately 15 carbons¹⁵¹. In recent electron nuclear double resonance studies (ENDOR) of cis and trans polyacetylene^{169,170} very small average spin densities were noticed due to the motion of the soliton. This implied delocalization of the soliton over 25 C-C pairs. A recent ab initio study¹⁶⁴ investigated models containing one kink and one unsaturated carbon end. It was noticed that the triplet state becomes more stable as the distance between the kink and the unsaturated end increases. It is in light of these solid state aspects, that the following ab initio results are discussed.

Since the solid state physicists mostly deal with singlet excited states, in that case the two solitons can annihilate each other by allowing complete relaxation. Thus the term 'soliton-antisoliton' pair ($S\bar{S}$) is justified. In the present study we are dealing with the lowest triplet excited state and therefore the two solitons cannot annihilate each other. The same terminology is extended but we prefer to use the notation SS in the triplet excited state as compared to $S\bar{S}$ in the singlet excited state.

4.2 Ab initio RHF and UHF Results

As is evident from the previous section crude theoretical models have been used to study polyenes. These models do not account for electron- electron interactions explicitly, and the treatment of the σ core is also crude. In the previous ab initio study geometry optimizations were not performed. In this section the ab initio RHF and UHF geometry optimization results for some retinal analogs are presented in the 3B excited state. Only the following planar chain analogs are investigated



The molecules studied were kept planar except for a control case when the 90° twisted conformation around the C11-C12 bond was studied in the 3B state in retinal PSB analog. The results predict the 90° twisted conformation to be 13.1 kJ mol^{-1} higher in energy than the planar trans conformation. In earlier studies the 90° twisted conformation was assumed, considering the similarity with an ethylenic bond rotation, to be a minimum on the potential energy surface. [B. Rosenberg in ref. 45]

The RHF optimized bond lengths with the STO-3G basis set for the retinal SB and retinal PSB analogs are shown in fig. 14. The split-valence 3-21G results for the same are given in fig. 15. Fig. 16 shows the UHF optimized bond lengths with the STO-3G and the 3-21G basis sets for the retinal SB and retinal PSB analogs. In each case the results obtained for the retinal analog and octatetraene are analogous to the retinal SB results and thus are not shown in these figures (refer to Appendix IV). For the retinal SB analog four different minima have been located two of which correspond to the localized SS structure and the other two correspond to the delocalized picture. The retinal PSB analog is the exception where only the delocalized structures are obtained. The retinal PSB analog also shows strong conjugation as

Figure 14

RIIF optimized bond lengths for different resonance structures in ^3B excited state of retinal SB and retinal PSB analogs with the STO-3G basis set. The resonance structures are shown schematically at the top of each diagram. The dots represent maximum spin densities.

Figure 15

RIHF optimized bond lengths for different resonance structures in 3B excited state of retinal SB and retinal PSB analogs with the 3-21G basis set. For other notations, see fig. 14.

3-21G Basis

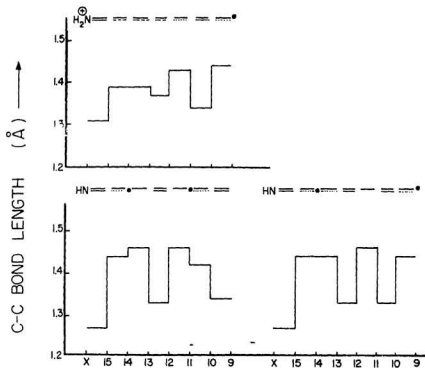


Figure 16

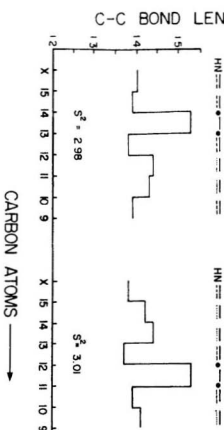
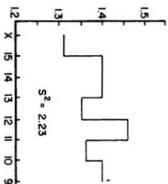
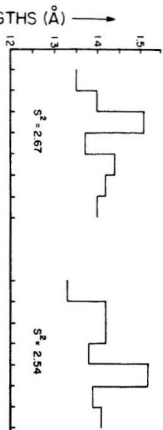
UHF optimized bond lengths for 3B excited state of retinal SB and retinal PSB analogs. The S^2 values obtained in the calculation are shown. The expected value for S^2 is 2. For other notations, see fig. 14.

UHF RESULTS:

STO-3G



3-21G



compared to the other analogs. Though a significant conjugation can be observed even in the retinal SB analog, the double and single bonds are well separated. The bond orders for octatetraene are shown as an example in fig. 17. With the split-valence 3-21G basis set only the minima corresponding to the most stable delocalized structures could be located.

However, at this point it is important to emphasize that the *ab initio* treatment of this problem runs into the difficulty that different locations of the SS pair may correspond to different minima on the same hypersurface. This leads to serious difficulties in choosing the appropriate initial geometry and more importantly the molecular orbitals to converge on the desired minimum. In fact, using the optimized ground state geometries as the initial guess usually leads to localized SS pair solutions. A very careful selection of the initial geometries and molecular orbitals permitted us to locate each relevant minimum on the potential hypersurface.

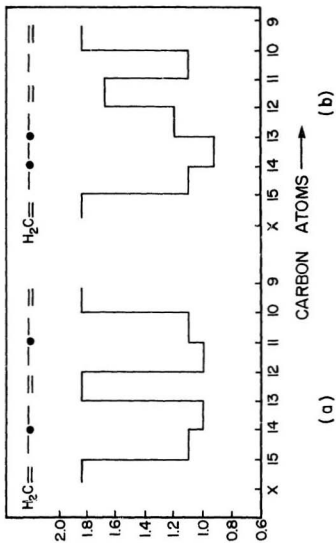
The energetics of the various structures is collected in table 25. Summarizing the RHF results, in each case the delocalized structures are lower in energy. For octatetraene, the delocalized structure is 59.6 kJ mol^{-1} lower in energy than the localized structure. In the retinal analog three different minima are observed, and the two possible localized structures are higher in energy by 58.1 and 59.9 kJ mol^{-1} . The situation is practically the same for the retinal SB case. In the case of retinal PSB only the delocalized structures could be located on the hypersurface. The energy difference between the two possible localized structures is very small: 1.8 kJ mol^{-1} for retinal analogs and 0.8 kJ mol^{-1} for retinal SB analogs.

Considering the analogy between the above results and the knowledge accumulated through solid state physics the following points can be made:

a. According to the solid state physics the 'soliton' and the 'antisoliton' would not be in close proximity as a soliton has a well defined extension or shape and even if the SS pair is enclosed into a very short domain of a few number of bonds, and thus

Figure 17

RHF optimized C-C bond orders for octatetraene in the 3B excited state.



have no room to expand to their optimum shape, they probably would prefer to be separated from each other as far as possible. The above ab initio results are in agreement with this as in each case the delocalized structures (delocalized in the sense that the soliton and antisoliton are far apart) are lower in energy.

b. The present results are also in agreement with the previous ab initio results¹⁶⁴ which predicted that the triplet state becomes more stable on increasing the distance between the phase kink and the end defect.

c. The above ab initio results indicate a very small energy difference between the two localized structures in each case. In the solid state language, this can be interpreted by saying that there is practically no interaction between the SS pair and the heteroatom. Strictly speaking, the small energy differences given above indicate a weak repulsion. This ab initio result is in contradiction with previous semiempirical studies¹⁵¹ which predicted an attractive interaction between a soliton and a heteroatom, although this may be the case for the singlet state.

d. The reason for the disappearance of the localized structures with the 3-21G basis set at the RHF level is not clear. However, the problems with the initial guess have been pointed out and the possibility that such minima could not be located cannot be ruled out. This point will also be discussed further in the upcoming sections.

4.2.1 UHF Results

In addition to the RHF results discussed above, UHF calculations have also been performed on the same 3B state. The results obtained for the UHF calculations with the STO-3G and the 3-21G basis sets are shown in fig. 16. The corresponding total energies for the STO-3G results are also collected in table 25. The UHF calculations are unable to account for the delocalized structures while the two localized ones are almost the same energy, the difference being only 10^{-3} a.u. (2.6 kJ mol^{-1}). It is evident from the S^2 values given in fig. 16 that the UHF wavefunctions suffer from significant spin contamination (also at the 3-21G level) and are thus probably not

Table 25 RHF and UHF total energies at different optimized nuclear configurations in ^3B state. The relative energies (kJ mol^{-1}) with respect to the absolute minimum for that model are given in brackets.

Molecule	E_{RHF} (a.u.) STO-3G	E_{UHF} (a.u.) STO-3G
$\text{=--}_s\text{--}_s\text{--}_s\text{=}$	-304.862646 (0.0)	
$\text{=--}_s\text{--}_s\text{--}_s\text{--}_s\text{=}$	-304.839953 (59.6)	-304.931229
$\text{=--=--}_s\text{--}_s\text{--}_s\text{=}$	-304.839953 (59.6)	-304.931228
$\text{=--}_s\text{--}_s\text{--}_s\text{--}_s\text{=O}$	-340.145535 (0.0)	
$\text{=--=--}_s\text{--}_s\text{--}_s\text{--}_s\text{=O}$	-340.122727 (59.0)	-340.224497 (0.0)
$\text{=--}_s\text{--}_s\text{--}_s\text{--}_s\text{--}_s\text{=O}$	-340.123402 (58.1)	-340.223521 (2.6)
$\text{=--}_s\text{--}_s\text{--}_s\text{--}_s\text{--}_s\text{=NH}$	-320.613913 (10.3)	
$\text{*--=--}_s\text{--}_s\text{--}_s\text{--}_s\text{--}_s\text{=NH}$	-320.617834 (0.0)	
$\text{=--}_s\text{--}_s\text{--}_s\text{--}_s\text{--}_s\text{--}_s\text{=NH}$	-320.591501 (69.1)	-320.688484 (2.6)
$\text{=--=--}_s\text{--}_s\text{--}_s\text{--}_s\text{--}_s\text{--}_s\text{=NH}$	-320.591211 (69.9)	-320.689466 (0.0)
$\text{=--}_s\text{--}_s\text{--}_s\text{--}_s\text{--}_s\text{--}_s\text{--}_s\text{=NH}_2^+$	-321.070532 (26.5)	
$\text{*--=--}_s\text{--}_s\text{--}_s\text{--}_s\text{--}_s\text{--}_s\text{--}_s\text{=NH}_2^+$	-321.080613 (0.0)	
$\text{=--}_s\text{--}_s\text{--}_s\text{--}_s\text{--}_s\text{--}_s\text{--}_s\text{--}_s\text{=NH}_2^+$		-321.110390 (0.0)
$\text{=--=--}_s\text{--}_s\text{--}_s\text{--}_s\text{--}_s\text{--}_s\text{--}_s\text{--}_s\text{=NH}_2^+$		-321.107117 (8.6)

suitable to calculate various physical properties like bond lengths, bond orders or spin densities to an acceptable accuracy.

4.3 Analogy with the allyl radical and methodological implications

In contrast to the discussion based on solid state aspects in the above sections, in this section the RHF results have been compared with some known results for the allyl radical and simple polyenes. The methodological implications that arise due to the comparison are also discussed.

4.3.1 The allyl radical structure and other related simple polyenes

The allyl radical has been repeatedly studied mainly due to the methodological problems encountered in describing its structure adequately^{171,172}. It is well known that in the case of the allyl radical at the RHF level two equivalent minima are predicted corresponding to the following resonance structures:



whereas the allyl radical is actually an equal mixture of these two structures.



This asymmetry in the allyl radical structure observed at the RHF level does not occur in the allyl radical computed at the UHF and multiconfiguration self-consistent field (MCSCF) levels and is related to the well known HF instability of RHF treatments¹⁷¹.

In the case of triplet ethylene, the relative energies of the conformations are not correlation sensitive. In contrast, it has recently been shown that for triplet butadiene the relative energies of the various conformations require a correlation energy correction¹⁴⁹. It was also shown that at the RHF level, the geometry of the singly-twisted allyl-methylene diradical triplet shows the same property as those encoun-

tered in the classic RHF instability of the allyl radical. The authors also concluded regarding the use of RHF or Nesbet open-shell-optimized structures that the intrinsic HF instabilities may be encountered in the situations in which the structures can be described as having allyl-like moieties¹⁴⁹. Further discussion on geometries and relative stabilities of planar and twisted hexatriene conformations and other longer polyenes has been given in ref. 147.

4.3.2 RHF Instability

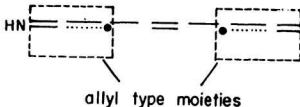
Before going further it is important to realize what actually is RHF instability. The instability of the RHF SCF solutions for the allyl radical (also referred to as the 'doublet instability') has been investigated by several authors at semiempirical and ab initio levels¹⁷³⁻¹⁷⁹. McKelvey and Berthier¹⁷⁵ studied the instability of the RHF solution for the allyl radical with respect to the size of the basis used in the calculation. The difference between the energies of the symmetry adapted and broken symmetry solutions decreased with increase in size of the basis set. Therefore, it was concluded that the instability of the HF solutions and symmetry breakings may be associated with the inadequacy of the basis set and may disappear on approaching the true HF limit.

However, Paldus and coworkers^{173,176,177} suggest that symmetry dilemma and related stability problems are completely general phenomena in the RHF solution, independent of the basis set used. Stability problems arise due to the existence of multiple solutions for the RHF problem. Paldus and coworkers also suggest that these phenomena are as pertinent to the exact HF solutions as to the approximate ones.

4.3.3 Retinal analogs as allyl-like moieties

In this section the present ab initio RHF results on triplet retinal analogs are compared with the above mentioned results for simple polyenes. A careful analysis of the structures obtained for the retinal SB and retinal PSB analogs with the RHF

wavefunction (c.f. figs. 14 and 15) indicates that these structures contain a number of allyl type moieties joined together in different ways. For example,



This raises the question of whether the results obtained are due to RHF instability giving rise to various minima on the same hypersurface corresponding to different resonance structures for the same molecule. In this case the true structure would be a mixture of the various resonance structures obtained. Before discussing the problems related to the search of the true structure a few more points can be made regarding the present RHF results.

In the case of retinal PSB analog only two minima were observed corresponding to the delocalized structures. (c.f. fig. 14) The spin density in the vicinity of the NH_2^+ group is highly delocalized due to the strong conjugation near the NH_2^+ group. Whereas, due to the lack of conjugation at the other end of the molecule two resonance structures are obtained. Since the retinal SB analog shows less conjugation as compared to the retinal PSB case (similar to the ground state results) spin density is not so delocalized and as a result a larger number of resonance structures are observed.

Once again, on comparing the STO-3G results with the 3-21G RHF results it appears that at the split-valence basis set level the structures start showing further resemblance to the allyl-type moieties as slightly more effect of delocalization can be seen. This is in accordance with the observation of McKelvey and Berthier¹⁷⁵ that the instability of the HF solutions may be associated with the inadequacy of the basis set.

4.3.4 Requirements for the search of the true structure of triplet retinal analogs

From the above discussion it is apparent that to describe the structure of triplet retinal analogs adequately one has to use a more sophisticated level of theory taking into account electron correlation effects. The basis set should also be preferably split valence type. Unfortunately, these requirements make the search for the true structure of triplet retinal analogs computationally very demanding and expensive.

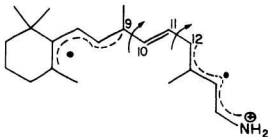
The above discussion also raises some intriguing questions regarding the solid state aspects:

Do these different resonance structures generated by allyl type moieties correspond to different locations of the soliton-antisoliton pairs? Since the solid state physicists mostly deal with crude theoretical models as π -electron models augmented with an empirical account of the core there is a possibility of methodological artifacts. For this reason it would be interesting to study the SS pair at a higher level of theory.

4.4 Projected Mechanistic Implications

Although it is realized that electron correlation would have to be taken into account, some useful predictions can be made using the RHF results. After carefully analysing the results, a reasonable structure can be predicted which could serve as a better initial guess for higher level calculations.

Using the arguments that the spin density would be highly delocalized in the vicinity of the NH_2^+ group and that the radicals would prefer to be as far apart as possible due to the electron-electron repulsion, the following structure can be predicted in the excited state



This leads to some very interesting mechanistic implications as now a bicycle pedal type mechanism around C9-C10 and C11-C12 bonds in the excited state would be favourable. It is emphasized that these predictions would have to be confirmed after performing further calculations in the excited state taking into account electron correlation effects.

The program developments along these lines are discussed in the following chapter.

5. PROGRAM DEVELOPMENTS FOR CONFIGURATION INTERACTION AND NATURAL ORBITALS

In the previous chapter it was shown that the open shell RHF and UHF methods alone are not capable of describing the structure of triplet retinal analogs adequately. Therefore, a higher level theoretical treatment taking into account the correlational effects may help, although this point is somewhat controversial. In this chapter the most commonly used procedure of configuration interaction (CI) is discussed.

5.1 CI Wavefunction

After solving the Roothaan equations in a finite basis set, a set of $2K$ spin orbitals $\{ \chi_i \}$ is obtained. (c.f. section 2.3) The determinant formed from the N lowest energy spin orbitals is the HF determinant $|\Psi_0\rangle$. In addition to $|\Psi_0\rangle$ a large number of other N -electron determinants can be formed from the $2K$ spin orbitals. These determinants are the singly excited determinants $|\Psi_a^r\rangle$ (generated by replacing spin orbital χ_a by χ_r), the doubly excited determinants $|\Psi_{ab}^{rs}\rangle$ (generated by replacing spin orbitals χ_a and χ_b by χ_r and χ_s), etc. up to and including N -tuply excited determinants. These determinants are now used as a basis to expand the exact wavefunction $|\Phi_0\rangle$.

$$|\Phi_0\rangle = C_0 |\Psi_0\rangle + \sum_{ar} C_a^r |\Psi_a^r\rangle + \sum_{a<b, r<s} C_{ab}^{rs} |\Psi_{ab}^{rs}\rangle \\ + \sum_{a<b<c, r<s<t} C_{abc}^{rst} |\Psi_{abc}^{rst}\rangle + \sum_{a<b<c<d, r<s<t<u} C_{abcd}^{rstu} |\Psi_{abcd}^{rstu}\rangle + \dots$$

This is referred to as the full CI wavefunction.

5.1.1 Conventional CI Procedure and Correlation Energy

The number of above mentioned N -tuply excited determinants is extremely large even for small molecules with basis sets of moderate size. But some of these

determinants can be eliminated by utilizing the fact that wavefunctions with different spin (having different eigenvalue for S_z) do not mix and linear combinations of some determinants can be taken to form proper spin-adapted configurations which are eigenfunctions of S^2 .

After forming the trial function the corresponding energies can be obtained by using the linear variational method. The CI Hamiltonian matrix is set up and its eigenvalues are calculated. This is referred to as the full CI procedure. The lowest eigenvalue is an upper bound to the ground state energy and other higher eigenvalues are upper bounds to excited states of the system. The difference between the lowest eigenvalue (\mathcal{E}_0) and the HF energy (E_0) is called the *correlation energy* (E_{corr}).

$$E_{corr} = \mathcal{E}_0 - E_0$$

5.2 Setting up the CI Hamiltonian Matrix

The following points are taken into consideration when setting up the CI matrix:

- a. According to Brillouin's theorem there is no mixing between the HF ground state and single excitations that is,

$$\langle \psi_0 | H | \psi_a^r \rangle = 0$$

- b. All matrix elements of the Hamiltonian between Slater determinants which differ by more than 2 spin orbitals are zero. For example:

$$\langle \psi_0 | H | \psi_{abc}^{rst} \rangle = 0$$

$$\text{and } \langle \psi_0 | H | \psi_{abcd}^{rstu} \rangle = 0$$

$$\text{but } \langle \psi_{ab}^{rs} | H | \psi_{cdef}^{tuvw} \rangle \neq 0 \text{ provided } a, b \in \{c, d, e, f\} \text{ and } r, s \in \{t, u, v, w\}$$

c. All the matrix elements can be calculated using the following rules:

Matrix elements between determinants for one electron operators in terms of spin orbitals are:

$$O_1 = \sum_{i=1}^N h(i)$$

$$(i) |K\rangle = |\dots mn \dots\rangle$$

$$\langle K | O_1 | K \rangle = \sum_m^N [m | h | m]$$

$$(ii) |K\rangle = |\dots mn \dots\rangle$$

$$|L\rangle = |\dots pn \dots\rangle$$

$$\langle K | O_1 | L \rangle = [m | h | p]$$

$$(iii) |K\rangle = |\dots mn \dots\rangle$$

$$|L\rangle = |\dots pq \dots\rangle$$

$$\langle K | O_1 | L \rangle = 0$$

Matrix elements between determinants for two electron operators in terms of spin orbitals are:

$$O_2 = \sum_{i=1}^N \sum_{j>i}^N r_{ij}^{-1}$$

$$(i) |K\rangle = |\dots mn \dots\rangle$$

$$\langle K | O_2 | K \rangle = \frac{1}{2} \sum_m^N \sum_n^N [mm | nn] - [mn | nm]$$

$$(ii) |K\rangle = |\dots mn \dots\rangle$$

$$|L\rangle = |\dots pn \dots\rangle$$

$$\langle K | O_2 | L \rangle = \sum_n^N [mp | nn] - [mn | np]$$

$$(iii) |K\rangle = |\dots mn \dots\rangle$$

$$|L\rangle = |\dots pq \dots\rangle$$

$$\langle K | O_2 | L \rangle = [mp | nq] - [mq | np]$$

The one and two electron integrals above are given in chemists notation that is

$$[i | h | j] = \int dx_1 \chi_i^*(x_1) H(r_1) \chi_j(x_1)$$

$$[ij | kl] = \int dx_1 dx_2 \chi_i^*(x_1) \chi_j(x_1) r_{12}^{-1} \chi_k^*(x_2) \chi_l(x_2)$$

5.3 Practical Considerations

Full CI is computationally feasible only for very small molecules. As the number of configurations grows very rapidly, the dimensionality of the full CI matrix becomes computationally impractical. Therefore, the CI expansion for the wavefunction has to be truncated. Most popular of all the truncated CI is the singly and doubly excited CI (SDCI) where only single and double excitations are considered. For small molecules SDCI recovers the major fraction of E_{corr} .

5.4 Direct CI

As mentioned above only a limited number of configurations can be used in the CI calculation mainly due to the available space in auxiliary memory devices for constructing and saving the hamiltonian matrix for its subsequent diagonalization. The time and space requirements increase as N_{conf}^2 , where N_{conf} is the dimension of the CI vector. To avoid these problems several methods have been proposed in the literature for extracting the eigenvalues and eigenvectors directly from the list of molecular one and two electron integrals¹⁸⁰⁻¹⁸³. Such methods involve an iterative procedure and do not require the construction of the hamiltonian matrix explicitly. These are referred to as the 'Direct CI' procedures. The major advantage with direct CI methods is that they are capable of handling larger problems.

The direct CI method programmed in MUNGAUSS is a general direct CI proposed by Handy et al¹⁸³ and is capable of handling closed shell singlets and open shell doublets, triplets, quartets. The iterative calculation of the lowest eigenvalue and corresponding eigenvector is based on the method proposed by Davidson¹⁸². The problem associated with this direct CI is that it is designed for the calculation of the lowest eigenvalue and eigenvector only. However, for the purposes of the present study it is of interest to calculate a few of the higher eigenvalues and their corresponding eigenvectors as well, to be able to study excited states level ordering.

5.5 Program developments

Due to the problems mentioned above necessary program changes were made to set up the full CI hamiltonian matrix and diagonalize it. Presently the dimensions of the matrix are set to handle 400 configurations.

5.6 One electron properties calculations from CI wavefunction

It has already been mentioned that from a mechanistic point of view it is important to study the properties of retinal analogs in the lowest lying singlet and triplet excited states. Due to the problems encountered in studying the retinal analogs in the lowest triplet excited state (refer to chapter 4) with the RIIF and UIIF wavefunctions, in this section the program developments for properties calculations with the CI wavefunctions are discussed.

Procedure

- 1 A SDCl calculation is performed.
- 2 From this wavefunction the reduced density matrix or the one matrix is obtained and diagonalized to determine the natural orbitals within the SDCl approximation.
- 3 Then the electronic properties are calculated utilizing the natural density matrix.

5.6.1 The reduced density matrix and natural orbitals

For the sake of simplicity the derivations in this and the following section will be presented in the second quantized formalism. For an introduction to the second quantized formalism the reader is directed to ref. 184. In second quantized notation a one-electron operator is given as

$$O_1 = \sum_{ij} \langle i | h | j \rangle a_i^\dagger a_j$$

where a_i^\dagger and a_j denote the creation and annihilation operators respectively. The matrix elements of the reduced density matrix are defined as

$$(\Gamma)_{ij} = \gamma_{ij} = \langle \Phi | a_j^\dagger a_i | \Phi \rangle$$

The density matrix is represented in the spin orbital space. In general, when Φ is not the HF ground state wavefunction Ψ_0 , the reduced density matrix Γ is not diagonal. However since Γ is a Hermitian matrix, it is possible to find a unique unitary matrix U which diagonalizes Γ .

$$\Lambda = U^\dagger \Gamma U$$

$$\lambda_{ij} = \delta_{ij} \lambda_i$$

The elements of the orthonormal set in which Γ is diagonal are called the *natural spin orbitals* (N.O.'s) and $\text{tr} \Gamma = N =$ total number of electrons.

$$\eta_i = \sum_k \chi_k U_{ki}$$

where η_i refers to natural spin orbitals and χ_k refers to spin orbitals. λ_i is called the *occupation number* of the natural spin orbital η_i in the wavefunction Φ .

5.6.2 Setting up the reduced density matrix

Since the density matrix is represented in the spin orbital space the overall structure of the density matrix is as follows:

$$\Gamma = \left(\begin{array}{c|c} \Gamma_{\alpha} & O \\ \hline O & \Gamma_{\beta} \end{array} \right)$$

For closed shell cases $\Gamma_{\alpha} = \Gamma_{\beta}$. Therefore, there is no need to construct both the blocks. Some general derivations for setting up matrix elements of the α block are discussed below in second quantized notation

The general expressions for a HF ground state, singly excited and doubly excited determinants can be written as follows:

$$|\Psi_0\rangle = |\psi_1\bar{\psi}_1 \dots \psi_M\bar{\psi}_M \dots \psi_M\bar{\psi}_M\rangle$$

$$|\Psi_s^{\bar{r}}\rangle = |S_s^{\bar{r}}\rangle = |\psi_1\bar{\psi}_1 \dots \psi_s \dots \psi_b\bar{\psi}_b \dots \psi_M\bar{\psi}_M\bar{\psi}_r\rangle$$

$$|\Psi_{s\bar{s}}^{\bar{r}\bar{r}}\rangle = |D_{s\bar{s}}^{\bar{r}\bar{r}}\rangle = |\psi_1\bar{\psi}_1 \dots \bar{\psi}_s \dots \psi_b \dots \psi_M\bar{\psi}_M\psi_r\bar{\psi}_{\bar{r}}\rangle$$

where $M = N/2$, the number of doubly occupied M.O.'s in the ground state. All the singly excited configurations are generated by exciting the β electrons. The possibility of generating the singly excited configurations by exciting the α electrons is not considered as only the unique configurations are generated based on spatial orbitals. The program does not deal with spin orbitals explicitly. All the derivations below are specific to this scheme for generating configurations and for setting up the α block only. a,b,c,... belong to the set of occupied orbitals and r,s,t,... belong to the set of virtuals in each of the following derivations.

Contribution from $|\Psi_0\rangle$

$$\begin{aligned}
 & \langle \Psi_0 | a_a^\dagger a_a | \Psi_0 \rangle = \\
 & \langle \psi_1 \bar{\psi}_1 \cdots \psi_a \bar{\psi}_a \cdots \psi_b \bar{\psi}_b \cdots \psi_M \bar{\psi}_M | a_a^\dagger a_a | \psi_1 \bar{\psi}_1 \cdots \psi_a \bar{\psi}_a \cdots \psi_b \bar{\psi}_b \cdots \psi_M \bar{\psi}_M \rangle = \\
 & \langle \psi_1 \bar{\psi}_1 \cdots \bar{\psi}_a \cdots \psi_b \bar{\psi}_b \cdots \psi_M \bar{\psi}_M \psi_a | a_a^\dagger a_a | \psi_1 \bar{\psi}_1 \cdots \bar{\psi}_a \cdots \psi_b \bar{\psi}_b \cdots \psi_M \bar{\psi}_M \rangle \\
 & \quad \text{odd number of permutations} \quad \quad \quad \text{even number of permutations} \\
 & = \gamma_{aa} = C_a C_a \text{ where } C_a \text{ is the CI expansion coefficient for } \Psi_0.
 \end{aligned}$$

Therefore the ground state HF configuration contributes to all γ_{aa} where $a = 1, 2, \dots, M$.

Contribution from singles

The singly excited configurations will contribute to the diagonal terms of the α block.

$$\begin{aligned}
 & \langle S_a^{\bar{r}} | a_a^\dagger a_a | S_a^{\bar{r}} \rangle \\
 & = \gamma_{aa} = - C_a^{\bar{r}} C_a^{\bar{r}}
 \end{aligned}$$

Therefore the singly excited configurations contribute to all γ_{aa} where $a = 1, 2, \dots, M$. A pair of two different singly excited configurations will not contribute to the α block.

Contribution from doubles

A doubly excited configuration will have the following contributions to the diagonal terms of the α block

$$\begin{aligned}
 & \langle D_{ab}^{r\bar{r}} | a_b^\dagger a_b | D_{ab}^{r\bar{r}} \rangle \\
 & = \gamma_{bb} = - C_{ab}^{r\bar{r}} \cdot C_{ab}^{r\bar{r}}
 \end{aligned}$$

Therefore the doubly excited configurations will contribute to all γ_{bb} where $b = 1, 2, \dots, M$ except when $b=a$ when it will contribute to γ_{rr}

$$\begin{aligned} & \langle D_{ab}^{\tau\bar{\tau}} | a_r^\dagger a_r | D_{ab}^{\tau\bar{\tau}} \rangle \\ & = \gamma_{rr} = -C_{ab}^{\tau\bar{\tau}} \cdot C_{ab}^{\tau\bar{\tau}} \end{aligned}$$

For all the diagonal elements considered above the sign will always be negative as either the bra or the ket will always lead to odd number of permutations. So far we have considered only the diagonal terms of the Γ_{rr} matrix. Considering the off diagonal terms for the Γ_{α} block, appropriate pairs of doubly excited configurations and pairs of singly and doubly excited configurations will contribute to the off diagonal terms. Pairs of singles will not contribute to the off diagonal terms of the α block.

Pairs of doubles

Consider a pair of doubles which differ by only one spin orbital.

$$\begin{aligned} & \langle D_{ab}^{\tau\bar{\tau}} | a_c^\dagger a_a | D_{cb}^{\tau\bar{\tau}} \rangle = \\ & \langle \psi_1 \bar{\psi}_1 \dots \bar{\psi}_a \dots \psi_b \dots \psi_c \bar{\psi}_c \dots \psi_M \bar{\psi}_M \psi_r \bar{\psi}_s | a_c^\dagger a_a | \psi_1 \bar{\psi}_1 \dots \psi_a \bar{\psi}_a \dots \psi_b \dots \bar{\psi}_r \dots \psi_M \bar{\psi}_M \psi_r \bar{\psi}_s \rangle \\ & = \gamma_{ac} = -C_{ab}^{\tau\bar{\tau}} \cdot C_{cb}^{\tau\bar{\tau}} \end{aligned}$$

It has to be remembered that by interchanging the bra and the ket it will contribute to matrix element γ_{ca} rather than γ_{ac} . (This is also true for other following cases.) The sign of the matrix elements in these cases depends on the relative positions of the orbitals. The sign of the matrix elements will be negative if orbital b lies in between orbital a and c. In other cases it will be positive as shown below by an example

$$\begin{aligned} & \langle D_{ab}^{\tau\bar{\tau}} | a_c^\dagger a_a | D_{cb}^{\tau\bar{\tau}} \rangle = \\ & \langle \psi_1 \bar{\psi}_1 \dots \psi_b \dots \bar{\psi}_a \dots \psi_c \bar{\psi}_c \dots \psi_M \bar{\psi}_M \psi_r \bar{\psi}_s | a_c^\dagger a_a | \psi_1 \bar{\psi}_1 \dots \psi_b \dots \psi_a \bar{\psi}_a \dots \bar{\psi}_r \dots \psi_M \bar{\psi}_M \psi_r \bar{\psi}_s \rangle \\ & = \gamma_{ac} = (-1)(-1) C_{ab}^{\tau\bar{\tau}} C_{cb}^{\tau\bar{\tau}} = C_{ab}^{\tau\bar{\tau}} \cdot C_{cb}^{\tau\bar{\tau}} \end{aligned}$$

Another pair of doubles is possible which differ by only one spin orbital and would contribute to the α block. Consider pairs of type

$$\begin{aligned} & \langle D_{ab}^{rf} | a_i^\dagger a_t | D_{ab}^{rf} \rangle \\ & = \gamma_{ti} = - C_{ab}^{rf} \cdot C_{ab}^{rf} \end{aligned}$$

The sign for matrix elements generated with these types of pairs will always be negative irrespective of the relative positions of occupied orbitals.

Pairs of singles and doubles

Certain pairs of singles and doubles can also contribute to some off-diagonal terms. Consider pairs of the type

$$\begin{aligned} & \langle S_b^f | a_s^\dagger a_r | D_{ab}^{rf} \rangle \\ & = \gamma_{rs} = - C_b^f \cdot C_{ab}^{rf} \end{aligned}$$

It can be shown that for cases where $b \leq a$ the sign for a matrix element will be positive.

After forming the reduced density matrix following the above steps, it is diagonalized to obtain the natural orbitals. The density matrix over N.O.'s is formed.

$$D_{\mu\nu}^{NO} = \sum_i \lambda_i C_{i\mu} C_{i\nu}$$

where λ_i is the occupancy of N.O. i and $C_{i\mu}$ and $C_{i\nu}$ are the corresponding M.O. coefficients.

5.6.3 Mulliken population analysis and one electron properties

Mulliken population can now be performed similar to the case of HF wavefunction. A measure of bond population between the atoms A and B can be estimated as

$$B_{AB} = \sum_{\mu \in A} \sum_{\nu \in B} D_{\mu\nu}^{NO} S_{\mu\nu}$$

Dipole moment can be calculated as follows:

$$\langle \mu_x \rangle = \sum_A Z_A x_A - \sum_{\mu} \sum_{\nu} D_{\mu\nu}^{NO} \int \chi_{\mu}^*(r) r \chi_{\nu}(r) dr$$

μ_y and μ_z can be calculated similarly. Other one electron properties may be calculated in analogy with the HF wavefunction using the existing program.

6. APPLICATIONS OF CI AND STA TO RETINAL ANALOGS

As mentioned in the introductory chapter CI calculations have been extensively applied to simple conjugated polyenes (c.f. section 1.5.5) to study their electronic spectra. Due to the analogy of retinal molecules with simple polyenes CI methods have also been applied to retinal analogs but usually within the PPP or INDO formalisms.

6.1 Objectives of CI studies

It has to be emphasized that CI studies on retinal analogs could be concentrated on a variety of aspects:

- a. Study electronic spectra, that is, excitation energies for several low lying excited states and generate the excited states level ordering.
- b. Change in excited states level ordering with the increase of chain length and relative excited states ordering in retinal and retinal PSB analogs.
- c. Calculate barriers to isomerization in the lowest lying singlet and triplet excited states.
- d. Calculate oscillator strengths and rotational strengths.
- e. Study the λ_{\max} regulation in visual pigments. It has been proposed that λ_{\max} regulation can be achieved by different combinations of double and single bond twistings⁸⁶.
- f. Structure elucidation and calculation of electronic properties in excited states.

6.2 Comparative study of excitation energies calculated using CI and STA

Ab initio HF SCF SDCl calculations have been performed on various analogs of retinal and retinal PSB. All singles and doubles CI calculations are performed with π electrons only. STA (refer to section 2.8) calculations are also performed and compared to the CI results. Calculated excitation energies for the lowest $\pi \rightarrow \pi^*$ transition are given in table 26.

Table 26 Excitation energies (eV) for lowest $\pi \rightarrow \pi^*$ transition.

Planar Analog	HFSCF-SDCI (π electrons only)	STA
	5.24	8.92
	5.20	8.87
	5.21	8.71
	4.21	6.71
	4.18	6.62
	4.05	6.53
	3.20	5.70
	4.71	7.89

The results indicate that a *cis* conformation around a single bond or a double bond leads to a 'red shift' in $\pi \rightarrow \pi^*$ excitation energy, that is, the excitation energy decreases. A larger 'red shift' in $\pi \rightarrow \pi^*$ excitation energies is also observed on going from retinal analog to the respective PSB. Both the CI and the STA results show the same trend. Although the STA values are overestimated, it is encouraging to see that it gives the correct trend. Present *ab initio* results are in agreement with the previous PPP-SCF-CI results on retinal¹⁴¹. The excitation energies obtained in the present results are higher than the results of ref. 141 because the present study deals with smaller analogs than full retinal. But the trend is the same.

In fig. 18 $\pi \rightarrow \pi^*$ STA excitation energies for planar all- *trans* retinal and retinal PSB analogs with varying chain lengths are shown. Results indicate a well known phenomenon in which excitation energy decreases as the chain length is increased.

6.3 λ_{\max} regulation

In fig. 19 STA $\pi \rightarrow \pi^*$ excitation energies are studied as a function of rotation around the C12-C13 single bond in a four double bond analog for retinal. Considering the lowest $\pi \rightarrow \pi^*$ excitation energy the results indicate that a successive 'blue shift' is observed as the rotation takes place from planar *trans* to the 90° twisted. Maximum blue shift is observed in the orthogonal conformation. On rotating further, a red shift is observed until *s-cis* conformation is reached. On comparing the $\pi \rightarrow \pi^*$ excitation energies for *s-trans* and *s-cis* the known 's-cis red shift' is observed. Fig. 20 shows $\pi \rightarrow \pi^*$ excitation energies calculated using a 4 x 4 SD-CI calculation as a function of rotation around the C12-C13 single bond in retinal analog. Again considering the changes in the lowest $\pi \rightarrow \pi^*$ excitation energy with rotation about the single bond, CI results show the same trend as observed with STA calculations. These results are in agreement with the former PPP-CI studies^{141,185}. The results also support the 'torsion model' proposed by Kakitani⁸⁶ based on self consistent HMO calculations and optical spectra of visual pigments. The torsion model suggests that

Figure 18

Variation in the lowest $\pi \rightarrow \pi^*$ excitation energy (calculated using STA) with the chain length.

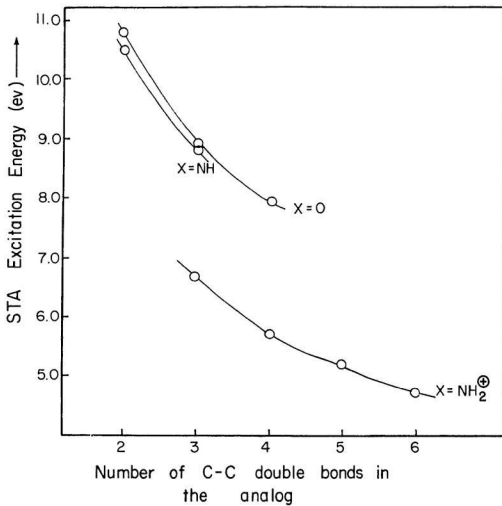


Figure 19

STA $\pi \rightarrow \pi^*$ excitation energies for a retinal chain analog as a function of torsion angle H13-C13-C12-H12. The torsion angle of 180° represents the 12-s-trans conformation. The excited states are labelled considering analogy with simple polyenes having C_{2h} symmetry.

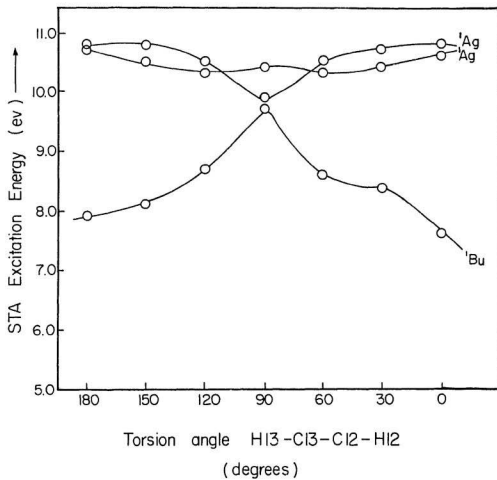
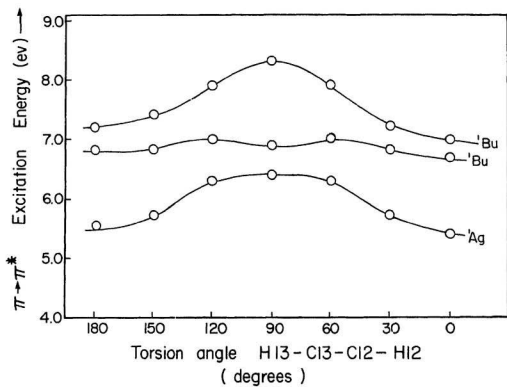


Figure 20

HFSCF-SDCI $\pi \rightarrow \pi^*$ excitation energies for a retinal chain analog as a function of torsion angle H13-C13-C12-H12. The torsion angle of 180° represents the 12-s-trans conformation. The excited states are labelled considering analogy with simple polyenes having C_{2h} symmetry.



twisting around single bonds leads to hypochromic shift (blue shift) and twisting around double bonds leads to bathochromic shift (red shift)⁸⁶. However, to test the torsion model completely, further calculations involving twisting around double bonds would have to be performed.

6.4 Comparison of excited states level ordering obtained with STA and CI calculations

Fig. 19 shows that the STA calculations predict the lowest $\pi \rightarrow \pi^*$ level to be 1B_u -like, corresponding to the strongly allowed transition from the ground state. The next two $\pi \rightarrow \pi^*$ levels are nearly degenerate 1A_g -like and correspond to forbidden transitions from the ground state. (One of the two 1A_g states becomes allowed in cis polyenes as the cis conformation destroys the inversion symmetry of the molecule.) It has to be remembered that the above discussion is based on the consideration that the retinal analog has the proper C_{2h} symmetry similar to simple polyenes. It is to be noted that the 12-s-cis and 12-s-trans structures have the same level ordering (c.f. fig. 19). At 90° in the twisted conformation the lowest $\pi \rightarrow \pi^*$ level is raised and one of the 1A_g -like states becomes nearly degenerate to the lowest 1B_u -like state.

Fig. 20 shows the level ordering obtained with the SDCl calculations for the same retinal analog. The lowest $\pi \rightarrow \pi^*$ level now corresponds to the 1A_g -like state. The next two near degenerate levels are the 1B_u -like states. The lowest $\pi \rightarrow \pi^*$ level now corresponds to the transition which is forbidden from the ground state. 12-s-cis and 12-s-trans structures show the same level ordering. Compared to the STA results, the SDCl calculations in general reduce the gap between the lowest $\pi \rightarrow \pi^*$ level and the next two $\pi \rightarrow \pi^*$ levels. All the excitation energies obtained with STA are overestimated due to the crude approximation. For the 90° twisted conformation the CI results also predict that the excitation energy for the lowest $\pi \rightarrow \pi^*$ transition increases such that the 1A_g -like state now lies very close to the next higher 1B_u -like state, but there is no crossing of the two states.

Comparing the above results with some previous PPP-CISD calculations on retinal¹⁸⁵ and simple polyenes¹⁸⁶ the following points are noted

- (1) Birge et al¹⁸⁵ reported a conformationally variant level ordering whereas the present HFSCF-CISD results show a conformationally invariant level ordering for retinal. In other words, the 12-s-cis and 12-s-trans structures are predicted to have the same level ordering. Both 12-s-cis and 12-s-trans structures have the 1A_g -like lowest lying excited state whereas the PPP-CISD calculations predicted that all 12-s-cis structures have a lowest excited 1B_u -like state and the 12-s-trans structures have a lowest excited 1A_g -like state.
- (2) Present STA results on retinal analog predict the 1B_u -like state to be the lowest and 1A_g -like for the next higher near degenerate states. In contrast the CI results predict the 1A_g -like state to be lowest and 1B_u -like for the next higher near degenerate states in retinal analog. Schulten and Karplus¹⁸⁶ reported PPP-SCI and PPP-SDCI results on octatetraene. It was noted that only singles CI was not adequate to predict the level ordering. Only after including all the double excitations in the CI calculation did the forbidden 1A_g -like state become lower than the allowed 1B_u -like state. Based on the present HFSCF-CISD calculations and the previous PPP-CISD calculations on simple polyenes it can be concluded that STA is not adequate for predicting excited state level ordering.

7. CONCLUDING REMARKS

The ground state properties of retinal are studied in detail by utilizing ab initio Hartree Fock STO-3G calculations on retinal analogs. The ground state results can be summarized as follows:

1. The convergence in bond lengths, bond orders and net atomic charges is studied with increase in chain length for retinal, retinal SB and retinal PSB analogs. The results indicate that it is possible to mimic some properties of retinal with a smaller analog. This holds for retinal PSB analogs only to a lesser extent.
2. Protonation of the SB causes more conjugational effects (i.e. elongation of double bonds and shortening of single bonds) in the vicinity of the NH_2^+ group which slowly dies off on moving towards the cyclohexene ring end of the molecule. This is reflected by the bond lengths and bond orders.
3. The various cis isomers show the same properties as the trans molecules.
4. The cyclohexene ring has little effect on bonding and charge distribution in the molecule, but simply causes local torsional distortions breaking the C_∞ symmetry of the chain.
5. The effect of methyl substituents at C1, C5 and C13 on the geometry of the analogs is studied in detail. In general the introduction of a methyl group in the chain reduces the effect of conjugation throughout the chain slightly. All the C-C single bonds become slightly longer and the C-C double bonds slightly shorter. However, the major effect of the methyl groups is reflected in torsions around the neighbouring single bonds which show distortion from planarity. This is because of the steric hindrance introduced by the presence of the methyl group. The introduction of a methyl group at C13 leads to a skewed geometry around C12-C13 and C10-C11 single bonds for retinal and retinal PSB analogs. The results indicate that for retinal PSB the preferred conformation is planar 11-cis, 12-s-trans as compared to 11-cis, skewed 12-s-cis in retinal. Since the energy difference between the two conformations

of retinal PSB is small, it can exist as an equilibrium mixture of the two in solution.

The major effect of the addition of the methyl groups on the cyclohexene ring is torsion angle around the C6-C7 single bond. Two stable skewed 6-s-cis conformations are obtained, one at 58.5° above the plane and the other at 65.0° below the plane, the plane being defined by C1-C6-C5-C4. The planar 6-s-trans conformation is predicted to be a transition state for the isolated chromophore. The barrier for interconversion from one skewed-s-cis to the other is calculated to be 18.9 kJ mol^{-1} if the transition state corresponds to planar-s-cis and 21.7 kJ mol^{-1} if the transition state corresponds to the planar-s-trans conformation. The present results also clarify that merely changing the ring puckering will not lead to an observation of the planar-s-trans minimum.

6. Net atomic charges alternate along the chain. This alternation is a result of induced local dipoles and is considerably stronger for retinal PSB analogs.

7. The charge distribution along the chain changes significantly at the SCF level when rotating around a double bond. This sudden charge polarization is shown to be an artifact of the closed shell HF calculations, which disappears if the properly correlated SLG wavefunction is used.

Apart from ground state studies the present study also deals with geometry relaxation in the lowest lying triplet excited state utilizing RHF and UHF methods. The results are compared with known results for simple polyenes and also discussed in light of solid state physics aspects. The following points summarize the excited state results:

1. The UHF wavefunctions suffer from significant spin contamination with both STO-3G and 3-21G basis sets and thus are not suitable for the purposes of the present study.

2. Geometry relaxation studies in the lowest triplet excited state using RHF wavefunctions show problems related to the intrinsic RHF instability. The results

indicate that the various minima observed on the same hypersurface may correspond to different resonance structures for the same molecule. The true structure in this case would be a mixture of the various resonance structures obtained. Despite these methodological problems, a careful analysis of the results leads to interesting mechanistic implications. The results suggest that a bicycle pedal type mechanism in the excited state around C9-C10 and C11-C12 bonds would be favourable. This is suggested based on the results that the spin density is highly delocalized in the vicinity of the NH_2^+ group and that the radicals prefer to be as far apart as possible.

3. The RHF results also raise the question whether the different resonance structures generated by allyl type moieties correspond to different locations of the soliton-antisoliton pairs.

4. STA and HFSCF SDCI calculations indicate that a 'red shift' is obtained in the lowest $\pi \rightarrow \pi^*$ excitation energy on going from planar trans conformation to planar cis conformation around a single bond or a double bond. A larger 'red shift' in $\pi \rightarrow \pi^*$ excitation energies is also observed on protonating the retinal SB.

5. STA results correctly indicate the lowering of $\pi \rightarrow \pi^*$ excitation energies with increase in chain length.

6. STA and SDCI results predict a 'blue shift' in the $\pi \rightarrow \pi^*$ excitation energy on rotating around the single bond, which supports the 'torsion model'.

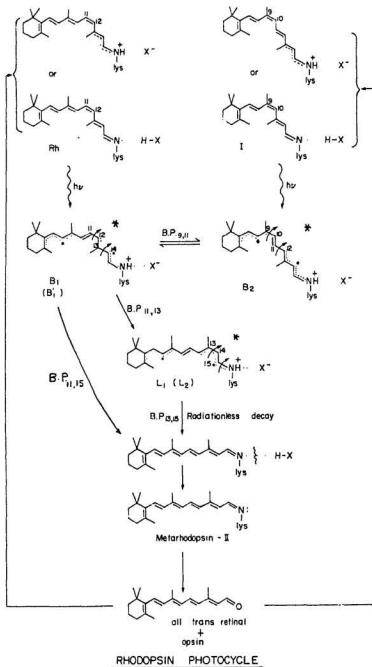
7. Both STA and SDCI calculations predict a conformationally invariant level ordering for excited states of retinal analog. Both the 12-s-cis and 12-s-trans conformations have the same level ordering.

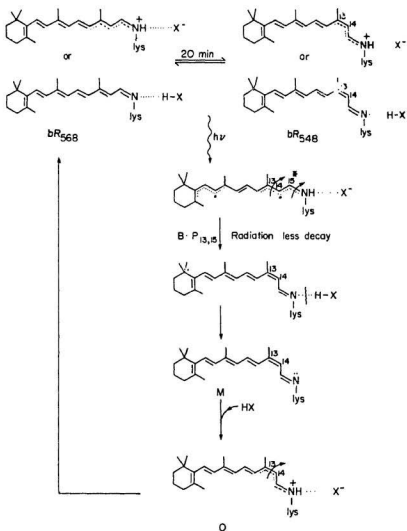
8. Present SDCI results predict the 1A_g -like state to be lowest and 1B_u -like for the next higher near degenerate states in retinal analog. Therefore the lowest lying excited state corresponds to the forbidden transition from the ground state.

9. The results obtained from STA are encouraging realizing the fact that a STA cal-

ulation is cheaper and faster to perform than a CI calculation. STA can be used for studying $\pi \rightarrow \pi^*$ excitation energies as a function of rotation around the single bonds. However, STA cannot be used to study the excited states level ordering.

Based on the above ground and excited state results, the projected mechanisms for Rh and bR photocycles are shown on the following pages.





BACTERIORHODOPSIN PHOTOCYCLE
(THE PROTON PUMP MECHANISM)

In the Rh photocycle the ground state is shown to be 11-cis retinal PSB. For isorhodopsin (I) the ground state is the 9-cis retinal PSB. Based on the arguments proposed by Sandorfy²⁸ the possibility of the $\Delta 13$ being H-bonded cannot be ruled out. After the photon absorption the structure in the excited state is based on the arguments that the spin density would be highly delocalized in the vicinity of the NH^+ -lys group and that the radicals would prefer to be as far apart as possible due to the electron-electron repulsion. The Schiff base of the chromophore still remains protonated as the conjugated Schiff bases are known to be more basic in the excited state¹⁸⁷. Isorhodopsin gives rise to intermediate B_2 which can undergo a bicycle pedal type simultaneous rotation about C9-C10 and C11-C12 bonds (B.P._{9,11}). Rh gives rise to intermediate B_1 which can undergo B.P. around C11-C12 and C13-C14 bonds. Bicycle pedal type simultaneous rotation around two bonds is suggested as compared to simple rotation about one bond because B.P. is a volume conserving process. Recent calculations have also shown that B.P. involves a lower barrier as compared to hula twist or simple isomerization process¹⁰⁵. When intermediate B_2 undergoes B.P._{9,11} it would give rise to an intermediate similar to B_1 (B_1'). Small differences between B_1 and B_1' could be arising due to clockwise or anticlockwise rotations. Recent photolysis experiments have suggested the presence of two batho intermediates arising from Rh or I⁵⁶. B_1 was noticed as the long lifetime component and B_2 as the short lifetime component. This can be explained if there is an equilibrium between B_2 and B_1 as they can interconvert through B.P._{9,11}. B_1 and B_1' then undergo B.P._{11,13} giving rise to L_1 and L_2 . L_1 and L_2 again could be identical or slightly different depending upon clockwise/anticlockwise rotations. L_1 and L_2 undergo B.P._{13,15} and decay (radiationless deactivation) to the ground state giving all-trans retinal PSB. There is an alternative pathway for the conversion of B_1 and B_1' to all-trans retinal PSB. B_1 and B_1' could undergo B.P._{11,15} giving all-trans retinal PSB in one step. However, B.P._{11,15} would involve a slightly higher barrier as

compared to B.P._{11,13} because in the excited state C15-N bond is expected to have more double bond character as compared to C13-C14 bond. Also, B.P._{11,15} does not explain the presence of intermediates L₁ and L₂. At this stage deprotonation can take place due to the reduced basicity of the Schiff base in the ground state and perhaps due to the conformational changes. The SB is then hydrolysed and the proton is separated. Later, through enzymatic processes Rh and I are regenerated.

In the case of bR the ground state is all-trans retinal PSB (light-adapted bR₅₆₈) or a 1:1 mixture of all-trans and 13-cis retinal PSB (dark-adapted). After the photon absorption the structure in the excited state is shown analogous to the case of Rh. B.P. around the C13-C14 and C15-N bonds is suggested which would have partial double bond characters. After isomerization the molecule decays to the ground state. In the ground state due to the reduced basicity of the Schiff base, deprotonation takes place and the proton is pumped outside the cell membrane. The molecule then gets reprotonated by a surrounding proton donor giving 13-cis retinal PSB. In the ground state the bond order of C13-C14 double bond is reduced due to the extra conjugation in the vicinity of the NH⁺-lys group. Therefore the molecule can isomerize thermally regenerating the all-trans bR₅₆₈.

These proposed mechanisms obviously do not account for each and every intermediate but give some insight about the structural aspects of certain intermediates. Further experimental and theoretical work would have to be done. Some desired further work is outlined below

1. Calculations of electronic properties in the excited states using CI wavefunctions leading to complete structure elucidation and study of properties in the lowest singlet and triplet excited states.
2. Complete understanding of the torsion model for λ_{\max} regulation in visual pigments.

3. Study models for the binding site at the ab initio HF level using the CAMM method of Sokalski and Poirier¹⁸⁸ or by studying the effect of external point charges on λ_{max} . Some semiempirical work has already been done in this direction.
4. It would be very interesting to get reliable X-ray crystallographic data for some salt of retinal PSB. The X-ray data could then be compared with the theoretical conformational studies and solid state ¹³C NMR data for retinal PSB salts.
5. Some experiments to investigate the proton transfer hypothesis are desired. For example, comparing the quantum yields for photoisomerization of methylated and demethylated visual pigments.

REFERENCES

1. a. G. Wald, *J. Gen. Physiol.*, **18**, 905 (1935) ; b. *ibid*, **19**, 351 (1935) ; c. *ibid*, **19**, 781 (1936).
2. G. Wald, *Nature (Lond.)*, **140**, 545 (1937).
3. I.M. Heilbron, A.E. Gillam, R.A. Morton, *Biochem. J.*, **25**, 1352 (1931)
4. H.N. Holmes, R.E. Corbet, *J. Am. Chem. Soc.*, **59**, 2042 (1937)
5. P. Karrer, R. Morf, K. Schopp, *Helv. Chim. Acta*, **14**, 1036 (1931)
6. J.G. Baxter, C.D. Robeson, *Science*, **92**, 203 (1940)
7. J.R. Edisbury, R.A. Morton, G.W. Simpkins, *Nature (Lond.)*, **140**, 234 (1937)
8. M.K. Salah, A.L. Stubbs, *Nature (Lond.)*, **159**, 744 (1947)
9. K.R. Farrer, J.C. Hamlet, H.B. Henbest, E.R.H. Jones, *J. Chem. Soc.*, 2657 (1952)
10. D. Bownds, *Nature (Lond.)*, **216**, 1178 (1967)
11. M. Akhtar, P.T. Blossie, P.B. Dewhurst, *Life Sci.*, **4**, 1221 (1965)
12. R.A. Marton and G.A.J. Pitt, *Biochem. J.*, **59**, 128 (1955) ; A. Kropf and R. Hubbard, *Ann. N.Y. Acad. Sci.*, **74**, 266 (1958)
13. K. vander Meer, J.J.C. Mulder and J. Lugtemburg, *Photochem. Photobiol.*, **24**, 363 (1976).
14. a. C.D. Robeson and J.G. Baxter, *J. Am. Chem. Soc.* **69**, 136 (1947) ; b. C.D. Robeson, W.P. Blum, J.M. Dieterle, J.D. Cawley, J.G. Baxter, *J. Am. Chem. Soc.* **77**, 4120 (1955).
15. W. Oroshnik, A.D. Mebane, *J. Am. Chem. Soc.* **76**, 5719, (1954).
16. W. Oroshnik, *J. Am. Chem. Soc.* **78**, 2651 (1956).
17. W. Oroshnik, P.K. Brown, R. Hubbard, G. Wald, *Proc. Natl. Acad. Sci. (Washington)* **42**, 578 (1956).

18. D. Oesterhelt and W. Stoeckenius, *Nature New Biol.* **233**, 149 (1971).
19. D. Oesterhelt and W. Stoeckenius, *Proc. Natl. Acad. Sci. (USA)*, **70**, 2853 (1973).
20. E.F. MacNicol, *Sci. Am.* **211**, 48 (1934).
21. L.Y. Fager and R.S. Fager, *Methods Enzymol.*, **81**, 160 (1982).
22. P. Liebman, *Biochemistry and Physiology of visual pigments Symposium*, 299 Springer, New York (1973).
23. S. Hecht, *Bull. N.Y. Acad. Med.* **14**, 21 (1938).
24. a. L. Zechmeister, *Chem. Rev.* **34**, 267 (1944) ; b. L. Zechmeister, *Experientia (Basel)* **10**, 1 (1954).
25. T. Yoshizawa and G. Wald, *Nature* **199**, 1279 (1963).
26. A. Kropf, *Nature (Lond.)* **264**, 92 (1976).
27. M.H. Abdel Kader, *Photochemistry and Photobiology: Proceedings of the International Conference*, **2**, 1397 (1983).
28. C. Sandorfy, *Int. J. Quantum Chem.* **26**, 907 (1984).
29. G.E. Bush, M.L. Applebury, A.A. Lamola and P.M. Rentzepis, *Proc. Natl. Acad. Sci. (USA)* **69**, 2802 (1972).
30. K. Peters, M.L. Applebury and P.M. Rentzepis, *Proc. Natl. Acad. Sci. (USA)* **74**, 3119 (1977).
31. P.M. Rentzepis, in *Spectroscopy of biological molecules* Ed: C. Sandorfy and T. Theophanides, Reidel 373 (1984).
32. T. Yoshizawa in *Photochemistry of vision*. Ed: H.J.A. Dartnall Vol. 7/1 of *Handbook of Sensory Physiology Springer, Berlin, Chapter 5*, 146 (1972)
33. B. Honig, *Ann. Rev. Phys. Chem.* **29**, 31 (1978).
34. B. Honig, *Curr. Top. Membr. Transp.*, **16**, 371 (1982).

35. M. Ottolenghi in *Advances in photochemistry* Vol. 12 Ed: J.N. Pitts, G.S. Hammond, K. Gollnick and D. Grosjean, Wiley-Interscience, New York, 97 (1980).
36. R.R. Birge, *Ann. Rev. Biophys. Bioeng.* 10, 315 (1981).
37. R. Uhl and E.W. Abrahamson, *Chem. Rev.* 81, 291 (1981).
38. W. Stoeckenius and R. Bogomolni, *Ann. Rev. Biochem.* 51, 587 (1982)
39. W. Stoeckenius, R.H. Lozier and R.A. Bogomolni, *Biochim. Biophys. Acta*, 505, 215 (1979).
40. H. Shichi in *Biochemistry of vision*, Academic Press, New York 1983.
41. V. Balogh-Nair and K. Nakanishi in *New comprehensive biochemistry* Vol. 3 Stereochemistry Ed: C. Tamm, Elsevier Biomedical, Amsterdam, 283 (1982)
42. D.S. Kliger, *Int. J. Quantum Chem.* 16, 809 (1979).
43. L. Packer (Ed.), *Biomembranes methods in enzymology*, Vol. 88, Parts II and I, Academic Press, New York (1982).
44. H. Langer (Ed.), *Biochemistry and Physiology of Visual Pigments*, Springer-Verlag, New York (1973).
45. J.B. Birks (Ed.), *Excited States of Biological Molecules*, John Wiley and Sons, London, 509 (1976).
46. C. Sandorfy and D. Vocelle, *Can. J. Chem.* 64, 2251 (1986).
47. T. Yoshizawa and S. Horiuchi, *Biochemistry and physiology of visual pigments* Ed: H. Langer, Springer-Verlag, Berlin, 69 (1973).
48. R.A. Mathies, *Spectroscopy of biological molecules* Eds: C. Sandorfy and T. Theophanides, D. Reidel Publishing Co., Holland, 303 (1984).
49. A.R. Oseroff and R.H. Callender, *Biochemistry*, 13, 4243 (1974).
50. R. Callender and B. Honig, *Ann. Rev. Biophys. Bioeng.*, 6, 33 (1977)
51. S.O. Smith, J. Lugtenburg and R.A. Mathies, *J. Membrane Biol.* 85, 95 (1985).

52. B. Curry, I. Palings, A.D. Brock, J.A. Pardoën, J. Lugtenburg and R.A. Mathies , *Advances in IR and Raman Spectroscopy*, vol. 12, Ed: R.J.H. Clark and R.E. Hester, Wiley Heyden, 114 (1985).
53. S.O. Smith, A.B. Myers, R.A. Mathies, J.A. Pardoën, C. Winkel, E.M.M. van den Berg and J. Lugtenburg, *Biophys. J.*, 47, 653 (1985).
54. S.O. Smith, J.A. Pardoën, J. Lugtenburg and R.A. Mathies, *J. Phys. Chem.*, 91, 804 (1987).
55. S.O. Smith, M.S. Braiman, A.B. Myers, J.A. Pardoën, J.M.L. Courtin, C. Winkel, J. Lugtenburg and R.A. Mathies, *J. Am. Chem. Soc.*, 109, 3108 (1987).
56. S.J. Hug, J.W. Lewis and D.S. Kliger, *J. Am. Chem. Soc.*, 110, 1998 (1988).
57. A.G. Doukas, M.R. Junnarkar, R.R. Alfano, R.H. Callender and V. Balogh-Nair, *Biophys. J.*, 47, 795 (1985).
58. G.S. Harbison, S.O. Smith, J.A. Pardoën, C. Winkel, J. Lugtenburg, J. Herzfeld, R. Mathies and R.G. Griffin, *Proc. Natl. Acad. Sci. (USA)*, 81, 1706 (1984).
59. J.M. Fang, J.D. Carriker, V. Balogh-Nair and K. Nakanishi, *J. Am. Chem. Soc.*, 105, 5162 (1983).
60. A. Albeck, N. Friedman, M. Sheves and M. Ottolenghi, *J. Am. Chem. Soc.*, 108, 4614 (1986).
61. C.H. Chang, R. Govindjee, T. Ebrey, K.A. Bagley, G. Dollinger, L. Eisenstein, J. Marque, H. Roder, J. Vittitow, J.M. Fang and K. Nakanishi, *Biophys. J.*, 47, 509 (1985).
62. U. Devi, M. Sheves, V. Rosenbach and M. Ottolenghi, *Photochem. Photobiol.*, 38, 197, (1983).

63. M. Sheves, T. Baasov, N. Friedman, M. Ottolenghi, R. Feinmann-Weinberg, V. Rosenbach, B. Ehrenberg, *J. Am. Chem. Soc.*, **106**, 2435 (1984).
64. G.S. Harbison, S.O. Smith, J.A. Pardoën, J.M.L. Courtin, J. Lugtenberg, J. Herzfeld, R.A. Mathies, R.G. Griffin, *Biochemistry*, **24**, 6955 (1985).
65. R.F. Childs, G.S. Shaw, R.E. Wasylshen, *J. Am. Chem. Soc.*, **109**, 5362 (1987).
66. G.S. Harbison, P.P.J. Mulder, H. Pardoën, J. Lugtenburg, J. Herzfeld, R.G. Griffin, *J. Am. Chem. Soc.*, **107**, 4809 (1985).
67. R. van der Steen, P.L. Biesheuvel, R.A. Mathies and J. Lugtenburg, *J. Am. Chem. Soc.*, **108**, 6410 (1986).
68. H.S. Rodman Gilson and B.H. Honig, *J. Am. Chem. Soc.*, **110**, 1943 (1988).
69. T. Hamanaka, T. Mitsui, T. Ashida and M. Kakudo, *Acta Crystallogr.*, **B28**, 214 (1972).
70. R.D. Gilardi, I.L. Karle, J. Karle, *Acta Crystallogr.*, **B28**, 2605 (1972).
71. G. Drikos, H. Ruppel, H. Dietrich and W. Sperling, *FEBS Lett.*, **131**, 23 (1981).
72. C.J. Simmons, R.S.H. Liu, M. Denny and K. Seff, *Acta Crystallogr.*, **B37**, 2197 (1981).
73. C.H. Stam and C.H. MacGillavry, *Acta Crystallogr.*, **16**, 62 (1963).
74. C.H. Stam, *Acta Crystallogr.*, **B28**, 2936 (1972).
75. E.L. Eichorn, C.H. MacGillavry, *Acta Crystallogr.*, **12**, 872 (1959).
76. W.E. Oberhansli, H.P. Wagner and O. Isler, *Acta Crystallogr.*, **B30**, 161 (1974).
77. H. Matsumoto, R.S.H. Liu, C.J. Simmons and K. Seff, *J. Am. Chem. Soc.*, **102**, 4259 (1980).
78. M.A. Gawinowicz, V. Balogh-Nair, J.S. Sabol and K. Nakanishi, *J. Am. Chem. Soc.*, **99**, 7720 (1977).
79. B. Honig, U. Dinur, K. Nakanishi, V. Balogh-Nair, M. Gawinowicz, M. Arna-

- boldi and M.G. Motto, *J. Am. Chem. Soc.*, **101**, 7084 (1979).
80. M. Sheves, K. Nakanishi and B. Honig, *J. Am. Chem. Soc.*, **101**, 7086 (1979).
81. M.G. Motto, M. Sheves, K. Tsujimoto, V. Balogh-Nair and K. Nakanishi, *J. Am. Chem. Soc.*, **102**, 7947 (1980).
82. K. Nakanishi, V. Balogh-Nair, M. Arnaboldi, K. Tsujimoto and B. Honig, *J. Am. Chem. Soc.*, **102**, 7945 (1980).
83. J.L. Spudich, D.A. McCain, K. Nakanishi, M. Okabe, N. Shimizu, H. Rodman, B. Honig and R.A. Bogomolni, *Biophys. J.*, **49**, 476 (1986).
84. J. Lugtenburg, M. Muradin-Szweykowska, C. Heeremans, J.A. Pardoën, G.S. Harbison, J. Herzfeld, R.G. Griffin, S.O. Smith and R.A. Mathies, *J. Am. Chem. Soc.*, **108**, 3104 (1986).
85. P.E. Blatz and J.H. Mohler, *Biochemistry*, **14**, 2304 (1975).
86. T. Kakitani and H. Kakitani, *Biophys. Struct. Mechanism*, **5**, 55 (1979).
87. A. Warshel, *Nature*, **260**, 679 (1976).
88. M.R. Fransen, W.C.M.M. Luyten, J. van Thuijl, J. Lugtenburg, P.A.A. Jansen, P.J.G.M. van Breugel and F.J.M. Daemen, *Nature*, **260**, 726 (1976).
89. K. Schulten and P. Tavan, *Nature*, **272**, 85 (1978).
90. R.S.H. Liu and A.E. Asato, *Proc. Natl. Acad. Sci. USA*, **82**, 259 (1985).
91. R.S.H. Liu, D. Mead and A.E. Asato, *J. Am. Chem. Soc.*, **107**, 6600 (1985).
92. A.E. Asato, M. Denny and R.S.H. Liu, *J. Am. Chem. Soc.*, **108**, 5032 (1986).
93. R.S.H. Liu, H. Matsumoto, A.E. Asato and D. Mead, *J. Am. Chem. Soc.*, **108**, 3796 (1986).
94. R.S.H. Liu and D.T. Browne, *Acc. Chem. Res.*, **19**, 42 (1986).
95. J. Langlet, B. Pullman and H. Berthod, *J. Mol. Struct.*, **6**, 139 (1970).

96. B. Honig, A. Warshel and M. Karplus, *Acc. Chem. Res.*, **8**, 92 (1975).
97. R. Rowan III, A. Warshel, B.D. Sykes and M. Karplus, *Biochemistry*, **13**, 970 (1974).
98. M.M. Dhingra and A. Saran, *Proc. Indian Acad. Sci. (Chem. Sci.)*, **90**, 485 (1981).
99. A. Saran and M.M. Dhingra, *Int. J. Quantum Chem., Quantum Biology Symposium* **9**, 145 (1982).
100. M.M. Dhingra and A. Saran, *Proc. Indian Acad. Sci. (Chem. Sci.)*, **90**, 497 (1981).
101. L. Salem and P. Bruckmann, *Nature*, **258**, 526 (1975).
102. L. Salem, *Acc. Chem. Res.*, **12**, 87 (1979).
103. A. Warshel and C. Deakyne, *Chem. Phys. Lett.*, **55**, 459 (1978).
104. T.R. Hays, S.H. Lin and H. Eyring, *Proc. Natl. Acad. Sci. USA*, **77**, 6314 (1980).
105. S. Seltzer, *J. Am. Chem. Soc.*, **109**, 1627 (1987).
106. G.J.M. Dormans, G.C. Groenenboom, W.C.A. van Dorst and H.M. Buck, *J. Am. Chem. Soc.*, **110**, 1406 (1988).
107. P. Tavan, K. Schulten, W. Gartner and D. Oesterhelt, *Biophys. J.*, **47**, 349 (1985).
108. R.R. Birge and L.M. Hubbard, *J. Am. Chem. Soc.*, **102**, 2195 (1980).
109. R.R. Birge and L.M. Hubbard, *Biophys. J.*, **34**, 517 (1981).
110. R.R. Birge, L.A. Findsen and B.M. Pierce, *J. Am. Chem. Soc.*, **109**, 5041 (1987).
111. P. Tavan and K. Schulten, *Biophys. J.*, **50**, 81 (1986).
112. H.S. Rodman Gilson, B.H. Honig, A. Croteau, G. Zarrilli and K. Nakanishi,

Biophys. J., **53**, 261 (1988).

113. T. Kakitani and H. Kakitani, *J. Phys. Soc. Jpn.*, **88**, 1455 (1975).
114. H. Kakitani, T. Kakitani and S. Yomosa, *J. Phys. Soc. Jpn.*, **42**, 1287 (1977).
115. T. Kakitani, A. Sarai and H. Kakitani, *J. Phys. Soc. Jpn.*, **51**, 3309 (1982).
116. T. Kakitani, A. Sarai and H. Kakitani, *J. Phys. Soc. Jpn.*, **51**, 3302 (1982).
117. L.J. Weimann, G.M. Maggiora and P.E. Blatz, *Int. J. Quantum Chem.: Quantum Biology Symp. No. 2*, 9 (1975).
118. T. Shoda, T. Noro, T. Nomura and K. Ohno, *Int. J. Quantum Chem.*, **30**, 289 (1986).
119. R.R. Birge, C.M. Einterz, H.M. Knapp and L.P. Murray, *Biophys. J.*, **53**, 367 (1988).
120. R.R. Birge and B.M. Pierce, *J. Chem. Phys.*, **70**, 165 (1979).
121. R.R. Birge, J.A. Bennett, L.M. Hubbard, H.L. Fang, B.M. Pierce, D.S. Klinger and G.E. Leroi, *J. Am. Chem. Soc.*, **104**, 2519 (1982).
122. R.R. Birge, L.P. Murray, B.M. Pierce, H. Akita, V. Balogh-Nair, L.A. Findsen and K. Nakanishi, *Proc. Natl. Acad. Sci. (USA)*, **82**, 4117 (1985).
123. R.R. Birge, *Acc. Chem. Res.*, **19**, 138 (1986).
124. R.R. Birge, L.P. Murray, R. Zidovetzki and H.M. Knapp, *J. Am. Chem. Soc.*, **109**, 2090 (1987).
125. R.A. Poirier, A. Yadav and M.R. Peterson, *MUNGAUSS*, Department of Chemistry, Memorial University of Newfoundland, St. John's, Newfoundland, Canada.
126. W.J. Hehre, R.F. Stewart and J.A. Pople, *J. Chem. Phys.*, **51**, 2657 (1969).
127. a. W.J. Pietro, B.A. Levi, W.J. Hehre and R.F. Stewart, *Inorg. Chem.*, **19**, 2225 (1980) ; b. W.J. Pietro, E.S. Blurock, R.F. Hout, Jr., W.J. Hehre, Defrees and

- R.F. Stewart, *Inorg. Chem.*, **20**, 3650 (1981) ; c. J.S. Binkley, J.A. Pople and W.J. Hehre, *J. Am. Chem. Soc.*, **102**, 939 (1980).
128. C.C.J. Roothaan, *Rev. Mod. Phys.*, **23**, 69 (1951).
129. F.W. Bobrowicz and W.A. Goddard III in *Methods of electronic structure theory*, Ed: H.F. Schaefer III, Plenum Press, New York, 79 (1977).
130. J.S. Binkley, J.A. Pople and P.A. Dobosh, *Mol. Phys.*, 1423 (1974).
131. J.A. Pople and R.K. Nesbet, *J. Chem. Phys.*, **22**, 571 (1954).
132. I. Mayer, *Chem. Phys. Lett.*, **97**, 270 (1983).
133. a. W.C. Davidon, *Math. Prog.*, **9**, 1 (1975). b. W.C. Davidon and L. Nazareth, *Technical Memo 308 and 306*, (1977). Applied Mathematics Division Argonne National Laboratories, Argonne, IL.
134. Ab initio molecular orbital calculations for chemists Eds: W.G. Richards and J.A. Horsley, Clarendon Press Oxford, 36 (1970).
135. a. P.R. Surján, *Phys. Rev. A*, **30**, 43 (1984). b. P.R. Surján, I. Mayer and I. Lukovits, *Phys. Rev. A*, **32**, 748 (1985). c. P.R. Surján, *Croatica Chemica Acta*, **57**, 833 (1984).
136. R.À. Poirier, A. Yadav and P.R. Surján, *Can. J. Chem.*, **65**, 892 (1987).
137. R.A. Poirier, A. Yadav and P.R. Surján, *J. Mol. Struc. (Theochem)*, **167**, 321 (1988).
138. P. Tavan, K. Schulten and D. Oesterhelt, *Biophys. J.*, **47**, 415 (1985).
139. B. Honig and T.G. Ebrey, *Ann. Rev. Biophys. Bioeng.*, **3**, 151 (1974).
140. D.J. Patel, *Nature*, **221**, 825 (1969).
141. B. Honig and M. Karplus, *Nature*, **229**, 558 (1971).
142. B. Pullman, J. Langlet and H. Berthod, *J. Theoret. Biol.*, **23**, 402 (1969).
143. R.A. Poirier and A. Yadav, *Chem. Phys. Lett.*, **156**, 122 (1989).

144. I. Gutman, *Theoret. Chim. Acta*, **50**, 287 (1979).
145. R.S.H. Liu, A.E. Asato, M. Denny and D. Mead, *J. Am. Chem. Soc.*, **106**, 8298 (1984).
146. E.M. Evleth, *Chem. Phys. Lett.*, **3**, 122 (1969).
147. N.C. Baird and R.M. West, *J. Am. Chem. Soc.*, **93**, 4427 (1971).
148. V. Bonacic-Koutecky and M. Persico, *Int. J. Quantum Chem.*, **23**, 517 (1983).
149. E.M. Evleth and R.A. Poirier, *J. Photochem.*, **30**, 423 (1985).
150. S. Basu, *Adv. Quantum Chem.*, **11**, 33 (1978).
151. M. Kertész and P.R. Surján, *Solid State Commun.*, **39**, 611 (1981).
152. H. Kuzmany, P.R. Surján and M. Kertész, *Solid State Commun.*, **48**, 243 (1983).
153. H.C. Longuet-Higgins and L. Salem, *Proc. Roy. Soc. London*, **A251**, 172 (1959).
154. S. Ramasesha and Z.G. Soos, *J. Chem. Phys.*, **80**, 3278 (1984).
155. P.R. Surján and H. Kuzmany, *Phys. Rev. B*, **33**, 2615 (1986).
156. A. Szabo, J. Langlet and J.P. Malrieu, *Chem. Phys.*, **13**, 173 (1976).
157. P.R. Surján, R.A. Poirier and A. Yadav in *Modelling of Structures and Properties of Molecules*, Ed: Z.B. Maksic, Chapter 5, **91**, Ellis Horwood Ltd., Chichester, England (1987).
158. H. Kuzmany, M. Mehring and S. Roth, *Springer Series in Solid State Sci.*, **63**, (1985) Springer, Berlin.
159. J.C. Chien, *Polyacetylene*, Academic Press, Orlando (1984).
160. C.F. Fincher Jr., C.E. Chen, A.J. Heeger, A.G. McDiarmid and J.B. Hastings, *Phys. Rev. Lett.*, **48**, 100 (1982).
161. R.E. Peierls, *Quantum Theory of Solids*, (1955), Calendron Press, Oxford.

162. M. Kertész, *Adv. Quant. Chem.*, **15**, 161 (1982).
163. M. Takahashi and J. Paldus, *Int. J. Quantum Chem.*, **26**, 349 (1984); *Can. J. Phys.*, **62**, 1226 (1984).
164. H. Wendel, P. Cho, M. Seel and J. Ladik, *Solid State Commun.*, **54**, 551 (1985).
165. W.P. Su, *Solid State Commun.*, **35**, 899 (1980).
166. W.P. Su, J.R. Schrieffer and A.J. Heeger, *Phys. Rev. Lett.*, **42**, 1698 (1979).
167. W.P. Su, J.R. Schrieffer and A.J. Heeger, *Phys. Rev. B*, **22**, 2099 (1980).
168. W.P. Su, J.R. Schrieffer and A.J. Heeger, *ibid.*, **28**, 1138 E (1983).
169. H. Thomann, L.R. Dalton, Y. Tomkiewicz, N.S. Shiren and T.C. Clarke, *Phys. Rev. Lett.*, **50**, 533 (1983).
170. S. Kuroda and H. Shirakawa, *Solid State Commun.*, **48**, 591 (1982).
171. O. Kikuchi, *Chem. Phys. Lett.*, **72**, 487 (1980).
172. T. Takada and M. Dupuis, *J. Am. Chem. Soc.*, **105**, 1716 (1983).
173. J. Paldus and J. Cizek, *J. Chem. Phys.*, **54**, 2293 (1971).
174. J. McKelvey and W.J. Hehre, *Mol. Phys.*, **25**, 983 (1973).
175. J. McKelvey and G. Berthier, *Chem. Phys. Lett.*, **41**, 476 (1976).
176. J. Paldus and A. Veillard, *Chem. Phys. Lett.*, **50**, 6 (1977).
177. J. Paldus, J. Cizek and B.A. Keating, *Phys. Rev. A*, **8**, 640 (1973).
178. J. Cizek and J. Paldus, *J. Chem. Phys.*, **47**, 3976 (1967); *ibid.*, **53**, 821 (1970).
179. J. Paldus and J. Cizek, *Phys. Rev. A*, **2**, 2268 (1970).
180. B. Roos, *Chem. Phys. Lett.*, **15**, 153 (1972).
181. I. Shavitt, *J. Comput. Phys.*, **11**, 90 (1973).
182. E.R. Davidson, *J. Comput. Phys.*, **17**, 87 (1975).
183. N.C. Handy, J.D. Goddard and H.F. Schaeffer III, *J. Chem. Phys.*, **71**, 426

(1979).

184. A. Szabo and Neil S. Ostlund in *Modern Quantum Chemistry: Introduction to advanced electronic structure theory, Chapter 2*, 89, Macmillan Publishing Co. Inc., New York (1982).
185. R.R. Birge, K. Schulten and M. Karplus, *Chem. Phys. Lett.*, **31**, 451 (1975).
186. K. Schulten and M. Karplus, *Chem. Phys. Lett.*, **14**, 305 (1972).
187. (a) Th. Forster, *Z. Elektrochem.*, **54**, 42 (1950). (b) R. Mathies and L. Stryer, *Proc. Natl. Acad. Sci. USA*, **73**, 2169 (1976).
188. W.A. Sokalski and R.A. Poirier, *Chem. Phys. Lett.*, **98**, 86 (1983).
189. R. Pariser and R.G. Parr, *J. Chem. Phys.*, **21**, 466 (1953).
190. J.D. Bene and H.H. Jaffe, *J. Chem. Phys.*, **48**, 1807 (1968).
191. I. Ohmine, M. Karplus and K. Schulten, *J. Chem. Phys.*, **68**, 2298 (1978).
192. P. Tavan and K. Schulten, *J. Chem. Phys.*, **70**, 5407 (1979).
193. A.C. Lasaga, R.J. Aerni and M. Karplus, *J. Chem. Phys.*, **73**, 5230 (1980).
194. B. Pullman and A. Saran, *Prog. Nucleic Acid Res. Mol. Biol.*, **18**, 215 (1976).
195. F. Jordan, M. Gilbert, J.P. Malrieu and U. Pincelli, *Theoret. Chim. Acta (Berlin)*, **15**, 211 (1969).
196. J.P. Malrieu, P. Claverie and S. Diner, *Theoret. Chim. Acta (Berlin)*, **13**, 18 (1969).

APPENDIX I

Symmetry labelling for states of trans butadiene (Under the π -electron Hückel Approximation)

Wavefunctions for each state may be written as:

$$\psi_N = \phi_1(a_u)^2 \phi_2(b_g)^2$$

$$\psi_{V_1} = \phi_1(a_u)^2 \phi_2(b_g)^1 \phi_3(a_u)^1$$

$$\psi_{V_2} = \phi_1(a_u)^2 \phi_2(b_g)^1 \phi_4(b_g)^1$$

$$\psi_{V_3} = \phi_1(a_u)^1 \phi_2(b_g)^2 \phi_3(a_u)^1$$

$$\psi_{V_4} = \phi_1(a_u)^1 \phi_2(b_g)^2 \phi_4(b_g)^1$$

The symmetry of each wavefunction is the symmetry of the product representations.

Wavefunction	Product	Product representation
ψ_N	$a_u \times a_u \times b_g \times b_g$	1A_g
ψ_{V_1}	$a_u \times a_u \times b_g \times a_u$	1B_u
ψ_{V_2}	$a_u \times a_u \times b_g \times b_g$	1A_g
ψ_{V_3}	$a_u \times b_g \times b_g \times a_u$	1A_g
ψ_{V_4}	$a_u \times b_g \times b_g \times b_g$	1B_u

APPENDIX II

a. Dependence of Fock matrix on Density matrix

The total charge density in a closed shell molecule described by a single determinant wavefunction with each occupied M.O. ψ_a containing two electrons is

$$\rho(r) = 2 \sum_a^{N/2} |\psi_a(r)|^2 \quad (16)$$

The integral of this charge density equals the total number of electrons

$$\begin{aligned} \int d\tau \rho(r) &= 2 \sum_a^{N/2} \int d\tau |\psi_a(r)|^2 \\ &= 2 \sum_a^{N/2} 1 = N \end{aligned}$$

Inserting the M.O. expansion (2) in the expansion for charge density (16)

$$\begin{aligned} \rho(r) &= 2 \sum_a^{N/2} \psi_a^*(r) \psi_a(r) \\ &= 2 \sum_a^{N/2} \sum_{\nu} C_{\nu a}^* \phi_{\nu}^*(r) \sum_{\mu} C_{\mu a} \phi_{\mu}(r) \\ &= \sum_{\mu\nu} [2 \sum_a^{N/2} C_{\mu a} C_{\nu a}^*] \phi_{\mu}(r) \\ &= \sum_{\mu\nu} P_{\mu\nu} \phi_{\mu}(r) \phi_{\nu}^*(r) \end{aligned}$$

Therefore, the density matrix elements can be defined as

$$P_{\mu\nu} = 2 \sum_a^{N/2} C_{\mu a} C_{\nu a}^* \quad (17)$$

Since the density matrix is directly related to the expansion coefficients, the results of closed-shell HF calculations can be characterized either by $C_{\mu i}$ or by the $P_{\mu\nu}$. The Fock matrix can now be expressed in terms of the density matrix.

We know that the Fock matrix has the elements

$$\begin{aligned} F_{\mu\nu} &= \int d\mathbf{r}_1 \phi_\mu^*(1) f(1) \phi_\nu(1) \\ &= \int d\mathbf{r}_1 \phi_\mu^*(1) h(1) \phi_\nu(1) + \sum_a^{\mathcal{N}/2} \int d\mathbf{r}_1 \phi_\mu^*(1) [2J_a(1) - K_a(1)] \phi_\nu(1) \\ &= H_{\mu\nu}^{\text{core}} + \sum_a^{\mathcal{N}/2} 2(\mu\nu | aa) - (\mu a | a\nu) \end{aligned}$$

Inserting the linear expansion for the M.O.(2) into the two electron terms:

$$\begin{aligned} F_{\mu\nu} &= H_{\mu\nu}^{\text{core}} + \sum_a^{\mathcal{N}/2} \sum_{\lambda\sigma} C_{\lambda a} C_{\sigma a}^* [2(\mu\nu | \sigma\lambda) - (\mu\lambda | \sigma\nu)] \\ &= H_{\mu\nu}^{\text{core}} + \sum_{\lambda\sigma} P_{\lambda\sigma} [(\mu\nu | \sigma\lambda) - \frac{1}{2} (\mu\lambda | \sigma\nu)] \\ &= H_{\mu\nu}^{\text{core}} + G_{\mu\nu} \end{aligned} \tag{18}$$

The Fock matrix thus contains a one electron part H^{core} which is fixed, given the basis set and a two electron part G that depends on the density matrix and a set of two-electron integrals.

$$H_{\mu\nu}^{\text{core}} = \int d\mathbf{r}_1 \phi_\mu^*(1) h(1) \phi_\nu(1)$$

The elements of the core Hamiltonian matrix are integrals involving the one electron operator $h(1)$, describing the kinetic energy and nuclear attraction of an electron

$$h(1) = -\frac{1}{2} \nabla_1^2 - \sum_A \frac{Z_A}{|\mathbf{r}_1 - \mathbf{R}_A|}$$

Therefore, the kinetic energy integrals and the nuclear attraction integrals have to be calculated to get the core Hamiltonian matrix.

$$T_{\mu\nu} = \int d\mathbf{r}_1 \phi_\mu^*(1) \left[-\frac{1}{2} \nabla_1^2 \right] \phi_\nu(1)$$

$$V_{\mu\nu}^{nucl} = \int d\mathbf{r}_1 \phi_{\mu}^*(1) \left[- \sum_A \frac{Z_A}{|\mathbf{r}_1 - \mathbf{R}_A|} \right] \phi_{\nu}(1)$$

$$H_{\mu\nu}^{core} = T_{\mu\nu} + V_{\mu\nu}^{nucl}$$

b. Orthogonalization of the basis:

Symmetric orthogonalization procedure has been used. It uses the inverse square root of \mathbf{S} as the transformation matrix.

$$\mathbf{S}^{-1/2} \mathbf{S} \mathbf{S}^{-1/2} = \mathbf{S}^0 = \mathbf{1}$$

APPENDIX III

Relationship between *ab initio* and *Semi-empirical* M.O. calculations

The various semi-empirical M.O. theories, which may be derived from the exact SCF formalism, include approximations and the use of empirical parameters to different degrees. The various approximate methods make increasingly drastic assumptions about the integrals which appear in the expressions for closed shell HIF, RHIF and UIH (see chapter 2 and appendix II), some being set equal to zero and the others replaced by semi-empirical estimates.

The valence electron approximation

In this approximation all 1s shells on the atoms constituting the molecule are considered to be part of an unpolarizable core and only the valence electrons are treated. Therefore, $H_{\mu\nu}^{core}$ now becomes,

$$H_{\mu\nu}^{core} = \int d\mathbf{r}_1 \phi_{\mu}^*(1) \left[-\frac{1}{2} \nabla_1^2 - \sum_A V_A(r) \right] \phi_{\nu}(1)$$

where $\sum_A V_A(r)$ is the electrostatic field of the core written as a sum of the potentials $V_A(r)$ for the various atoms in the molecule. It is to be noted that this method still comes under the category of *ab initio* methods. In the following paragraphs different semi-empirical methods are discussed:

A. Neglect of diatomic differential overlap (NDDO)

The valence shell approximation is made and along with that the atomic orbitals included in the basis set are assumed to form an orthonormal set. So that $S_{\mu\nu} = \delta_{\mu\nu}$. In addition differential overlap in two electron integrals is neglected. This means that the overlapping charge densities of basis orbitals on different atoms are neglected $(\mu\nu|\lambda\sigma) = 0$ unless μ and ν belong to the same atom A and λ and σ to B. The remaining integrals may be calculated from a small basis set of atomic orbitals or chosen empirically. Dewar's MINDO method is also very similar to this method.

B. Intermediate Neglect of Differential Overlap (INDO)

In this approximation all interatomic overlaps are ignored. All two electron integrals which depend on the overlapping of charge densities of different atomic basis orbitals are neglected, i.e. $(\mu\nu|\lambda\sigma) = 0$. Some one centre integrals are not ignored, example: $(s_A \cdot p_{xA} | s_A \cdot p_{xA})$ and $(p_{xA} \cdot p_{yA} | p_{xA} \cdot p_{yA})$.

C. Complete Neglect of Differential Overlap (CNDO)

This approximation goes even one stage further than the INDO method. All two-electron integrals which depend on the overlapping of charge densities of different atomic basis orbitals are neglected, that is $(\mu\nu|\lambda\sigma) = 0$ unless $\mu = \nu$ and $\lambda = \sigma$ in which case the integral can be written as $\gamma_{\mu\lambda} = (\mu\mu|\lambda\lambda)$. This is a fairly drastic approximation since some one-centre integrals are ignored, example $(2s_A \cdot 2p_{xA} | 2s_A \cdot 2p_{xA})$. The electron interaction integrals $\gamma_{\mu\nu}$ are assumed to be dependent only on the atoms to which ϕ_μ and ϕ_ν belong and not to the particular type of atomic orbital. As a result only a single set of integrals γ_{AB} is left which can be interpreted as an average repulsion between an electron in a valence shell on atom A and another valence electron in an atomic orbital on B. The matrix elements now become

$$H_{\mu\mu} = H_{\mu\mu}^{core} - \frac{1}{2} P_{\mu\mu} \gamma_{AA} + \sum_A P_{AA} \gamma_{AA} + \sum_{B \neq A} P_{BB} \gamma_{AB}$$

μ belongs to atom A and $P_{BB} = \sum_{\nu}^B P_{\nu\nu}$

$$H_{\mu\mu}^{core} = \langle \mu | -\frac{1}{2} \nabla^2 + V_A | \mu \rangle - \sum_{B \neq A} \langle \mu | V_B | \mu \rangle$$

The first term is the energy of the atomic orbital ϕ_μ on A (can be estimated semi-empirically) and the second term is the interaction of an electron in ϕ_μ with the cores of atoms B.

If ϕ_μ and ϕ_ν are on different atoms

$$H_{\mu\nu}^{\text{core}} = \beta_{\mu\nu} = \beta_{AB}^0 \cdot S_{\mu\nu}$$

β_{AB}^0 is a parameter depending only on atoms A and B. Now that most of the atomic integrals have been eliminated or set equal to parameters the LCAO-SCF equations can be solved.

D. Extended Huckel Theory (EHT)

It starts with the Roothaan equations but leaves the Hamiltonian undefined.

$$H C_{\mu i} \phi_\mu = \epsilon_i C_{\mu i} \phi_\mu$$

The coefficients $C_{\mu i}$ and the orbital energies ϵ_i are obtained by solving the secular determinant

$$| H_{\mu\nu} - \epsilon S_{\mu\nu} | = 0$$

The explicit form of $H_{\mu\nu}$ is not sought and nearly all the integrals are represented by empirical parameters. The complete secular determinant is treated, all interactions are accounted for and the off-diagonal terms are retained. Matrix elements $H_{\mu\mu}$ are taken as measures of the electron attracting power of particular atoms. $H_{\mu\nu}$ are approximated as $0.5 K (H_{\mu\mu} + H_{\nu\nu}) S_{\mu\nu}$. K is a parameter. Simple diagonalization of the determinant yields ϵ_i and the M.O. coefficients. There is no self-consistency as the resulting orbitals are not used in computing the matrix elements. Total Huckel energy = $2\sum \epsilon_i$ for a closed shell system. The coefficients are used to determine approximate charge distributions in the molecule.

E. The π -electron approximation

There are a whole series of approximate M.O. methods that roughly follow the hierarchy of complexity as the above methods but the π -electron approximation is used as an additional assumption. This has been applied mainly for conjugated systems.

In this approximation a series of states of conjugated molecules are assumed to have a constant σ electron framework and it is assumed that differences are only due to the π -electrons. The complete wavefunction is $\Psi = \Sigma \Pi$. Σ and Π are proper antisymmetric wave functions describing the appropriate sets of electrons. The hamiltonians can be written as

$$H = H_{\sigma}^0 + H_{\pi}^0 + H_{\sigma\pi}$$

H_{σ}^0 and H_{π}^0 are of the usual Hartree-Fock form but refer only to σ and π electrons respectively.

$$H_{\sigma\sigma} = \sum_i^{n\sigma} \sum_j^{n\pi} \frac{1}{r_{ij}}$$

$$H^{\pi} = H_{\pi}^0 + H_{\sigma\sigma}$$

Including $H_{\sigma\sigma}$ in the core

$$H^{\pi} = \sum_i^{n\pi} h^{core}_i + \sum_{i < j}^{n\pi} \frac{1}{r_{ij}}$$

Hartree-Fock operator is then $H = h^{core} + \sum_j^{n\pi} (2 J_j - K_j) = h^{core} + G_{\pi}$.

To obtain solution to these equations further approximations are made. A brief outline of some of the π -electron methods is as follows:

(a). The Goepfert-Meyer-Sklar method

This method works within the π -electron approximation but makes very few further assumptions. The M.O. are expanded in a basis of $2p_z$ atomic orbitals assumed to be orthogonal. The J and K integrals are calculated completely except that three and four centre integrals are neglected, but h^{core} is simplified by the following approximation. σ - π effects are neglected as are the effects of hydrogen nuclei.

$$h^{core} = -\frac{1}{2} \nabla_i^2 + \sum_s V_{si}$$

and we assume $h_{i1}^{\text{core}} = W_{2p} \psi_i$

W_{2p} = ionization potential of carbon in an sp^2 valence state.

(b). The Pariser-Parr-Pople method

There are several possible modifications of this particular scheme, but most are at about the same level of sophistication. The starting point is the Roothaan equation in the form

$$\left\{ h^{\text{core}} + 2J_i - K_i \right\} \sum_{\mu} C_{\mu i} \phi_{\mu} = \epsilon_i \sum_{\mu} C_{\mu i} \phi_{\mu}$$

The CNDO approximation is made, that is $S_{\mu\nu} = \delta_{\mu\nu}$ and any integral of the form

$$\int d\mathbf{r}_1 d\mathbf{r}_2 \phi_{\mu}^*(1) \phi_{\nu}(1) \frac{1}{r_{12}} \phi_{\lambda}^*(2) \phi_{\sigma}(2)$$

is set equal to $\delta_{\mu\nu} \delta_{\lambda\sigma} \gamma_{\mu\lambda}$

and $\gamma_{\mu\lambda} = \int d\mathbf{r}_{12} \phi_{\mu}^2(1) \phi_{\lambda}^2(2)$ is taken as an empirical parameter.

For the core integrals a type of Goeppert-Meyer-Sklar approximation is made.

$h_{\mu\nu}^{\text{core}} = 0$ if $\mu \neq \nu$ unless μ and ν are on neighbouring atoms. If they are on neighbouring atoms $h_{\mu\nu}^{\text{core}} = \beta_{\mu\nu}$ (another empirical parameter).

$$h_{\mu\mu}^{\text{core}} = \int d\mathbf{r}_1 \phi_{\mu}^*(1) \left[-\frac{1}{2} \nabla^2 - V_{\mu} \right] \phi_{\mu}(1) + \sum_{\mu \neq \nu} \int d\mathbf{r}_1 \phi_{\mu}^*(1) V_{\mu} \phi_{\mu}(1)$$

The first term is replaced by an empirical parameter I_{μ} = modified ionization potential and the second term = $-Z_{\nu} \gamma_{\mu\nu}$ which is electron-nuclear attraction with other atoms.

V_{μ} and V_{ν} are potentials due to atoms μ and ν .

(c). The Huckel Method

This is a very well known method and is the most drastic of all the approximations. It is within the π -approximation and furthermore assumes an effective Hamiltonian H that does not treat inter-electron repulsions specifically.

$$H \sum_{\mu} C_{\mu i} \phi_{\mu} = \epsilon_i \sum_{\mu} C_{\mu i} \phi_{\mu}$$

This gives secular equations

$$\sum_{\mu} C_{\mu i} (H_{\mu\nu} - \epsilon S_{\mu\nu}) = 0$$

which have a non-trivial solution when

$$\det |H_{\mu\nu} - \epsilon S_{\mu\nu}| = 0.$$

To solve this determinant the following assumptions are made about matrix elements:

$$H_{\mu\mu} = \alpha \text{ an empirical parameter}$$

$$H_{\mu\nu} = \beta \text{ (if } \mu \text{ and } \nu \text{ are neighbours) an undefined parameter.}$$

$$H_{\mu\nu} = 0 \text{ if } \mu \text{ and } \nu \text{ are not neighbours}$$

$$S_{\mu\nu} = \delta_{\mu\nu}$$

Energies are normally quoted in β units.

In the above paragraphs the relationship between the ab initio M.O. calculations and the semiempirical methods has been stressed and the position of each in the hierarchy of complexity has been indicated. Each method has been the subject of a lengthy monograph. For further details the reader is directed to references 120, 189-196.

APPENDIX IV

RHF optimized C-C bond lengths for different resonance structures for octatetraene and corresponding retinal analog with the STO-3G basis set.

Bond	Bond lengths (Å °)					
	X=—, —, —, —=		X=—, —, —=—=		X=—=—, —, —=	
	X=C	X=O	X=C	X=O	X=C	X=O
X-C15	1.3106	1.2260	1.3224	1.2280	1.3156	1.2225
C14-C15	1.4634	1.4858	1.4548	1.4786	1.4798	1.4996
C13-C14	1.4841	1.4834	1.5385	1.5385	1.3359	1.3336
C12-C13	1.3231	1.3230	1.4402	1.4407	1.4400	1.4422
C11-C12	1.4841	1.4842	1.3358	1.3356	1.5384	1.5389
C10-C11	1.4636	1.4638	1.4798	1.4801	1.4548	1.4550
C9-C10	1.3196	1.3195	1.3156	1.3156	1.3224	1.3223

NOTES

